
An unbiased spectral line survey observation toward the low-mass star-forming region L1527

**Kento YOSHIDA,^{1,2,*} Nami SAKAI,² Yuri NISHIMURA,^{1,3,4} Tomoya
TOKUDOME,¹ Yoshimasa WATANABE,^{5,6} Takeshi SAKAI,⁷ Shuro TAKANO,⁸
and Satoshi YAMAMOTO^{1,9}**

¹Department of Physics, The University of Tokyo, 7-3-1, Hongo, Bunkyo-ku, Tokyo 113-0033, Japan

²Star and Planet Formation Laboratory, RIKEN Cluster for Pioneering Research (CPR), 2-1, Hirosawa, Wako, Saitama 351-0198, Japan

³Institute of Astronomy, The University of Tokyo, 2-21-1, Osawa, Mitaka, Tokyo 181-0015, Japan

⁴Chile Observatory, National Astronomical Observatory of Japan, 2-21-1, Osawa, Mitaka, Tokyo 181-8588, Japan

⁵Division of Physics, Faculty of Pure and Applied Sciences, University of Tsukuba, Tsukuba, Ibaraki 305-8571, Japan

⁶Tomonaga Center for the History of the Universe, University of Tsukuba, Tsukuba, Ibaraki 305-8571, Japan

⁷Department of Communication Engineering and Informatics, Graduate School of Informatics and Engineering, The University of Electro-Communications, Chofugaoka, Chofu, Tokyo 182-8585, Japan

⁸Department of Physics, General Studies, College of Engineering, Nihon University, 1, Nakagawara, Tokusada, Tamuramachi, Koriyama, Fukushima 963-8642, Japan

⁹Research Center for the Early Universe, The University of Tokyo, 7-3-1, Hongo, Bunkyo-ku,

Tokyo 113-0033, Japan

*E-mail: yoshida@taurus.phys.s.u-tokyo.ac.jp

Received (reception date); Accepted (acceptation date)

Abstract

An unbiased spectral line survey toward a solar-type Class 0/I protostar, IRAS04368+2557, in L1527 has been carried out in the 3 mm band with the Nobeyama 45 m telescope. L1527 is known as a warm carbon-chain chemistry (WCCC) source, which harbors abundant unsaturated organic species such as C_nH ($n = 3, 4, 5, \dots$) in a warm and dense region near the protostar. The observation covers the frequency range from 80 to 116 GHz. A supplementary observation has also been conducted in the 70 GHz band to observe fundamental transitions of deuterated species. In total, 69 molecular species are identified, among which 27 species are carbon-chain species and their isomers, including their minor isotopologues. This spectral line survey provides us with a good template of the chemical composition of the WCCC source.

Key words: astrochemistry — ISM: individual (LDN 1527) — ISM: molecules

1 Introduction

In the last decade, it has been established that the chemical composition of low-mass protostellar sources shows significant diversity, even if their evolutionary stages are similar to one another (e.g., Sakai & Yamamoto 2013; Watanabe et al. 2012). One distinct case is hot corino chemistry characterized by rich saturated complex organic molecules (COMs) in a hot region around a protostar (e.g., Cazaux et al. 2003; Sakai et al. 2006; Öberg et al. 2011; Taquet et al. 2015; Codella et al. 2016). A representative hot corino source is IRAS 16293-2422 in Ophiuchus (e.g., Cazaux et al. 2003; Bottinelli et al. 2004; Kuan et al. 2004). Recent ALMA observations revealed that saturated COMs such as HCOOCH_3 , $(\text{CH}_3)_2\text{O}$, and even glycolaldehyde are abundant in the innermost part of the protostellar core having a temperature higher than 100 K (e.g., Jørgensen et al. 2012; 2016; Favre et al. 2014; Oya et al. 2016; 2018). On the other hand, the warm carbon-chain chemistry (WCCC) is characterized by high abundances of carbon-chain molecules and related species concentrated around a protostar (e.g., Sakai et al. 2008b; 2009a; 2010a; Hirota, Sakai & Yamamoto 2010). A prototypical source is IRAS

04368+2557 in L1527 in the Taurus molecular cloud. In WCCC, unsaturated hydrocarbons such as carbon-chain molecules and their isomers are efficiently produced in the gas phase in a lukewarm region around a protostar ($T \sim 30$ K and $R \sim 1000$ au). Their production is triggered by sublimation of CH_4 from grain mantles.

Hot corino chemistry and WCCC show exclusive nature: carbon-chain molecules are deficient in the hot corinos, while COMs are deficient in the WCCC sources (Sakai et al. 2008b; Sakai & Yamamoto 2013; Lefloch et al. 2018). It is proposed that this chemical variation would originate from the duration time of starless core phase after shielding of the interstellar UV radiation from outside of the parent molecular cloud (Sakai et al. 2009a; Sakai & Yamamoto 2013). If the duration time is long enough for the gas-phase formation of CO from carbon atom, CO is depleted onto dust grains rather than C atom, resulting in the formation of CH_3OH through a series of reactions with the H atom on dust surface (e.g., Watanabe & Kouchi 2002; Soma et al. 2015). COMs are thought to be formed on dust surfaces as in the case of CH_3OH , or by subsequent gas-phase reactions starting from sublimated CH_3OH (e.g., Garrod & Herbst 2006; Vasyunin & Herbst 2013; Balucani et al. 2015; Soma et al. 2018). On the other hand, if the duration time of the starless core phase is close to the free-fall time (i.e., the core collapse starts just after the UV shielding), the C atom still survives in the gas phase without being converted to CO, and can be depleted onto dust grains. This situation leads to the efficient production of CH_4 on dust surfaces by hydrogenation of the C atom (Aikawa et al. 2008). After the onset of star formation, molecules in dust mantles are released into the gas phase, and chemical diversity emerges in the gas phase.

A detailed understanding of the origin and the fate of the chemical diversity is of great interest for astrochemistry in relation to the origin of the Solar System. As the first step toward this goal, it is important to reveal the chemical compositions of representative low-mass protostellar sources in an unbiased way. Although spectral line survey observations toward the hot corino source IRAS 16293-2422 have been conducted not only with single-dish telescopes but also with interferometers (Caux et al. 2011; Jørgensen et al. 2016; Ligterink et al. 2017), no spectral line survey observations toward WCCC sources have been reported except for that recently published by Lefloch et al. (2018) (See below). With this in mind, we conducted the unbiased spectral line survey toward the prototypical WCCC source L1527 in the 3 mm band with the Nobeyama 45m telescope (hereafter referred to as NRO 45 m), as part of the legacy project of Nobeyama Radio Observatory. Here, we report the whole result of the survey. Presence of highly unsaturated hydrocarbons is the most characteristic feature of interstellar chemistry. Hence, revealing the whole chemical composition of the WCCC source and its

comparison with other sources such as starless cores showing cold carbon-chain chemistry (e.g., TMC-1 (CP); Kaifu et al. 2004) will give us valuable information on formation of these molecules in space.

As an independent study, a similar spectral line survey observation toward this source was also carried out with the IRAM 30 m telescope, as part of the ASAI (Astrochemical Surveys At Iram) program. Its summary result has recently been reported (Lefloch et al. 2018), although detailed data exploitation has not been presented. The ASAI survey almost covers the frequency range of our survey in the 3 mm band with a larger beam size by a factor of 1.5. Nevertheless, independent spectral line surveys with different telescopes are always important for the fundamental sources such as L1527, because they give opportunities to confirm the consistency of the results, and also provide additional information such as the source sizes by taking advantage of the different beam sizes. Here, we report the results of our spectral line survey with NRO 45 m.

2 Observation

The spectral line survey observations of L1527 were carried out with NRO 45 m during the seasons from 2006 to 2012. The frequency range was from 79.8 GHz to 116.8 GHz. The observed position was $(\alpha_{2000}, \delta_{2000}) = (4^{\text{h}}39^{\text{m}}53^{\text{s}}89, 26^{\circ}03'11''.0)$, which is the position of the protostar (Sakai et al. 2008b). In this observation, we used the SIS mixer receivers, S80 and S100, simultaneously from 2006 to 2008, while we employed the dual-polarization sideband-separating SIS receiver T100H/V (Nakajima et al. 2008) from 2009 to 2012. The system temperatures varied from 250 to 350 K in the former and from 150 to 250 K in the latter. The intensity scale was calibrated by using the chopper-wheel method, and the calibration uncertainty is estimated to be better than 20%. The telescope pointing was checked once every 1 to 1.5 hour by observing the nearby SiO maser sources (NML-Tau and Ori-KL). The pointing accuracy was ensured to be better than $6''$. The main-beam efficiency (η_{mb}) at 86 GHz was 0.43 from 2006 to 2008, 0.49 in 2009, and 0.42 from 2010 to 2012, as reported on the NRO website. The antenna temperature (T_{A}^*) is converted to the main-beam brightness temperature (T_{mb}) by $T_{\text{mb}} = T_{\text{A}}^*/\eta_{\text{mb}}$. The beam size was $19''$ at 86 GHz and $15''$ at 110 GHz. A position switching mode with the off-position $(\alpha_{2000}, \delta_{2000}) = (4^{\text{h}}42^{\text{m}}35^{\text{s}}9, 25^{\circ}53'23''.3)$, which is free from the emission of CO isotopologue lines, was employed in all the observations.

Before 2010, we used a bank of acousto-optical radio spectrometers (AOSs), whose bandwidth, resolution, and channel spacing are 250 MHz, 250 kHz, and 125 kHz, respectively. In

2011-2012, we used a bank of autocorrelators, SAM45 (Spectral Analysis Machine for the 45 m telescope), whose bandwidth, resolution, and channel spacing were set to be 1 GHz, 244 kHz, and 244 kHz, respectively. The frequency resolution corresponds to the velocity resolution of $\sim 0.8 \text{ km s}^{-1}$ at 90 GHz. This resolution is larger than the typical line width in this source ($\sim 0.5\text{--}0.8 \text{ km s}^{-1}$). Nevertheless, we chose this resolution to cover the whole 3 mm band within the limited observation time. Although the lines are partly frequency-diluted, the integrated intensity is reliable.

In addition to the observations in the 3 mm band, a supplementary observation was conducted in the 4 mm band with NRO 45 m from February to April 2012. This observation mainly aims at investigating the deuterium fractionation of some fundamental molecular species. Thus, only selected lines were observed. The side-band-separating (2SB) SIS mixer receiver T70H/V was used as the front end with a typical system noise temperature of 200–300 K. The back end was SAM45, whose resolution was set to be 60.1 kHz. The beam size was $22''$ at 75 GHz. The main-beam efficiency at 75 GHz was 0.45.

3 Results

3.1 Overall results

Figure 1 is an overview of the observed spectrum in the 3 mm band, while Figure 2 shows its zoomed view. Figure 3 shows the spectra of the supplementary observation in the 70 GHz band. Typically, the rms noise at the native spectral resolution ranges from 5 to 15 mK in T_{mb} in the 3 mm band. This rms noise level is similar to or even better than that of the spectral line survey toward the outflow shocked region L1157 B1, which was also conducted with NRO 45 m as part of the legacy project of Nobeyama Radio Observatory (Sugimura et al. 2011; Yamaguchi et al. 2012). The detected lines are identified on the basis of spectral line databases, the Cologne Database for Molecular Spectroscopy managed by University of Cologne (CDMS; Müller et al. 2001; 2005) and the Submillimeter, Millimeter, and Microwave Spectral Line Catalog provided by Jet Propulsion Laboratory (JPL; Pickett et al. 1998). A line detection criterion is that the peak intensity of the line exceeds four times the rms noise level at its expected frequency. In total, 243 emission lines and one absorption line ($\text{CH}_3\text{OH } 3_{1,3}\text{--}4_{1,4}, \text{A}^+$ at 107.01 GHz) are detected in the frequency range from 79.8 to 116.9 GHz (Figures 1 and 2). Hence, the line density is 6.5 GHz^{-1} with this sensitivity. From the detected emission lines, 69 molecular species are identified in the 3 and 4 mm bands, among which 37 species are isotopologues. These numbers are higher than those of L1157 B1 (line density: 3.4 GHz^{-1} , detected species:

47 species including 15 isotopologues). This clearly shows chemical complexity of L1527. The detected molecules are summarized in Table 1.

In this survey, *c*-C₃D is detected for the first time in interstellar clouds. Although *c*-C₃D is detected with the signal-to-noise (S/N) ratio higher than 4σ , the velocity resolution is not high enough to determine the line parameters by Gaussian fits. C₂O, C₃S, C₆H, HCNO, HCO₂⁺, C₄D, C₂H₃CN, and CH₂DOH are tentatively detected with the S/N ratio higher than 3σ . In addition, CC¹³CCH, *l*-C₃D and CH₃CCD are also tentatively detected, because multiple lines are marginally seen. Among the tentatively detected species in this survey, the detections of C₆H, HCNO, HCO₂⁺, C₄D, and *l*-C₃D have already been reported by the higher sensitivity observations (Sakai et al. 2007; Marcelino et al. 2009; Sakai et al. 2008c; Sakai et al. 2009b).

For unidentified lines with the S/N ratio higher than 4σ , we carefully inspect whether they are also detected in the ASAI survey, and find that none of them have corresponding features in the ASAI data. Most of the unidentified lines that appeared only in this survey are likely spurious lines, which are mainly caused in the AD converters of the autocorrelators during the period of our observations. Significant features of such spurious lines are shown in some panels of Figure 2. In the frequency range observed only with NRO 45 m, 2 lines are unidentified, and they should be verified in future observations. The intensity, line-of-sight velocity and FWHM line width of the detected lines are determined by a single Gaussian fit. If the line profile is blended with multiple lines such as nearby hyperfine components, multiple Gaussian functions are employed to determine the line parameters. For the hyperfine components of N₂D⁺ and CH₂CN, we assume that the line width and the line-of-sight velocity are identical among all the components, and that the intensities are proportional to the line strengths, because the hyperfine splittings are too small to fit them independently (Figure ??). Tables 2 and 3 present lists of the line parameters of the identified molecular lines including tentatively detected ones and unidentified lines. Note that some of the hyperfine components of CCD show significant offsets in ΔV_{LSR} (Table 3). This is probably because of insufficient accuracy of the rest frequencies listed in CDMS (See the Appendix).

As listed in Table 1, 27 species are carbon-chain species and their isomers. For saturated molecules, the most fundamental species, CH₃OH and CH₃CHO, which are already detected in many cold starless cores (e.g., Kaifu et al. 2004; Vastel et al. 2014; Soma et al. 2018), are detected. However, larger complex organic molecules such as (CH₃)₂O and HCOOCH₃ are not detected in this survey, while spectral lines of these species are detected in the 3 mm band with peak intensities of a few 10 mK or stronger toward the hot corino sources such as IRAS 16293-2422 and NGC1333 IRAS4A (e.g., Caux et al. 2011; Bottinelli et al. 2004).

A deficiency of complex organic molecules in L1527 was also reported on the basis of high sensitivity observations (Sakai et al. 2008a).

3.2 Column densities and rotation temperatures

In this observation, multiple transition lines with different upper-state energies were detected for many species. Assuming a local thermodynamic equilibrium (LTE) condition, we determine the rotation temperature and the beam-averaged column density for each species by using the least-squares method with the following formula:

$$T_b = \frac{h\nu}{k} \left[\frac{1}{\exp(h\nu/kT_{\text{rot}}) - 1} - \frac{1}{\exp(h\nu/kT_{\text{bg}}) - 1} \right] (1 - e^{-\tau}),$$

and

$$\tau = \frac{8\pi^3 S \mu^2}{3h\Delta\nu U(T_{\text{rot}})} \left[\exp\left(\frac{h\nu}{kT_{\text{rot}}}\right) - 1 \right] \exp\left(-\frac{E_u}{kT_{\text{rot}}}\right) N,$$

where T_b is the brightness temperature, h the Planck constant, ν the transition frequency, k the Boltzmann constant, T_{rot} the rotation temperature, T_{bg} the cosmic microwave background temperature of 2.7 K, τ the optical depth, S the line strength, μ the dipole moment, $\Delta\nu$ the line width at half maximum, $U(T_{\text{rot}})$ the partition function, E_u the upper state energy, and N the total column density.

The partition function is numerically calculated from energies and degeneracies of the rotational levels, which are taken from the spectroscopy databases CDMS and JPL. The beam-filling factor is not included for simplicity. This assumption is reasonable especially for carbon-chain molecules, because distributions of carbon-chain molecules such as CCH and C₄H are reported to be extended over 20''–40'' (Sakai et al. 2010a), which is comparable to or larger than the typical beam size of the observation ($\sim 20''$). Uncertainties of the derived column densities include the rms noise, the fitting error, and the intensity calibration uncertainty of 20%. Table 4 shows the column densities and the rotation temperatures derived by the above analysis. The large uncertainty for C₃N originates from large scattering of the data due to the poor S/N ratios.

For molecules for which only one transition line or multiple lines with almost the same upper-state energies are detected, the column densities are derived under the LTE assumption with the excitation temperatures of 10 K and 15 K. The range of the excitation temperature is chosen on the basis of the rotation temperatures derived for other molecules in the above analysis. The column densities thus evaluated are summarized in Table 5. A change in the temperature by 5 K does not result in a substantial change in the column density ($\sim 20\%$ or

less for most of the species). Optical depths of the lines are also listed in Table 5. Most of them are less than 1. Hence, the column densities are reasonably estimated. An exception is the HCCNC case. The column density of HCCNC changes by a factor of 2 between 10 K and 15 K. This is likely due to the relatively high upper-state energy of the detected line ($J = 10-9$; $E_u = 26$ K). Moreover, if we employ the $J = 9-8$ line ($E_u = 21$ K) tentatively detected with the 3σ confidential level, the column density is derived to be about a half of that from the $J = 10-9$ line, assuming the excitation temperature of 10 K or 15 K. The column density of HCCNC therefore has a relatively large uncertainty.

It should be noted that some molecules having an extended distribution might have the excitation temperature less than 10 K, because of contributions from less dense and colder parts. However, the excitation temperature of 5 K does not cause a substantial change in the column density ($\sim 20\%$ or less) and the optical depth (0.4 or less) for most of the species. For DNC and H^{13}CO^+ , the column densities becomes ~ 2 times higher and optical depths becomes ~ 2 , if the excitation temperature were 5 K.

The low excitation temperature indicates that the emissions are not truly in the LTE condition, but are sub-thermally excited. To examine whether LTE is a good approximation for this observation, we compare the derived column densities with those obtained with the non-LTE radiative transfer code RADEX (van der Tak et al. 2007). Simple molecules such as C^{18}O , CS, SO, HC^{15}N , HC^{18}O^+ , and CCH are examined, for which the collisional cross sections are available. As summarized in Table 6, the column densities derived by RADEX and those derived by the LTE analysis agree within the error over a range of $n(\text{H}_2) = 3 \times 10^5 - 3 \times 10^6 \text{ cm}^{-3}$ and $T_k = 10-30$ K except for CS. The difference in the column density of CS is about a factor of 2, which does not change the conclusion of the discussion in Section 4.2 (see Figures 5 and 6). Yoshida et al. (2015) reported the column density of $\text{c-C}_3\text{H}_2$ with RADEX by using the NRO 45 m and the IRAM 30 m telescope, which only differ from those derived with LTE by 20%. Larger molecules tend to exist in the denser part of the cloud, and hence, the non-LTE effect could be smaller than the above cases. The non-LTE effect on isotopic ratios is also negligible, because uncertainties of the derived column densities are mostly caused by assumptions of temperature and H_2 density, and their effects are canceled out in the ratios. Thus, we employ the results obtained with LTE in the following analysis and discussions.

The spectral lines of CO, ^{13}CO , CS, HCO^+ , HCN, and HNC are optically thick, judging from the isotopologue lines. Hence, the column densities of these molecules shown in Table 5 are derived from the isotopologue lines, assuming the following isotopic ratios in the local interstellar matter (ISM): $^{12}\text{C}/^{13}\text{C} = 60$, $^{16}\text{O}/^{18}\text{O} = 560$, and $^{32}\text{S}/^{34}\text{S} = 22$ (Lucas & Liszt 1998;

Wilson & Rood 1994; Chin et al. 1996). As discussed later (Section 4.1.2), the $^{12}\text{C}/^{13}\text{C}$ ratios of carbon-chain molecules are higher than the local ISM value. However, we here employ the standard values for the above fundamental species. Although the optical depths of C^{18}O and H^{13}CO^+ lines are also high, the derived column densities are consistent with those derived from the C^{17}O , $^{13}\text{C}^{18}\text{O}$, and HC^{18}O^+ lines ($^{18}\text{O}/^{17}\text{O}=3.2$; Wilson & Rood 1994).

For molecules having the ortho and para species due to symmetry, they are analyzed separately under the assumption of the same rotation temperatures, if the lines of both species are detected. Free parameters for the fit are the total column density, the rotation temperature, and the ortho-to-para ratio. For $l\text{-C}_3\text{H}_2$, $c\text{-C}_3\text{H}_2$, C_4H_2 and CH_2CO , the ortho-to-para ratios are derived to be 2.81 ± 0.14 , 2.2 ± 0.3 , 3.2 ± 0.2 and 3.2 ± 1.2 , respectively. $c\text{-C}_3\text{H}_2$ shows lower ortho-to-para ratio than 3, probably because an optically-thick ortho line is used for the evaluation. For molecules of which only ortho lines are detected, we assume the statistical ortho-to-para ratios: 3 for H_2^{13}CO , H_2CS , NH_2D , $c\text{-H}_2\text{C}_3\text{O}$, $c\text{-}^{13}\text{CCCH}_2$ and CH_2CN , and 2 for D_2CO and $c\text{-C}_3\text{D}_2$. For CH_3CCH and CH_3CN , the A and E states caused by the internal rotation are analyzed separately under the assumption of the identical rotation temperature. The A/E ratios are derived to be 0.98 ± 0.14 and 1.07 ± 0.02 for CH_3CCH and CH_3CN , respectively. For CH_3CHO and CH_3OH , the A/E ratio is assumed to be 1, because only one line of the A state is detected. The column densities shown in Tables 4 and 5 represent the total column densities. The error of the column density of NH_2D is large because of the poor S/N ratio of the detected line.

We derive the upper limit to the column densities for important undetected species, OCS , HCOOCH_3 , and $(\text{CH}_3)_2\text{O}$, to compare them with those derived in IRAS 16293-2422. A spectral line for which the highest S/N ratio is expected in the observed frequency range (i.e., $J=7-6$ at 85.14 GHz for OCS , $4_{14}-3_{13}\text{EE}$ at 99.32 GHz for $(\text{CH}_3)_2\text{O}$, and $9_{09}-8_{08}\text{A}$ at 100.68 GHz for HCOOCH_3) is used for the evaluation for each species. The 3σ upper limit is derived from the rms noise under the assumption of the line width of 1.0 km s^{-1} , as shown in Table 5.

In order to derive the beam-averaged fractional abundances of molecules relative to H_2 ($X = N/N(\text{H}_2)$), we evaluate the beam-averaged column density of H_2 , $N(\text{H}_2)$, from the C^{17}O data. The $N(\text{H}_2)$ value is derived to be $(8.2 \pm 1.6) \times 10^{22} \text{ cm}^{-2}$ by assuming the rotation temperature of 15 K and the $N(\text{C}^{17}\text{O})/N(\text{H}_2)$ ratio of 2.6×10^{-8} (Jørgensen, Schöier & van Dishoeck 2002). Note that this ratio is derived from the C^{17}O and dust continuum observations, and is lower than the ratio reported by Frerking, Langer, & Wilson (1982). The fractional abundances of molecules are listed in Table 7. Here, we adopt the column densities derived with the excitation temperature of 15 K for the species listed in Table 5.

4 Discussion

4.1 Isotopic ratios

4.1.1 Deuterated species

Since we detect 12 deuterated species with reasonably good S/N ratios, we here derive their abundance ratio relative to the normal species, as summarized in Table 8. For the isotopic species, we adopt the same rotation temperatures as those for the normal species. For molecules for which the rotation temperatures are not derived by the fit, the ratios are derived by assuming the excitation temperature of 15 K. Note that the results do not change within the error limits, even if we adopt the excitation temperature of 10 K. The D/H ratio (i.e., what fraction of the hydrogen atom is replaced by the deuterium atom in the species of interest) is not the same as the abundance ratio, when the molecular species contains multiple equivalent H or D atoms. The D/H ratios translated from the derived abundance ratios are also shown in Table 8.

The abundance ratios derived in this study are consistent with the previous reports, as shown in Table 8. Carbon-chain molecules (CCH and HC₃N) and standard species (HCN, HCO⁺, N₂H⁺, and HNC) show moderate D/H ratios of ~ 0.04 – 0.05 . Note that the D/H ratios of HCO⁺ and HNC can be regarded as an upper limit and lower limit, respectively. The H¹³CO⁺ and DNC lines could be optically thick, if we adopt the excitation temperature lower than 10 K. For overcoming this situation, using the double isotope species such as DN¹³C to evaluate the D/H ratio would be preferable. CH₂DCCH is statistically favored by a factor of 3, because there are three equivalent hydrogen atoms in the methyl group to be deuterated. Thus, the [CH₂DCCH]/[CH₃CCH] ratio of 0.141 means a similar level of deuterium fractionation to the other carbon-chain species, when the statistical weight is considered.

The moderate D/H ratio observed in this study is consistent with the interpretation reported by Sakai et al. (2009b) and Sakai & Yamamoto (2013). In the WCCC sources, the starless-core phase would be shorter than the chemical timescale of the C-to-CO conversion ($\sim 10^6$ yr). The starless-core phase is not long enough for deuterium transfer reactions and CO depletion onto dust grains to occur. Thus, the D/H ratios should be relatively low in the WCCC sources (Sakai et al. 2009b). This is in contrast to the hot corino sources, which is thought to be a consequence of a longer cold starless-core phase with high degree of CO depletion. In fact, the [CCD]/[CCH] ratio is reported to be 0.18 in the hot core source IRAS 16293-2422 (van Dishoeck et al. 1995), which is much higher than that in L1527 (0.037).

On the other hand, the D/H ratios of c-C₃D₂, D₂CO, and HDCS are found to be high in comparison with those of other species. This trend is seen in other low-mass star-forming

regions, as described below. The $[\text{HDCS}]/[\text{H}_2\text{CS}]$ ratio is 0.29, which is much higher than the abundance ratios of the other species. The D/H ratio is still as high as 0.14, in which the statistical weight of 2 due to the two equivalent hydrogen atoms is taken into account. The high $[\text{HDCS}]/[\text{H}_2\text{CS}]$ ratio (0.29) is previously reported in the evolved starless core, Barnard 1, which is higher than the D/H ratios of the other molecules observed in this source (Marcelino et al. 2005). Marcelino et al. (2005) reproduced the high abundance ratio of HDCS in their steady-state gas-phase chemical model.

The derived $[\text{D}_2\text{CO}]/[\text{H}_2\text{CO}]$ ratio of 0.014 is also high, because the D/H ratio ($\sqrt{[\text{D}_2\text{CO}]/[\text{H}_2\text{CO}]}$) is as high as 0.12. The high $[\text{D}_2\text{CO}]/[\text{H}_2\text{CO}]$ ratio is often revealed in many low-mass star-forming regions including L1527 (e.g., Roberts & Millar 2007; Parise et al. 2006). Parise et al. (2006) reported the $[\text{D}_2\text{CO}]/[\text{H}_2\text{CO}]$ ratio in L1527 (0.44), while Roberts & Millar (2007) reported the $[\text{D}_2\text{CO}]/[\text{H}_2\text{CO}]$ ratio of 0.016. Our result is close to the result by Roberts & Millar (2007). Several mechanisms both in the gas-phase and the solid-phase are proposed to account for the high D_2CO abundance. Taquet, Ceccarelli & Kahane (2012) modeled the high D/H ratio, considering the abstraction and substitution of H by D atom on grain surface (e.g., $\text{H}_2\text{CO} + \text{D} \rightarrow \text{HDCO} + \text{H}$; $\text{HDCO} + \text{D} \rightarrow \text{D}_2\text{CO} + \text{H}$). Roueff et al. (2007) suggested that the D/H ratio of formaldehyde is related to the deuterium fractionation through CH_3^+ (i.e., $\text{CH}_3^+ + \text{HD} \rightarrow \text{CH}_2\text{D}^+ + \text{H}_2 + 390 \text{ K}$) in their steady-state gas-phase model, because CH_3 produced from CH_3^+ reacts with O atoms to form formaldehyde.

The derived $[\text{c-C}_3\text{D}_2]/[\text{c-C}_3\text{HD}]$ ratio of 0.11 in L1527 is higher than the $[\text{c-C}_3\text{HD}]/[\text{c-C}_3\text{H}_2]$ ratio (0.044). The $[\text{c-C}_3\text{HD}]/[\text{c-C}_3\text{H}_2]$ ratio of 0.044 is even lower than those of other molecules, when the equivalent two H atoms in $\text{c-C}_3\text{H}_2$ are considered. Since the abundance ratio of a doubly deuterated species, $[\text{XD}_2]/[\text{XHD}]$, should be statistically 4 times lower than that of the singly deuterated one, $[\text{XHD}]/[\text{XH}_2]$, this result means that $\text{c-C}_3\text{HD}$ is more readily deuterated than $\text{c-C}_3\text{H}_2$. On the other hand, Spezzano et al. (2013) reported that the $[\text{c-C}_3\text{D}_2]/[\text{c-C}_3\text{HD}]$ ratio is comparable to the $[\text{c-C}_3\text{HD}]/[\text{c-C}_3\text{H}_2]$ ratio in the starless cores L1544 and TMC-1C, although the errors of the ratios are large. They concluded that the observed D/H ratios can be explained by simple gas-phase reactions (e.g., the successive deuteration of $\text{c-C}_3\text{H}_2$ by the reaction with H_2D^+ , D_2H^+ , and D_3^+). However, the situation can be different in L1527, because the overabundance of $\text{c-C}_3\text{D}_2$ relative to $\text{c-C}_3\text{HD}$ cannot be explained by considering only a single formation pathway. Hence, the result is puzzling, and chemical models may need to be revisited.

Note that the anomalous D/H ratios may also be related to the large beam size of the single-dish telescope. Recently, Yoshida et al. (in preparation) have conducted high angular

resolution observations of D₂CO and H₂CO in L1527 with ALMA, revealing their different distributions: the normal species mainly resides in the protostar position, whereas the deuterated species mainly resides in the outer envelope. The D/H ratios derived from the single-dish observations may therefore suffer from systematic errors caused by the simplified assumption of the same emitting region and the same excitation temperature. Thus, observations with high spatial resolution are needed to solve the origin of the high D/H ratios of some molecules in this source.

4.1.2 ¹³C-substituted species

In this survey, the ¹³C species of CO, C¹⁸O, CN, HCO⁺, DCO⁺, HNC, HCN, CCH, *c*-C₃H₂, HC₃N, and H₂CO are detected. Among them, we derive the ¹²C/¹³C ratios for the cases that the column densities of the corresponding normal species are reasonably determined without suffering from the high optical depth problem. The ratios for C¹⁸O, CN, CCH, HC₃N, and *c*-C₃H₂ are summarized in Table 9. For molecules for which the rotation temperatures are not derived by the fit, the ratios are derived by assuming the excitation temperature of 15 K. Note that the results do not change within the error limits, even if the excitation temperature of 10 K is adopted.

Recent studies revealed that the ¹²C/¹³C ratios of molecules produced from C⁺ in the starless cores (TMC-1, L1521E, L1521B, and L134N) and L1527 are significantly higher than the elemental ¹²C/¹³C ratio in the local interstellar medium (60–70; Lucas & Liszt 1998; Milam et al. 2005). In L1527, CCH, HC₃N and *c*-C₃H₂ show dilution of ¹³C species except for HCC¹³CN and *c*-CC¹³CH₂ (Sakai et al. 2010b; Araki et al. 2016; Taniguchi, Saito & Ozeki 2016; Yoshida et al. 2015). For CCH, the dilution is confirmed in this survey, where the column density of the normal species is derived from the optically-thin hyperfine components ($J = 3/2-1/2$, $F = 1-1$; $\tau = 0.14$, and $J = 3/2-1/2$, $F = 1-0$; $\tau = 0.13$). On the other hand, the derived ¹²C/¹³C ratios of HC₃N are much less accurate than the reported values, because the sensitivity of this survey is not as good as the previous work (Araki et al. 2016). The derived ¹²C/¹³C ratios of *c*-C₃H₂ are 1.5 times lower than those reported by Yoshida et al. (2015). This discrepancy would originate from the limited numbers of detected lines. Yoshida et al. (2015) used 41 lines including optically thin lines in 1.3–3 mm bands to derive the column density of the normal species, while only 7 lines are detected in this survey. Moreover, some of them are relatively optically thick. The optically-thick lines suppress the column density of the normal species, which would make the ¹²C/¹³C ratio low.

The dilution of ¹³C species was theoretically predicted by Langer, Graedel & Armentrout

(1984). In molecular clouds, the main reservoir of ^{13}C is ^{13}CO , and $^{13}\text{C}^+$ is produced by the reaction with He^+ . However, $^{13}\text{C}^+$ can quickly go back to ^{13}CO through the isotope exchange reaction,



Because this reaction is exothermic (Watson, Anicich, & Huntress 1978), the backward reaction is less likely to occur at low temperature conditions. This leads to the dilution of $^{13}\text{C}^+$, resulting in high $^{12}\text{C}/^{13}\text{C}$ ratios of molecules produced from C^+ . On the other hand, molecules produced directly from CO are expected to have the $^{12}\text{C}/^{13}\text{C}$ ratio of 60–70, because ^{13}CO is the main reservoir of ^{13}C . This phenomenon is already confirmed in the cold starless core TMC-1: various carbon-chain molecules show the dilution of ^{13}C (Sakai et al. 2007; 2010b; 2013), while CH_3OH , which is formed through successive hydrogenation of CO on dust grains (Watanabe & Kouchi 2002), shows the normal $^{12}\text{C}/^{13}\text{C}$ ratio (Soma et al. 2015). Since the derived $[\text{C}^{18}\text{O}]/[^{13}\text{C}^{18}\text{O}]$ ratio in L1527 is consistent with the elemental ratio within the error, our study further confirms the dilution of ^{13}C species of carbon-chain molecules in the protostellar core, L1527.

The above situation is different from a high $[\text{C}^{18}\text{O}]/[^{13}\text{C}^{18}\text{O}]$ ratio caused by the isotope selective photodissociation (e.g., Visser, van Dishoeck, & Black 2009). This mechanism enhances the $^{13}\text{C}^+$ abundance, and subsequently decreases the $^{12}\text{C}/^{13}\text{C}$ ratio in various molecules formed from $^{13}\text{C}^+$ (enrichment of the ^{13}C species). This is opposite to our observational trend. Thus, this mechanism seems unimportant in this source. It is also suggested that a high $[\text{C}^{18}\text{O}]/[^{13}\text{C}^{18}\text{O}]$ ratio in the gas phase is caused by the difference of the binding energy between ^{13}CO and ^{12}CO (Smith et al. 2015; Jørgensen et al. 2018). This can cause the lower abundance of $^{13}\text{C}^+$ relative to $^{12}\text{C}^+$, resulting in lower abundances of the ^{13}C species of various molecules. However, the dilution of the ^{13}C species are widely found even in cold clouds, and this mechanism seems less important than the mechanism mentioned in the above paragraph.

The derived $[\text{CN}]/[^{13}\text{CN}]$ ratio (61 ± 17) is also comparable to the elemental ratio. In diffuse clouds, dilution of $^{13}\text{C}^+$ is not significant due to high temperature. If CN produced in this earlier phase of molecular cloud evolution still remains, the $^{12}\text{C}/^{13}\text{C}$ ratio of CN is close to 60–70. The derived $^{12}\text{C}/^{13}\text{C}$ ratio of CN is consistent with the possible formation pathway of HC_3N : $\text{C}_2\text{H}_2 + \text{CN} \rightarrow \text{HC}_3\text{N} + \text{H}$ (Fukuzawa & Osamura 1996; Woon & Herbst 1996; 1997; Takano et al. 1998). In the formation reaction of HC_3N , the C-N bond in CN is considered to be preserved. Thus, the $[\text{HC}_3\text{N}]/[\text{HCC}^{13}\text{CN}]$ ratio would be similar to the $[\text{CN}]/[^{13}\text{CN}]$ ratio of 61. This expectation is now verified in L1527 by the $[\text{HC}_3\text{N}]/[\text{HCC}^{13}\text{CN}]$ ratio of 49 ± 15 (this study) and 64.2 ± 1.1 (Araki et al. 2016).

4.1.3 ^{15}N -substituted species

The ^{15}N species of CN, HCN, and HNC are detected in this survey. The $^{14}\text{N}/^{15}\text{N}$ ratios of the three species are consistent with one another within the error, as shown in Table 10. Sources where the $^{14}\text{N}/^{15}\text{N}$ ratios of CN, HCN, and HNC are derived are limited to Barnard 1 and the protocluster OMC-2 FIR4. In both sources, the $^{14}\text{N}/^{15}\text{N}$ ratios of the above three species are comparable to one another (Daniel et al. 2013; Kahane et al. 2018), and the ratios are similar to those derived in L1527 (Table 10). This result is consistent with the astrochemical models, which predict that the molecules bearing the nitrile functional group (-CN) have a common fractionation process (e.g., Rodgers & Charnley 2008). On the other hand, the $^{14}\text{N}/^{15}\text{N}$ ratio of CN is reported to be significantly higher than that of HCN in the starless core L1544 (Hily-Blant et al. 2013a; 2013b). This report contradicts with our result in L1527. Further observations are thus needed to solve this discrepancy.

Araki et al. (2016) reported that the $^{14}\text{N}/^{15}\text{N}$ ratio of HC_3N is 338 ± 12 in L1527. If HC_3N is produced from the reaction mentioned above ($\text{C}_2\text{H}_2 + \text{CN} \rightarrow \text{HC}_3\text{N} + \text{H}$), the $^{14}\text{N}/^{15}\text{N}$ ratios of HC_3N and CN should be similar. On the other hand, the $^{14}\text{N}/^{15}\text{N}$ ratio of CN (230 ± 80) is derived to be lower than that of HC_3N . However, the error of this study is large, and is a target for future observations.

4.2 Comparison with other sources

4.2.1 TMC-1

In Figure 5, the column densities of molecules derived in this study in L1527 are compared with those reported for TMC-1, which is the representative carbon-chain rich starless core. Basically, the column densities are well correlated between the two sources. We note the following trends.

1. The column density ratios ($N_{\text{TMC-1}}/N_{\text{L1527}}$) of the nitrogen-bearing species (e.g., HC_3N and HC_5N) and the sulfur-bearing species (e.g., CCS and H_2CS) are higher than those of the hydrocarbons.
2. For C_nH , longer chain molecules have relatively low $N_{\text{TMC-1}}/N_{\text{L1527}}$ ratios. For instance, the column densities of CCH and *c/l*- C_3H are higher than those in TMC-1, while the column densities of C_4H and C_5H are lower. This trend is more significant in longer chains as reported by Sakai et al. (2008b). Note that Araki et al. (2017) reported that C_7H and C_6H_2 are the exception: relative abundances of C_7H and C_6H_2 in L1527 compared to TMC-1 are higher than those of C_6H and C_4H_2 , respectively.

The characteristics of WCCC, which are originally suggested by Sakai et al. (2008b), are further

confirmed. In WCCC, carbon-chain molecules are efficiently regenerated from CH_4 , which is sublimated from grain mantle after the onset of star formation. Longer chains tend to be deficient in comparison with TMC-1, because they are produced more slowly than shorter chains. The formation timescale of N-bearing chains can also be long due to slow neutral-neutral reactions, suppressing the abundances of HC_nN and other N-bearing species in WCCC sources relative to the carbon-chain molecules. S-bearing species can remain deficient, if sulfur is still depleted on dust grains.

As for COMs, the column density ratios relative to CH_3OH in L1527 and TMC-1 are compared in Table 11. The column densities in TMC-1 are taken from Soma et al. (2018). The column density ratios in L1527 are almost comparable to those in TMC-1, suggesting that, unlike the hot corino case, the formation of COMs is inefficient. This is consistent with the WCCC mechanism (e.g., Sakai & Yamamoto 2013).

4.2.2 IRAS 16293-2422

Figure 6 shows the correlation plot of the column densities derived in L1527 and those in IRAS 16293-2422. This source is known to be a binary source, and the chemistry of each component has been studied by interferometric observations (e.g., Jørgensen et al. 2016). However, we here discuss the beam averaged column densities at the protostellar core scale (a few 1000 au) for a fair comparison with our line survey result for L1527 at a similar size scale. The beam-averaged column densities (beam size $\sim 11''$ – $28''$) of CH_3CHO , HCOOCH_3 , and $(\text{CH}_3)_2\text{O}$ in IRAS 16293-2422 are derived from the data reported by Cazaux et al. (2003) by using a least-squares method, under the assumption of the LTE condition. For other species, the beam-averaged column densities are derived from the spectral line survey observation in 0.9–3 mm bands (TIMASSS; Caux et al. 2011) with the same method as for L1527 described in Section 3. We note the following trends.

1. The column density ratios ($N_{\text{IRAS16293}}/N_{\text{L1527}}$) of the carbon-chain related molecules, CCH, C_4H , HC_3N , and $\text{c-C}_3\text{H}_2$, are around 0.1–1.
2. On the other hand, the column density ratios of the CH_3OH , H_2CO , and CH_3CHO are higher than ~ 10 . Complex organic molecules such as HCOOCH_3 and $(\text{CH}_3)_2\text{O}$, which are characteristic species to hot corino sources, are not detected in L1527. The upper limits of HCOOCH_3 and $(\text{CH}_3)_2\text{O}$ in L1527 suggest that these species are significantly less abundant than in IRAS 16293-2422 by two orders of magnitude or more. Table 11 shows the column density ratios of COMs relative to CH_3OH in L1527 and IRAS 16293-2422. The ratios of HCOOCH_3 and $(\text{CH}_3)_2\text{O}$ relative to methanol in IRAS 16293-2422 are much higher than

those derived toward L1527, indicating the efficient production of COMs in the hot corino. The ratio of the column density of H₂CO in L1527 relative to that in IRAS 16293-2422 is higher than the corresponding ratios of COMs (CH₃CHO, HCOOCH₃, and (CH₃)₂O) relative to CH₃OH. The high abundance of H₂CO relative to CH₃OH in L1527 is consistent with the fast contraction scenario in WCCC, because the timescale for the formation of CH₃OH on dust grains is longer than that of H₂CO (Taquet, Ceccarelli & Kahane 2012). On the other hand, CH₃CHO shows the similar ratio among the 3 sources shown in Table 11. This result implies that CH₃CHO may not be enhanced by the hot corino chemistry.

3. The column density ratios of the S-bearing species are around 10–100 except for CCS. CCS is efficiently produced during chemically young cold-core phase (Suzuki et al. 1992), and is not enhanced by the activity of the central protostar (Hirota, Sakai & Yamamoto 2010). The faster contraction timescale in L1527 may result in the higher abundance of ‘remnant’ CCS in comparison with other S-bearing species.

As shown in Figure 6, the $N_{\text{IRAS16293}}/N_{\text{L1527}}$ ratios range from 10^2 – 10^3 (COMs) to 0.1 (carbon-chain molecules). Chemical difference with such a high dynamic range of the column density ratio ($\gtrsim 3$ orders of magnitude) is noteworthy. For instance, Watanabe et al. (2012) conducted a spectral line survey toward the Class 0–I protostar R CrA IRS7B, revealing a higher abundance of CCH and lower abundances of CH₃OH and SO₂ in comparison with IRAS 16293-2422. The dynamic range of the column density ratios is 2–3 orders of magnitude, which is lower than the case between L1527 and IRAS 16293-2422. Watanabe et al. (2012) concluded that R CrA IRS7B is a source with a mixture of hot corino chemistry and WCCC or a source under a strong influence of the external UV radiation. The higher dynamic range of the column density ratios shown in Figure 6 further confirms that the hot corinos such as IRAS 16293-2422 and the WCCC sources such as L1527 are the two distinct cases in chemical composition.

The full chemical composition of sources can be characterized without any preconception only by an unbiased spectral line survey with high sensitivity that can detect not only the major species but also the minor species such as the COMs and carbon-chain molecules. Since unbiased spectral line survey observations toward low-mass star-forming regions have been carried out only toward a few representative sources such as IRAS 16293-2422, R CrA IRS7B, and L1527, those toward other low-mass star-forming regions are of particular importance to understand the origin of the chemical diversity.

Acknowledgments

The authors thank Cecilia Ceccarelli and Bertrand Lefloch for valuable discussions, particularly for communication of the ASAI data prior to publication, and Sheng-Yuan Liu for valuable comments. The authors are grateful to the Nobeyama Radio Observatory (NRO) staff for great support in the observations with the 45m telescope. The Nobeyama Radio Observatory is a branch of the National Astronomical Observatory of Japan, National Institutes of Natural Sciences. K. Y. acknowledges the RIKEN Junior Research Associate Program and the JSPS fellowship. This study is supported by Grant-in-Aids from the Ministry of Education, Culture, Sports, Science, and Technology of Japan (Nos. 21740132, 23740142, 25400223, 16H03964, and 25108005). N. S. and S. Y. acknowledge financial support by JSPS and MAEE under the Japan-France integrated action program.

Appendix. Observed frequencies of the $N = 1-0$ transition of CCD

Some of the hyperfine components of the CCD $N = 1-0$ transition are observed with slightly different frequencies from those reported in CDMS, as can be seen in Figure 3 (e.g., the top middle panel). The observed frequencies are summarized in Table 12. The rest frequencies reported in CDMS may be inaccurate, because they are calculated based on the laboratory measurements of the higher N transitions (Bogey, Demuynck, & Destombes 1985; Vrtilek et al. 1985). The accurate rest frequencies need to be determined in the future laboratory experiment.

References

- Aikawa, Y., Wakelam, V., Garrod, T., & Herbst, E. 2008, *ApJ*, 674, 884
- Araki, M., Takano, S., Sakai, N., Yamamoto, S., Oyama, T., Kuze, N., & Tsukiyama, K. 2016, *ApJ*, 833, 291
- Araki, M., Takano, S., Sakai, N., Yamamoto, S., Oyama, T., Kuze, N., & Tsukiyama, K. 2017, *ApJ*, 847, 51
- Balucani, N., Ceccarelli, C., & Taquet, V. 2015, *MNRAS*, 449, L16
- Bogey, M., Demuynck, C., Destombes, J. L. 1985, *A&A*, 144, 15
- Bottinelli, S., et al. 2004, *ApJL*, 617, L69
- Caux, E., et al. 2011, *A&A*, 532, A23
- Cazaux, S., et al. 2003, *ApJL*, 593, L51
- Chin, Y.-N., Henkel, C., Whiteoak, J. B., Langer, N., Churchwell, E. B., 1996, *A&A*, 305, 960
- Codella, C., et al. 2016, *A&A*, 586, L3
- Crapsi, A., Caselli, P., Walmsley, C. M., Myers, P. C., Tafalla, M., Lee, C. W., Bourke, T. L., 2005, *ApJ*, 619, 379
- Daniel, F., et al. 2013, *A&A*, 560, A3

- Favre, C., Jørgensen, J. K., David, F., Christian, B., Bisschop, S. E., Bourke, T. L., Hogerheijde, M. R., & Frieswijk, W. W. F. 2014, *ApJ*, 790, 55
- Flower, D. R. 1999, *MNRAS*, 305, 651
- Frerking, M. A., Langer, W. D., & Wilson, R. W. 1982, *ApJ*, 262, 590
- Fukuzawa, K., & Osamura, Y., 1996, Abstract of IAU symposium 178, *Molecules in Astrophysics: Probes & Processes*, ed. D. J. Jansen, M. R. Hogerheijde, and E. F. van Dishoeck (Sterrewacht Leiden), p. 186.
- Garrod, R. T., & Herbst, E. 2006, *A&A*, 457, 927
- Gratier, P., Majumdar, L., Ohishi, M., Roueff, E., Loison, J. C., Hickson, K. M., & Wakelam, V. 2016, *ApJ*, 225, 25
- Green, S., & Thaddeus, P. 1974, *ApJ*, 191, 653
- Hily-Blant, P., Bonal, L., Faure, A., & Quirico, E. 2013, *iracus*, 223, 582
- Hily-Blant, P., Pineau des Forêts, G., Faure, A., Le Gal, R., & Padovani, M. 2013, *A&A*, 557, A65
- Hirota, T., Yamamoto, S., Mikami, H., & Ohishi, M. 1998, *ApJ*, 503, 717
- Hirota, T., Ikeda, M. & Yamamoto, S. 2001, *ApJ*, 547, 814
- Hirota, T., Sakai, N. & Yamamoto, S. 2010, *ApJ*, 720, 1370
- Jørgensen, J. K., Favre, C., Bisschop, S. E., Bourke, T. L., van Dishoeck, E. F., & Schmalzl, M. 2012, *ApJL*, 757, L4
- Jørgensen, J. K., et al. 2016, *A&A*, 595, A117
- Jørgensen, J. K., Schöier, F. L., & van Dishoeck, E. F. 2002, *A&A*, 389, 908
- Jørgensen, J. K., Schöier, F. L., & van Dishoeck, E. F. 2004, *A&A*, 416, 603
- Jørgensen, J. K., et al. 2018, *A&A*, 620, A170
- Kahane, C., Al-Edhari, A. J., Ceccarelli, C., López-Sepulcre, A., Fontani, F., & Kama, M. 2018, *ApJ*, 852, 130
- Kaifu, N., et al. 2004, *PASJ*, 56, 69
- Kuan, Y.-J., et al. 2004, *ApJL*, 616, L27
- Langer, W. D., Graedel, T. E. & Armentrout, P. B. 1984, *ApJ*, 277, 581
- Ligterink, N. F. W., et al. 2017, *MNRAS*, 469, 2
- Lique, F., Spielfiedel, A., & Cernicharo, J. 2006, *A&A*, 451, 1125
- Lefloch, B. et al. 2018, *MNRAS*, 477, 4792
- Loison, J. C., et al. 2017, *MNRAS*, 470, 4075
- Lucas, R., & Liszt, H. 1998, *A&A*, 337, 246
- Marcelino, N., Cernicharo, J., Roueff, E., Gerin, M. & Mauersberger, R. *ApJ*, 2005, 620, 308
- Marcelino, N., Cernicharo, J., Tercero, B., & Roueff, E. *ApJL*, 2009, 690, L27

Milam, S. N., Savage, C., Brewster, M. A., Ziurys, L. M. & Wyckoff, S. 2005, *ApJ*, 634, 1126

Müller, H. S. P., Thorwirth, S., Roth, D. A. & Winnewisser, G. 2001, *A&A*, 370, L49

Müller, H. S. P., Schlöder, F., Stutzki, J. & Winnewisser, G. 2005, *J. Mol. Struct.*, 742, 215

Nakajima, T. et al. 2008, *PASJ*, 60, 435

Öberg, K., van der Marel, N., Kristensen, L. E., & van Dishoeck, E. F. 2011, *ApJ*, 740, 14

Oya, Y., Sakai, N., López-Sepulcre, A., Watanabe, Y., Ceccarelli, C., Lefloch, B., Favre, C., & Yamamoto, S. 2016, *ApJ*, 824, 88

Oya, Y., et al. 2018, *ApJ*, 854, 96

Parise, B., Ceccarelli, C., Tielens, A. G. G. M., Castets, A., Caux, E., Lefloch, B., & Maret, S. 2006, *A&A*, 453, 949

Persson, M. V. et al. 2018, *A&A*, 610, 54

Pickett, H. M., Poynter, R. L., Cohen, E. A., Delitsky, M. L., Pearson, J. C., & Müller, H. S. P. 1998, *J. Quant. Spectrosc. & Rad. Transfer*, 60, 883

Rabli, D., & Flower, D. R. 2010, *MNRAS*, 406, 95

Roberts, H., Fullar, G. A., Millar, T. J., Hatchell, J., Buckle, J. V. 2002, *A&A*, 381, 1026

Roberts, H. & Millar, T. J. 2007, *A&A*, 471, 849

Rodgers, S. D., & Charnley, S. B. 2008, *ApJ*, 689, 1448

Roueff, E., Parise, B., & Herbst, E. 2007, *A&A*, 464, 245

Sakai, N, Sakai, T., & Yamamoto, S. 2006, *PASJ*, 58, L15

Sakai, N, Sakai, T., Osamura, Y., & Yamamoto, S. 2007, *ApJL*, 667, L65

Sakai, N, Sakai, T., & Yamamoto, S. 2008, *Ap&SS*, 313, 153

Sakai, N, Sakai, T., Hirota, T., & Yamamoto, S. 2008, *ApJ*, 672, 371

Sakai, N, Sakai, T., Aikawa, Y., & Yamamoto, S. 2008, *ApJL*, 675, L89

Sakai, N. 2008, PhD thesis, The University of Tokyo

Sakai, N, Sakai, T., Hirota, T., Burton, M., & Yamamoto, S. 2009, *ApJ*, 697,769

Sakai, N, Sakai, T., Hirota, T., & Yamamoto, S. 2009, *ApJ*, 702, 1025

Sakai, N., Sakai, T., Hitora, T., & Yamamoto, S. 2010a, *ApJ*, 722, 1633

Sakai, N., Saruwatari, O, Sakai, T., Takano, S., & Yamamoto, S. 2010b, *A&A*, 512, A31

Sakai, N., Takano, S., Sakai, T., Shiba, S., Sumiyoshi, Y., Endo, Y., & Yamamoto, S. 2013, *JPCA*, 117, 9831

Sakai, N., & Yamamoto, S. 2013, *Chemical Review*, 113, 8981

Smith, R. L., Pontoppidan, K. M., Young, E. D., & Morris, M. R. 2015, *ApJ*, 813, 120

Soma, T., Sakai, N., Watanabe, Y., & Yamamoto, S. 2015, *ApJ*, 802, 74

Soma, T., Sakai, N., Watanabe, Y., & Yamamoto, S. 2018, *ApJ*, 854, 116

Spezzano, S., et al. 2013, ApJL, 769, L19

Spielfiedel, A., Feautrier, N., Najar, F., Ben Abdallah, D., Dayou, F., Senent, M. L., & Lique, F. 2012, MNRAS, 421, 1891

Sugimura, M., et al. 2011, PASJ, 63, 459

Suzuki, H., Yamamoto, S., Ohishi, M., Kaifu, N., Ishikawa, S., Hirahara, Y., & Takano, S. 1994, ApJ, 392, 551

Takano, S. et al. 1998, A&A, 329, 1156

Taniguchi, K., Ozeki, H., Saito, M., Sakai, N., Nakamura, F., Kamenno, S., Takano, S., & Yamamoto, S. 2016a, ApJ, 817, 147

Taniguchi, K., Saito, M., & Ozeki, H. 2016b, ApJ, 830, 106

Taquet, V., Ceccarelli, C., & Kahane, C. 2012, A&A, 538, A42

Taquet, V., Charnley, S., & Sipilä, O. 2014, ApJ, 791, 120

Taquet, V., López-Sepulcre, A., Ceccarelli, C., Neri, R., Kahane, C., & Charnley, S. 2015, ApJ, 804, 81

Vastel, C., Ceccarelli, C., Lefloch, B., & Bachiller, R. 2014, ApJ, 795, L2

van der Tak, F. F. S., Black, J. H., Schöier, F. L., Jansen, D. J., & van Dishoeck, E. F. 2007, A&A, 468, 627

van Dishoeck, E. F., Blake, G. A., Jansen, D. J., & Groesbeck, T. D. 1995, ApJ, 447, 760

Vasyunin, A. I., & Herbst, E. 2012, ApJ, 769, 34

Visser, R., van Dishoeck, E. F., & Black, J. H. 2009, A&A, 503, 323

Vrtilek, J. M., Gottlieb, C. A., Langer, W. D., Thaddeus, P., & Wilson, R. W. 1985, ApJ, 296, 35

Watanabe, N., & Kouchi, A. 2002, ApJL, 571, L173

Watanabe, Y., Sakai, N., Lindberg, J. E., Jørgensen, J. K., Bisschop, S. E. & Yamamoto, S. 2012, ApJ, 745, 126

Watson, W. D., Anicich, V. G., & Huntress, W. T., Jr. 1976, ApJL, 205, L165

Wilson, T. L., & Rood, R. T. 1994, ARA&A, 32, 191

Woon, D. E., & Herbst, E. 1996, in IAU symposium 178, Molecules in Astrophysics: Probes & Processes, (Sterrewacht Leiden), Poster B33

Woon, D. E., & Herbst, E. 1997, ApJ, 477, 204

Yamaguchi, T., et al. 2012, PASJ, 64, 105

Yang, B., Stancil, P. C., Balakrishnan, N., & Forrey, R. C. 2010, ApJ, 718, 1062

Yoshida, K., et al. 2015, ApJ, 807, 66

Table 1. Molecules detected in this study

Carbon-chain molecules and the isomers
CCH, ^{13}CCH , C^{13}CH , CCD, C_2O^* , CCS,
C_3O , C_3N , l- C_3H , l- C_3D^* , c- C_3H , c- C_3D ,
c- C_3H_2 , c- $^{13}\text{CCCH}_2$, c- $\text{CC}^{13}\text{CH}_2$, c- C_3HD , c- C_3D_2 ,
l- C_3H_2 , C_3S^* , CH_3CCH , CH_2DCCH , CH_3CCD^* ,
HCCNC, HC_3N , DC_3N , H^{13}CCCN , HC^{13}CCN , HCC^{13}CN ,
C_4H , C_4D^* , $\text{CC}^{13}\text{CCH}^*$, C_4H_2 , C_5H , HC_5N , C_6H^*
Complex organic molecules
CH_3OH , CH_2DOH^* , CH_3CHO , c- $\text{H}_2\text{C}_3\text{O}$, HCCCHO, $\text{C}_2\text{H}_3\text{CN}^*$
Other species
CO , ^{13}CO , C^{18}O , C^{17}O , $^{13}\text{C}^{18}\text{O}$, CS, C^{34}S , C^{33}S ,
CN, ^{13}CN , C^{15}N , SO, HNC, HN^{13}C , H^{15}NC , DNC,
HCN, H^{13}CN , HC^{15}N , DCN, N_2H^+ , N_2D^+ ,
HCO^+ , H^{13}CO^+ , HC^{18}O^+ , DCO^+ , D^{13}CO^+
HCS^+ , HCO, HNCO, NH_2D , H_2^{13}CO , D_2CO ,
H_2CS , HDCS, CH_2CN , CH_2CO , CHDCO, HCO_2^{+*} , HCNO^*

* Tentative detection

Table 2. Line parameters observed in the 3 mm band*.

Frequency (GHz)	Molecule	Transition	E_u (cm^{-1})	ΔV_{LSR}^* (km s^{-1})	T_{mb}^* (K)	Δv^* (km s^{-1})	$\int T_{\text{mb}} dv$ (K km s^{-1})	rms (mK)
79.812333	c-C ₃ H ₂ D	2 _{1,2} -1 _{0,1}	4.1	-0.059(7)	0.477(6)	1.164(18)	0.600(9)	6.7
79.876710	HC ₅ N	30-29	41.3	-0.04(2)	0.118(5)	1.25(6)	0.170(5)	4.8
80.046678	C ₄ H ₂	9 _{1,9} -8 _{1,8}	22.7	-0.10(3)	0.145(6)	1.40(7)	0.239(9)	6.4
80.047537	c-CC ¹³ CH ₂	2 _{0,2} -1 _{1,1}	4.4	-0.07(2)	0.164(6)	1.26(5)	0.229(8)	7.4
80.076652	CH ₂ CO	4 _{1,4} -3 _{1,3}	15.7	0.02(5)	0.088(7)	1.36(11)	0.140(11)	8.2
80.383887	C ₄ H ₂	9 _{0,9} -8 _{0,8}	13.4	-0.22(2)	0.101(4)	1.19(5)	0.135(5)	4.2
80.412848	l-C ₃ H	² Π _{1/2} , $J = 7/2-5/2$, $F = 3-2, f$	19.4	0.0(2)	0.015(4) [†]	1.6(5)	0.029(9)	6.1
80.420646	l-C ₃ H	² Π _{1/2} , $J = 7/2-5/2$, $F = 4-3, f$	19.4	-0.1(2)	0.014(4) [†]	1.6(5)	0.030(6)	5.0
80.422052	l-C ₃ H	² Π _{1/2} , $J = 7/2-5/2$, $F = 3-2, f$	19.4	0.4(3)	0.013(5) [†]	1.7(7)	0.043(7)	5.7
80.480188	CH ₂ CN	4 _{0,4} -3 _{0,3} , $J = 9/2-7/2$, $F_1 = 7/2-5/2, F = 9/2-7/2$	6.7	0.03(4)	0.0222(12)	1.50(9)	0.026(7)	5.0
80.480411	CH ₂ CN	4 _{0,4} -3 _{0,3} , $J = 9/2-7/2$, $F_1 = 9/2-7/2, F = 11/2-9/2$	6.7	0.03(4)	0.0267(15)	1.50(9)	0.029(7)	5.0
80.480454	CH ₂ CN	4 _{0,4} -3 _{0,3} , $J = 9/2-7/2$, $F_1 = 11/2-9/2, F = 13/2-11/2$	6.7	0.03(4)	0.0322(18)	1.50(9)	0.037(7)	5.0
80.481639	CH ₂ CN	4 _{0,4} -3 _{0,3} , $J = 9/2-7/2$, $F_1 = 7/2-5/2, F = 7/2-5/2$	6.7	0.03(4)	0.0161(9) [‡]	1.50(9)	0.003(7)	5.0
80.482217	CH ₂ CN	4 _{0,4} -3 _{0,3} , $J = 9/2-7/2$, $F_1 = 9/2-7/2, F = 9/2-7/2$	6.7	0.03(4)	0.0202(11)	1.50(9)	0.004(7)	5.0
80.483158	CH ₂ CN	4 _{0,4} -3 _{0,3} , $J = 9/2-7/2$, $F_1 = 11/2-9/2, F = 11/2-9/2$	6.7	0.03(4)	0.0252(14)	1.50(9)	0.020(7)	5.0
80.484890	CH ₂ CN	4 _{0,4} -3 _{0,3} , $J = 9/2-5/2$, $F_1 = 11/2-7/2, F = 9/2-7/2$	6.7	0.03(4)	0.0195(11) [‡]	1.50(9)	0.005(7)	5.0
80.487232	CH ₂ CN	4 _{0,4} -3 _{0,3} , $J = 7/2-7/2$, $F_1 = 9/2-9/2, F = 9/2-7/2$	6.7	0.03(4)	0.0218(12)	1.50(9)	0.039(7)	5.0
80.488519	CH ₂ CN	4 _{0,4} -3 _{0,3} , $J = 7/2-5/2$, $F_1 = 7/2-5/2, F = 7/2-5/2$	6.7	0.03(4)	0.0160(9) [‡]	1.50(9)	0.022(7)	5.0

Table 2. (Continued)

Frequency (GHz)	Molecule	Transition	E_u (cm^{-1})	ΔV_{LSR}^* (km s^{-1})	T_{mb}^* (K)	Δv^* (km s^{-1})	$\int T_{\text{mb}} dv$ (K km s^{-1})	rms (mK)
80.490250	CH ₂ CN	$4_{0,4}-3_{0,3}, J = 7/2-5/2,$ $F_1 = 9/2-7/2, F = 11/2-$ $9/2$	6.7	0.03(4)	0.0274(15)	1.50(9)	0.079(7)	5.0
80.490706	CH ₂ CN	$4_{0,4}-3_{0,3}, J = 7/2-5/2,$ $F_1 = 7/2-5/2, F = 9/2-$ $7/2$	6.7	0.03(4)	0.0218(12)	1.50(9)	0.071(7)	5.0
80.491239	CH ₂ CN	$4_{0,4}-3_{0,3}, J = 7/2-5/2,$ $F_1 = 5/2-3/2, F = 7/2-$ $5/2$	6.7	0.03(4)	0.0171(9) [‡]	1.50(9)	0.049(7)	5.0
80.577159	CH ₂ DCCH	$5_{1,5}-4_{1,4}$	11.9	0.26(12)	0.017(5) [‡]	0.8(2)	0.014(4)	4.7
80.718829	C ₄ H ₂	$9_{1,8}-8_{1,7}$	22.9	-0.03(3)	0.140(8)	1.15(7)	0.164(11)	8.8
80.723180	c-C ₃ H ₂	$4_{2,2}-4_{1,3}$	20.0	-0.07(4)	0.124(5)	1.72(9)	0.253(9)	5.8
80.775347	c-CC ¹³ CH ₂	$3_{1,2}-3_{0,3}$	10.9	0.19(16)	0.021(5) [‡]	1.5(4)	0.036(9)	6.2
80.832117	CH ₂ CO	$4_{0,4}-3_{0,3}$	6.7	0.04(6)	0.045(4)	1.26(14)	0.069(7)	5.3
80.902226	CH ₂ DCCH	$5_{0,5}-4_{0,4}$	8.1	0.02(6)	0.048(5)	1.16(14)	0.061(6)	6.1
80.928180	C ₃ S	$14-13$	20.2	-0.6(2)	0.019(5) [‡]	1.5(5)	0.020(7)	6.2
81.150881	c- ¹³ CCCH ₂	$2_{0,2}-1_{1,1}$	4.4	0.09(18)	0.016(4) [†]	1.3(4)	0.021(7)	5.5
81.228145	CH ₂ DCCH	$5_{1,4}-4_{1,3}$	11.9	0.30(13)	0.043(12) [‡]	0.9(3)	0.030(12)	13.0
81.505170	CCS	$N = 6-5, J = 7-6$	10.7	0.05(4)	0.207(11)	1.53(9)	0.384(17)	11.7
81.534111	HC ¹³ CCN	$9-8$	13.6	0.18(7)	0.064(9)	1.01(17)	0.059(12)	10.3
81.541981	HCC ¹³ CN	$9-8$	13.6	0.08(5)	0.077(5)	1.53(12)	0.120(10)	6.9
81.586230	CH ₂ CO	$4_{1,3}-3_{1,2}$	15.9	0.09(5)	0.097(7)	1.34(12)	0.141(13)	9.3
81.777856	C ₆ H	$^2\Pi_{3/2}, J = 59/2-57/2, e$	41.4	-0.37(15)	0.049(12) [‡]	1.3(4)	0.078(19)	14.5
81.801237	C ₆ H	$^2\Pi_{3/2}, J = 59/2-57/2, f$	41.4	-0.05(18)	0.041(7) [‡]	2.0(4)	0.081(15)	11.4
81.881468	HC ₃ N	$9-8$	13.7	0.063(5)	2.163(18)	1.308(12)	3.121(14)	13.1
82.093544	c-C ₃ H ₂	$2_{0,2}-1_{1,1}$	4.5	-0.150(13)	1.52(3)	1.40(3)	2.48(5)	34.3
82.303747	c- ¹³ CCCH ₂	$2_{1,2}-1_{0,1}$	4.4	-0.17(12)	0.048(11) [‡]	1.1(3)	0.049(13)	12.6
82.384050	C ₆ H	$^2\Pi_{1/2}, J = 59/2-57/2, f$	57.3	0.12(16)	0.030(14) [†]	0.8(4)	0.009(10)	11.4
82.395089	l-C ₃ H ₂	$4_{1,4}-3_{1,3}$	16.2	-0.02(3)	0.182(9)	1.26(7)	0.249(13)	9.6
82.424912	HCCCHO	$9_{1,9}-8_{1,8}$	15.9	0.05(13)	0.040(6)	1.6(3)	0.075(13)	8.5
82.539039	HC ₅ N	$31-30$	44.1	-0.05(6)	0.089(6)	1.55(13)	0.127(10)	8.1
82.966200	c-C ₃ H ₂	$3_{1,2}-3_{0,3}$	11.2	-0.101(7)	1.131(14)	1.255(17)	1.596(20)	15.2
83.165345	l-C ₃ H ₂	$4_{0,4}-3_{0,3}$	6.9	-0.05(2)	0.139(6)	1.11(5)	0.154(8)	6.6
83.207505	C ₂ H ₃ CN	$9_{1,9}-8_{1,8}$	15.4	-0.10(16)	0.016(8) [†]	0.7(4)	0.009(5)	6.0
83.474137	c-CC ¹³ CH ₂	$3_{2,2}-3_{1,3}$	11.0	-0.02(16)	0.022(5) [‡]	1.5(4)	0.033(10)	6.8

Table 2. (Continued)

Frequency (GHz)	Molecule	Transition	E_u (cm^{-1})	ΔV_{LSR}^* (km s^{-1})	T_{mb}^* (K)	Δv^* (km s^{-1})	$\int T_{\text{mb}} dv$ (K km s^{-1})	rms (mK)
83.541399	C ₅ H	${}^2\Pi_{1/2}, J=35/2-33/2, e$	25.7	-0.01(5)	0.056(5)	1.15(12)	0.070(6)	6.1
83.546917	C ₅ H	${}^2\Pi_{1/2}, J=35/2-33/2, f$	25.7	0.17(7)	0.047(5)	1.37(17)	0.066(7)	6.7
83.775819	HCCCHO	9 _{0,9} -8 _{0,8}	14.0	0.08(5)	0.049(5)	1.13(12)	0.063(7)	5.3
83.933699	l-C ₃ H ₂	4 _{1,3} -3 _{1,2}	16.3	-0.001(12)	0.195(4)	1.15(3)	0.248(6)	5.0
84.119329	¹³ CCH	$N=1-0, J=3/2-1/2,$ $F_1=2-1, F=5/2-3/2$	2.8	0.00(5)	0.048(5)	0.97(12)	0.048(6)	5.4
84.124143	¹³ CCH	$N=1-0, J=3/2-1/2,$ $F_1=2-1, F=3/2-1/2$	2.8	0.06(6)	0.037(5)	0.99(15)	0.036(6)	5.5
84.151352	¹³ CCH	$N=1-0, J=3/2-1/2,$ $F_1=1-0, F=1/2-1/2$	2.8	-0.05(18)	0.019(3) [‡]	2.1(4)	0.060(7)	5.1
84.153305	¹³ CCH	$N=1-0, J=3/2-1/2,$ $F_1=1-0, F=3/2-1/2$	2.8	0.04(8)	0.031(4)	1.27(20)	0.033(5)	4.9
84.185635	c-CC ¹³ CH ₂	2 _{1,2} -1 _{0,1}	4.4	0.015(10)	0.215(4)	1.18(2)	0.276(5)	4.3
84.192487	¹³ CCH	$N=1-0, J=1/2-1/2,$ $F_1=1-1, F=1/2-3/2$	2.8	-0.2(2)	0.010(6) [†]	0.9(6)	0.006(5)	5.9
84.206865	¹³ CCH	$N=1-0, J=1/2-1/2,$ $F_1=1-1, F=3/2-3/2$	2.8	0.14(10)	0.023(5)	1.0(2)	0.018(5)	5.2
84.429814	DC ₃ N	10-9	15.5	0.20(3)	0.113(5)	1.14(6)	0.145(7)	5.5
84.521169	CH ₃ OH	5 _{-1,5} -4 _{0,4} , E	28.1	0.12(14)	0.029(4)	2.2(3)	0.060(8)	6.0
84.727688	c-C ₃ H ₂	3 _{2,2} -3 _{1,3}	11.2	0.150(5)	0.525(5)	1.154(12)	0.668(7)	5.5
84.748625	c-C ₃ HD	6 _{3,3} -6 _{2,4}	36.9	0.6(2)	0.007(4) [†]	0.8(6)	0.001(3)	3.8
84.946000	C ₂ H ₃ CN	9 _{0,9} -8 _{0,8}	14.2	0.32(18)	0.014(4) [†]	1.3(4)	0.013(6)	5.1
85.139103	OCS	7-6	11.4	-	-	-	-	6.7
85.162223	HC ¹⁸ O ⁺	1-0	2.8	0.332(10)	0.341(6)	1.15(2)	0.423(7)	5.5
85.201340	HC ₅ N	32-31	46.9	0.39(4)	0.075(6)	1.18(11)	0.114(6)	6.1
85.229335	C ¹³ CH	$N=1-0, J=3/2-1/2,$ $F_1=2-1, F=5/2-3/2$	2.8	0.46(4)	0.074(5)	1.29(11)	0.128(7)	6.4
85.232805	C ¹³ CH	$N=1-0, J=3/2-1/2,$ $F_1=2-1, F=3/2-1/2$	2.8	0.46(7)	0.053(6)	1.14(16)	0.057(8)	6.9
85.247728	C ¹³ CH	$N=1-0, J=3/2-1/2,$ $F_1=1-0, F=1/2-1/2$	2.8	0.25(14)	0.018(5) [‡]	0.9(3)	0.011(5)	5.6
85.256988	C ¹³ CH	$N=1-0, J=3/2-1/2,$ $F_1=1-0, F=3/2-1/2$	2.8	0.49(6)	0.046(5)	1.10(14)	0.053(7)	5.8
85.272335	c-C ₃ H	3 _{1,2} -3 _{1,3} , $J=5/2-5/2,$ $F=3-3, 2-2$	10.3	0.31(13)	0.032(3)	2.4(3)	0.069(8)	5.8
85.296727	CH ₂ DOH	1 _{1,0} -1 _{0,1}	4.3	-0.2(2)	0.013(5) [†]	1.2(5)	0.011(6)	5.7

Table 2. (Continued)

Frequency (GHz)	Molecule	Transition	E_u (cm^{-1})	ΔV_{LSR}^* (km s^{-1})	T_{mb}^* (K)	Δv^* (km s^{-1})	$\int T_{\text{mb}} dv$ (K km s^{-1})	rms (mK)
85.303990	C^{13}CH	$N = 1-0, J = 1/2-1/2,$ $F_1 = 1-1, F = 1/2-3/2$	2.9	0.37(9)	0.025(5)	1.0(2)	0.030(6)	5.1
85.307459	C^{13}CH	$N = 1-0, J = 1/2-1/2,$ $F_1 = 1-1, F = 3/2-3/2$	2.9	0.54(9)	0.040(7)	1.0(2)	0.031(8)	8.5
85.314092	C^{13}CH	$N = 1-0, J = 1/2-1/2,$ $F_1 = 0-1, F = 1/2-1/2$	2.9	0.17(17)	0.020(6) [†]	1.2(4)	0.014(7)	6.9
85.331926	CC^{13}CCH	$N = 9-8, J = 19/2-17/2$	14.2	...	0.014 [†]	5.0
85.338894	$c\text{-C}_3\text{H}_2$	$2_{1,2}-1_{0,1}$	4.5	0.340(6)	2.76(3)	1.239(14)	3.80(3)	21.1
85.347890	HCS^+	$2-1$	4.3	0.50(4)	0.057(4)	1.18(10)	0.077(5)	5.3
85.361195	HCCCHO	$9_{1,8}-8_{1,7}$	16.4	0.45(7)	0.033(4)	1.26(17)	0.040(5)	4.8
85.370342	CC^{13}CCH	$N = 9-8, J = 17/2-15/2$	14.2	0.45(15)	0.018(6) [‡]	0.9(3)	0.021(5)	5.5
85.450766	CH_3CCH	$J_K = 5_2-4_2$	28.6	0.04(9)	0.071(9)	1.5(2)	0.106(17)	12.2
85.455667	CH_3CCH	$J_K = 5_1-4_1$	13.6	-0.07(3)	0.50(3)	1.07(7)	0.602(15)	12.7
85.457300	CH_3CCH	$J_K = 5_0-4_0$	8.6	-0.08(3)	0.56(3)	1.21(6)	0.844(14)	13.6
85.531512	HCO_2^+	$4_{0,4}-3_{0,3}$	7.1	0.87(15)	0.045(12) [‡]	1.1(3)	0.039(13)	13.6
85.634010	C_4H	$N = 9-8, J = 19/2-17/2$	14.3	0.048(6)	1.198(12)	1.101(13)	1.454(14)	11.3
85.656431	$c\text{-C}_3\text{H}_2$	$4_{3,2}-4_{2,3}$	20.2	-0.010(9)	0.464(8)	1.16(2)	0.571(9)	7.4
85.672580	C_4H	$N = 9-8, J = 17/2-15/2$	14.3	-0.011(6)	1.016(10)	1.197(13)	1.324(14)	11.3
85.694978	$c\text{-C}_3\text{H}$	$3_{1,2}-3_{1,3}, J = 7/2-7/2,$ $F = 3-3$	10.3	-1.0(2)	0.030(5) [‡]	2.4(5)	0.093(14)	9.4
85.702495	$c\text{-C}_3\text{H}$	$3_{1,2}-3_{1,3}, J = 7/2-7/2,$ $F = 4-4$	10.3	-0.08(14)	0.046(9)	1.6(3)	0.111(13)	11.0
85.926278	NH_2D	$1_{1,1}-1_{0,1}$	14.4	0.2(9)	0.05(4)	2(2)	0.136(12)	8.3
86.054966	HC^{15}N	$1-0$	2.9	0.14(2)	0.101(5)	1.07(6)	0.113(7)	5.5
86.093950	SO	$N = 2-1, J = 2-1$	13.4	0.22(9)	0.034(4)	1.5(2)	0.067(6)	5.2
86.181391	CCS	$N = 7-6, J = 6-5$	16.2	0.00(8)	0.041(5)	1.34(19)	0.074(6)	5.7
86.338733	H^{13}CN	$J = 1-0, F = 1-1$	2.9	0.07(3)	0.136(6)	1.31(7)	0.205(7)	6.4
86.340163	H^{13}CN	$J = 1-0, F = 2-1$	2.9	0.07(2)	0.168(5)	1.32(5)	0.247(5)	4.9
86.342251	H^{13}CN	$J = 1-0, F = 0-1$	2.9	-0.0(2)	0.06(2)	1.2(5)	0.069(5)	4.5
86.593678	C_3O	$9-8$	14.4	0.00(4)	0.121(10)	1.10(10)	0.125(14)	11.7
86.670760	HCO	$1_{0,1}-0_{0,0}, J = 3/2-1/2,$ $F = 2-1$	2.9	0.28(4)	0.144(7)	1.41(8)	0.228(13)	9.5
86.708360 [§]	HCO	$1_{0,1}-0_{0,0}, J = 3/2-1/2,$ $F = 1-0$	2.9	0.34(6)	0.090(8)	1.38(14)	0.129(13)	10.0
86.708379 [§]	C_3S	$15-14$	23.1	0.41(6)	0.090(8)	1.38(14)	0.130(13)	10.0

Table 2. (Continued)

Frequency (GHz)	Molecule	Transition	E_u (cm^{-1})	ΔV_{LSR}^* (km s^{-1})	T_{mb}^* (K)	Δv^* (km s^{-1})	$\int T_{\text{mb}} dv$ (K km s^{-1})	rms (mK)
86.754288	H^{13}CO^+	1-0	2.9	-0.011(5)	2.60(2)	1.271(12)	3.764(15)	11.4
86.777460	HCO	$1_{0,1}-0_{0,0}$, $F=1-1$, $J=1/2-1/2$,	2.9	0.21(5)	0.106(9)	1.23(12)	0.134(13)	10.6
86.805780	HCO	$1_{0,1}-0_{0,0}$, $F=0-1$, $J=1/2-1/2$,	2.9	-0.21(13)	0.043(9)	1.4(3)	0.030(11)	10.4
87.090825	HN^{13}C	1-0	2.9	0.31(7)	0.61(7)	1.38(17)	0.91(11)	85.5
87.284105	CCH	$N=1-0$, $J=3/2-1/2$, $F=1-1$	2.9	0.025(5)	1.506(19)	1.154(12)	1.458(9)	8.4
87.312812	$\text{C}_2\text{H}_3\text{CN}$	$9_{1,8}-8_{1,7}$	16.1	...	0.030 ‡	7.9
87.316898	CCH	$N=1-0$, $J=3/2-1/2$, $F=2-1$	2.9	-0.050(6)	4.18(4)	1.271(14)	5.971(13)	10.4
87.328585	CCH	$N=1-0$, $J=3/2-1/2$, $F=1-0$	2.9	-0.056(5)	2.95(2)	1.244(11)	4.091(10)	8.1
87.347994	C_6H	$^2\Pi_{3/2}$, $J=63/2-61/2$, f	47.2	0.2(5)	0.016(5) †	2.8(11)	0.046(15)	9.5
87.401989	CCH	$N=1-0$, $J=1/2-1/2$, $F=1-1$	2.9	-0.031(6)	2.86(3)	1.315(15)	4.213(17)	13.4
87.407165	CCH	$N=1-0$, $J=1/2-1/2$, $F=0-1$	2.9	0.018(6)	2.24(2)	1.135(14)	2.866(15)	12.4
87.435318	$c\text{-C}_3\text{H}_2$	$5_{4,2}-5_{3,3}$	31.5	-0.2(2)	0.032(7) ‡	2.0(5)	0.057(14)	10.4
87.446470	CCH	$N=1-0$, $J=1/2-1/2$, $F=1-0$	2.9	-0.002(6)	1.435(15)	1.224(15)	1.990(12)	9.9
87.863630	HC_5N	33-32	49.8	0.16(7)	0.057(7)	1.12(17)	0.063(9)	8.9
87.925237	HNCO	$4_{0,4}-3_{0,3}$	7.3	0.217(12)	0.196(5)	0.90(3)	0.187(6)	5.4
87.967595	C_6H	$^2\Pi_{1/2}$, $J=63/2-61/2$, f	63.1	0.22(13)	0.019(6) ‡	0.9(3)	0.021(6)	5.8
88.166832	H^{13}CCCN	10-9	16.2	0.39(9)	0.030(6)	0.9(2)	0.018(5)	6.3
88.308034	C_4D	$N=10-9$, $J=21/2-19/2$	16.2	...	0.010 †	6.5
88.315148	C_5H	$^2\Pi_{1/2}$, $J=37/2-35/2$, e	28.7	0.09(13)	0.028(9) ‡	0.8(3)	0.011(7)	8.9
88.318557	$1\text{-C}_3\text{D}$	$^2\Pi_{1/2}$, $J=9/2-7/2$, e	7.9	0.5(3)	0.019(6) †	1.9(7)	0.032(15)	9.5
88.320879	C_5H	$^2\Pi_{1/2}$, $J=37/2-35/2$, f	28.7	0.24(16)	0.028(6) ‡	1.6(4)	0.036(10)	8.5
88.344000	C_4D	$N=10-9$, $J=19/2-17/2$	16.2	-0.20(13)	0.025(7) ‡	1.0(3)	0.021(7)	7.3
88.345803	$1\text{-C}_3\text{D}$	$^2\Pi_{1/2}$, $J=9/2-7/2$, f	7.9	-0.0(3)	0.013(6) †	1.0(6)	0.016(7)	7.5
88.630416	HCN	$J=1-0$, $F=1-1$	3.0	-0.19(4)	0.75(3)	2.00(10)	1.787(14)	9.0
88.631848	HCN	$J=1-0$, $F=2-1$	3.0	-0.23(3)	1.14(3)	2.00(7)	2.705(14)	9.1
88.633936	HCN	$J=1-0$, $F=0-1$	3.0	-0.00(4)	0.72(4)	1.51(10)	1.403(16)	11.4
88.865690	H^{15}NC	1-0	3.0	0.00(3)	0.139(7)	0.96(6)	0.122(7)	7.4

Table 2. (Continued)

Frequency (GHz)	Molecule	Transition	E_u (cm^{-1})	ΔV_{LSR}^* (km s^{-1})	T_{mb}^* (K)	Δv^* (km s^{-1})	$\int T_{\text{mb}} dv$ (K km s^{-1})	rms (mK)
88.940236	C ₄ H ₂	10 _{1,10} -9 _{1,9}	25.7	-0.12(3)	0.113(5)	1.24(6)	0.163(6)	5.9
89.045583	C ₃ N	$N=9-8, J=19/2-17/2$	14.9	0.02(9)	0.030(10)	0.7(3)	0.017(5)	6.3
89.064347	C ₃ N	$N=9-8, J=17/2-15/2$	14.9	...	0.010 [†]	8.1
89.188525	HCO ⁺	1-0	3.0	-0.23(3)	2.27(5)	2.68(7)	6.73(5)	27.9
89.307563	C ₄ H ₂	10 _{2,8} -9 _{2,7}	54.0	-0.45(18)	0.017(5) [†]	1.2(4)	0.016(6)	6.0
89.314548	C ₄ H ₂	10 _{0,10} -9 _{0,9}	16.4	-0.15(3)	0.081(4)	1.24(8)	0.121(6)	5.2
89.407817	CH ₂ DOH	2 _{0,2} -1 _{0,1}	4.5	-0.33(11)	0.019(8) [‡]	0.7(3)	0.012(5)	6.1
89.419300	HCCNC	9-8	14.9	0.04(14)	0.022(6) [‡]	1.0(3)	0.014(6)	6.8
89.687047	C ₄ H ₂	10 _{1,9} -9 _{1,8}	25.9	-0.051(19)	0.135(5)	1.17(5)	0.171(7)	5.6
90.525890	HC ₅ N	34-33	52.8	0.04(7)	0.049(6)	1.01(16)	0.068(6)	6.6
90.593059	HC ¹³ CCN	10-9	16.6	...	0.017 [†]	8.9
90.601777	HCC ¹³ CN	10-9	16.6	0.00(14)	0.034(8) [‡]	1.2(3)	0.048(12)	9.9
90.663568	HNC	1-0	3.0	0.222(7)	2.286(19)	1.654(16)	4.133(12)	8.3
90.686381	CCS	$N=7-6, J=7-6$	18.2	0.30(10)	0.047(6)	1.4(2)	0.060(9)	8.6
90.979023	HC ₃ N	10-9	16.7	0.192(5)	2.44(3)	1.059(13)	2.850(6)	6.4
91.494349	c-C ₃ H	2 _{1,2} -1 _{1,1} , $J=5/2-3/2$, $F=3-2$	3.1	0.093(8)	0.404(6)	1.077(20)	0.491(5)	5.8
91.497608	c-C ₃ H	2 _{1,2} -1 _{1,1} , $J=5/2-3/2$, $F=2-1$	3.1	0.183(14)	0.247(6)	1.14(3)	0.306(6)	5.8
91.512969	c-C ₃ H	2 _{1,2} -1 _{1,1} , $J=5/2-3/2$, $F=2-2$	3.1	0.15(10)	0.025(6)	0.9(2)	0.018(5)	6.1
91.572516	HCCCHO	10 _{1,10} -9 _{1,9}	18.9	-0.22(16)	0.019(5) [†]	1.2(4)	0.020(6)	6.3
91.681696	c-C ₃ H	2 _{1,2} -1 _{1,1} , $J=3/2-1/2$, $F=1-1$	3.1	0.03(6)	0.033(4)	0.90(14)	0.032(4)	4.7
91.692752	c-C ₃ H	2 _{1,2} -1 _{1,1} , $J=3/2-1/2$, $F=1-0$	3.1	-0.05(3)	0.093(4)	1.25(6)	0.137(5)	4.6
91.699471	c-C ₃ H	2 _{1,2} -1 _{1,1} , $J=3/2-1/2$, $F=2-1$	3.1	0.061(12)	0.226(5)	1.19(3)	0.299(5)	5.3
91.747372	c-C ₃ H	2 _{1,2} -1 _{1,1} , $J=3/2-3/2$, $F=1-1$	3.1	0.14(6)	0.043(5)	0.99(14)	0.045(5)	5.7
91.751320	HCNO	4-3	7.7	0.13(15)	0.015(4) [‡]	1.1(3)	0.023(6)	5.0
91.780518	c-C ₃ H	2 _{1,2} -1 _{1,1} , $J=3/2-3/2$, $F=2-2$	3.1	0.12(9)	0.039(4)	1.8(2)	0.091(7)	6.0
91.985314	CH ₃ CN	$J_K=5_1-4_1$	14.2	0.15(8)	0.035(5)	1.10(19)	0.029(6)	6.4
91.987088	CH ₃ CN	$J_K=5_0-4_0$	9.2	0.06(8)	0.044(6)	1.21(19)	0.050(9)	7.8

Table 2. (Continued)

Frequency (GHz)	Molecule	Transition	E_u (cm^{-1})	ΔV_{LSR}^* (km s^{-1})	T_{mb}^* (K)	Δv^* (km s^{-1})	$\int T_{\text{mb}} dv$ (K km s^{-1})	rms (mK)
92.227853	C ₂ O	$N = 4-3, J = 5-4$	7.7	0.24(14)	0.021(5) [‡]	1.2(3)	0.031(6)	6.2
92.363286	C ₂ O	$N = 4-3, J = 4-3$	8.0	-0.09(18)	0.025(9) [†]	0.9(4)	0.017(9)	10.4
92.426250	C ₂ H ₃ CN	10 _{1,10} -9 _{1,9}	18.5	-0.05(15)	0.041(14) [†]	0.9(4)	0.023(13)	15.3
92.517433	c-H ₂ C ₃ O	7 _{1,7} -6 _{1,6}	13.2	...	0.038 [†]	13.6
92.872375	DC ₃ N	11-10	18.6	0.14(6)	0.130(13)	1.14(13)	0.162(15)	15.6
92.894848	C ₆ H	$^2\Pi_{3/2}, J = 67/2-65/2, f$	53.3	...	0.035 [†]	20.2
92.981601	HDCS	3 _{0,3} -2 _{0,2}	6.2	0.27(8)	0.053(11)	0.78(17)	0.048(11)	11.2
93.088901	C ₅ H	$^2\Pi_{1/2}, J = 39/2-37/2, e$	31.8	0.18(11)	0.043(9)	1.0(3)	0.061(10)	10.4
93.094854	C ₅ H	$^2\Pi_{1/2}, J = 39/2-37/2, f$	31.8	-0.3(3)	0.028(8) [†]	1.8(6)	0.043(16)	12.8
93.171925	N ₂ H ⁺	$J = 1-0, F_1 = 1-1$	3.1	-0.00(4)	1.17(8)	1.02(9)	1.440(19)	12.4
93.173763	N ₂ H ⁺	$J = 1-0, F_1 = 2-1$	3.1	0.30(4)	1.22(5)	1.79(9)	2.26(2)	10.3
93.176254	N ₂ H ⁺	$J = 1-0, F_1 = 0-1$	3.1	0.18(8)	0.57(9)	0.92(16)	0.544(15)	10.4
93.188123	HC ₅ N	35-34	56.0	0.04(11)	0.077(12)	1.23(20)	0.124(17)	12.0
93.580859	CH ₃ CHO	5 _{1,5} -4 _{1,4} , A ⁺	10.9	...	0.019 [†]	13.0
93.595276	CH ₃ CHO	5 _{-1,5} -4 _{-1,4} , E	11.0	0.3(4)	0.028(14) [†]	1.5(9)	0.06(2)	14.7
93.870107	CCS	$N = 7-6, J = 8-7$	13.8	-0.00(4)	0.231(9)	0.97(5)	0.257(10)	8.4
94.088936	CHDCO	5 _{0,5} -4 _{0,4}	9.4	...	0.038	9.1
94.276636	C ₂ H ₃ CN	10 _{0,10} -9 _{0,9}	17.3	...	0.021 [†]	8.4
94.371354	c-C ₃ D ₂	3 _{0,3} -2 _{1,2}	6.8	0.0(2)	0.035(9) [‡]	1.1(3)	0.028(12)	9.2
94.833681	HCCCHO	10 _{1,9} -9 _{1,8}	19.5	0.21(18)	0.044(18)	1.0(5)	0.048(12)	7.9
95.150393	C ₄ H	$N = 10-9, J = 21/2-19/2$	17.5	0.132(6)	0.93(2)	1.08(3)	1.057(11)	7.3
95.188947	C ₄ H	$N = 10-9, J = 19/2-17/2$	17.5	0.135(7)	0.87(3)	1.07(4)	1.001(16)	10.0
95.850335	HC ₅ N	36-35	59.2	0.03(7)	0.068(11)	1.2(3)	0.094(11)	8.0
95.947340	CH ₃ CHO	5 _{0,5} -4 _{0,4} , E	9.7	-0.1(2)	0.024(7) [‡]	1.5(5)	0.029(11)	7.2
95.963380	CH ₃ CHO	5 _{0,5} -4 _{0,4} , A ⁺	9.6	0.0(2)	0.023(18) [‡]	1.0(10)	0.013(9)	7.4
95.994082	c-C ₃ HD	2 _{1,1} -1 _{1,0}	5.3	0.09(4)	0.131(7)	0.99(6)	0.142(9)	6.1
96.214619	C ₃ O	10-9	17.7	...	0.091	6.2
96.412949	C ³⁴ S	2-1	4.8	-0.02(4)	0.169(8)	1.76(10)	0.353(13)	6.3
96.691587	CH ₂ DCCCH	6 _{1,6} -5 _{1,5}	15.1	...	0.039	7.9
96.739362	CH ₃ OH	2 _{-1,2} -1 _{-1,1} , E	8.7	0.088(10)	0.496(19)	1.09(5)	0.595(13)	8.2
96.741375	CH ₃ OH	2 _{0,2} -1 _{0,1} , A ⁺	4.8	-0.021(12)	0.827(11)	0.912(16)	0.838(13)	8.8

Table 2. (Continued)

Frequency (GHz)	Molecule	Transition	E_u (cm^{-1})	ΔV_{LSR}^* (km s^{-1})	T_{mb}^* (K)	Δv^* (km s^{-1})	$\int T_{\text{mb}} dv$ (K km s^{-1})	rms (mK)
96.744550	CH ₃ OH	2 _{0,2} -1 _{0,1} , E	14.0	-0.05(10)	0.082(10)	1.03(14)	0.090(13)	8.4
96.983001	H ¹³ CCCN	11-10	19.4	0.16(15)	0.043(14)	1.1(4)	0.066(14)	8.7
97.080728	CH ₂ DCCH	6 _{0,6} -5 _{0,5}	11.3	...	0.093	6.4
97.172064	C ³³ S	2-1	4.9	0.64(15)	0.044(9)	1.0(2)	0.040(14)	8.9
97.175928	C ₄ D	$N = 11-10$, $J = 21/2-19/2$	19.5	-0.0(3)	0.027(14) [†]	1.0(7)	0.031(16)	10.2
97.472736	CH ₂ DCCH	6 _{1,5} -5 _{1,4}	15.2	...	0.028 [†]	18.4
97.761978	c-C ₃ D ₂	3 _{1,3} -2 _{0,2}	6.9	...	0.042	9.1
97.833632	C ₄ H ₂	11 _{1,11} -10 _{1,10}	29.0	0.07(5)	0.132(9)	1.05(9)	0.132(13)	8.5
97.862577	C ₅ H	$^2\Pi_{1/2}$, $J = 41/2-39/2$, e	35.0	-0.1(3)	0.017(6) [†]	1.9(8)	0.040(12)	7.1
97.868769	C ₅ H	$^2\Pi_{1/2}$, $J = 41/2-39/2$, f	35.0	...	0.037	6.8
97.980953	CS	2-1	4.9	0.05(2)	1.34(2)	2.58(5)	3.67(2)	9.1
97.995166	l-C ₃ H	$^2\Pi_{1/2}$, $J = 9/2-7/2$, $F = 5-4$, e	8.7	...	0.480	26.0
97.995913	l-C ₃ H	$^2\Pi_{1/2}$, $J = 9/2-7/2$, $F = 4-3$, e	8.7	0.07(16)	0.19(9)	1.1(7)	0.34(3)	26.4
98.011611	l-C ₃ H	$^2\Pi_{1/2}$, $J = 9/2-7/2$, $F = 5-4$, f	8.7	0.04(12)	0.28(6)	0.9(2)	0.273(10)	8.1
98.012524	l-C ₃ H	$^2\Pi_{1/2}$, $J = 9/2-7/2$, $F = 4-3$, f	8.7	...	0.253	7.8
98.244930	C ₄ H ₂	11 _{0,11} -10 _{0,10}	19.7	-0.00(7)	0.064(6)	1.06(17)	0.075(9)	6.1
98.512524	HC ₅ N	37-36	62.4	0.14(9)	0.050(7)	1.10(16)	0.077(7)	5.6
98.655094	C ₄ H ₂	11 _{1,10} -10 _{1,9}	29.1	0.00(5)	0.162(12)	0.83(8)	0.161(7)	6.0
98.863328	CH ₃ CHO	5 _{1,4} -4 _{1,3} , E	11.5	...	0.023	5.7
98.900948	CH ₃ CHO	5 _{1,4} -4 _{1,3} , A^-	11.5	0.00(15)	0.028(6)	1.0(2)	0.028(7)	5.8
98.940009	C ₃ N	$N = 10-9$, $J = 21/2-19/2$	18.2	0.00(17)	0.033(7)	1.0(2)	0.033(8)	6.7
98.958770	C ₃ N	$N = 10-9$, $J = 19/2-17/2$	18.2	0.13(14)	0.034(12)	0.9(4)	0.028(7)	6.0
99.299870	SO	$N = 2-1$, $J = 3-2$	6.4	-0.00(2)	0.58(2)	1.26(5)	0.884(11)	6.7
99.325217 ^{ll}	(CH ₃) ₂ O	4 _{1,4} -3 _{0,3} , EE	7.1	-	-	-	-	6.1
99.354250	HCCNC	10-9	18.2	0.07(13)	0.031(7)	1.3(4)	0.040(8)	6.0
99.461077	c-H ₂ C ₃ O	7 _{3,4} -6 _{3,3}	20.7	...	0.018 [†]	6.4
99.651849	HC ¹³ CCN	11-10	19.9	0.05(10)	0.055(10)	1.0(2)	0.061(9)	6.0

Table 2. (Continued)

Frequency (GHz)	Molecule	Transition	E_u (cm^{-1})	ΔV_{LSR}^* (km s^{-1})	T_{mb}^* (K)	Δv^* (km s^{-1})	$\int T_{\text{mb}} dv$ (K km s^{-1})	rms (mK)
99.661467	HCC ¹³ CN	11–10	19.9	−0.05(10)	0.050(8)	0.91(19)	0.052(8)	5.4
99.866521	CCS	$N = 8-7, J = 7-6$	19.6	0.03(17)	0.033(5)	2.0(4)	0.062(11)	6.5
100.076392	HC ₃ N	11–10	20.0	−0.057(5)	3.140(16)	0.849(6)	2.942(7)	6.3
100.094514	CH ₂ CO	$5_{1,5}-4_{1,4}$	19.1	0.08(3)	0.165(7)	0.87(5)	0.159(8)	6.1
100.598231	CH ₂ CN	$5_{0,5}-4_{0,4}, J = 11/2-9/2,$ $F_1 = 9/2-7/2, F = 11/2-9/2$	10.1	−0.00(3)	0.0381(19)	0.84(5)	0.033(11)	6.6
100.598399	CH ₂ CN	$5_{0,5}-4_{0,4}, J = 11/2-9/2,$ $F_1 = 11/2-9/2, F = 13/2-11/2$	10.1	−0.00(3)	0.045(2)	0.84(5)	0.047(11)	6.6
100.598421	CH ₂ CN	$5_{0,5}-4_{0,4}, J = 11/2-9/2,$ $F_1 = 13/2-11/2, F = 15/2-13/2$	10.1	−0.00(3)	0.052(3)	0.84(5)	0.055(11)	6.6
100.599454	CH ₂ CN	$5_{0,5}-4_{0,4}, J = 11/2-9/2,$ $F_1 = 9/2-7/2, F = 9/2-7/2$	10.1	−0.00(3)	0.0299(15)	0.84(5)	0.050(11)	6.6
100.599932	CH ₂ CN	$5_{0,5}-4_{0,4}, J = 11/2-9/2,$ $F_1 = 11/2-9/2, F = 11/2-9/2$	10.1	−0.00(3)	0.0359(18)	0.84(5)	0.059(11)	6.6
100.600535	CH ₂ CN	$5_{0,5}-4_{0,4}, J = 11/2-9/2,$ $F_1 = 9/2-7/2, F = 7/2-5/2$	10.1	−0.00(3)	0.0228(11) [‡]	0.84(5)	0.039(12)	6.6
100.600607	CH ₂ CN	$5_{0,5}-4_{0,4}, J = 11/2-9/2,$ $F_1 = 13/2-11/2, F = 13/2-11/2$	10.1	−0.00(3)	0.043(2)	0.84(5)	0.042(11)	6.6
100.601342	CH ₂ CN	$5_{0,5}-4_{0,4}, J = 11/2-9/2,$ $F_1 = 11/2-9/2, F = 9/2-7/2$	10.1	−0.00(3)	0.0286(14)	0.84(5)	0.025(11)	6.6
100.602444	CH ₂ CN	$5_{0,5}-4_{0,4}, J = 11/2-9/2,$ $F_1 = 13/2-11/2, F = 11/2-9/2$	10.1	−0.00(3)	0.0355(18)	0.84(5)	0.010(12)	6.6
100.606261	CH ₂ CN	$5_{0,5}-4_{0,4}, J = 9/2-7/2,$ $F_1 = 11/2-9/2, F = 11/2-9/2$	10.1	−0.00(3)	0.0377(19)	0.84(5)	0.031(11)	6.6
100.607363	CH ₂ CN	$5_{0,5}-4_{0,4}, J = 9/2-7/2,$ $F_1 = 9/2-7/2, F = 9/2-7/2$	10.1	−0.00(3)	0.0298(15)	0.84(5)	0.026(12)	6.6
100.608262	CH ₂ CN	$5_{0,5}-4_{0,4}, J = 9/2-7/2,$ $F_1 = 7/2-5/2, F = 7/2-5/2$	10.1	−0.00(3)	0.0235(12) [‡]	0.84(5)	0.027(11)	6.6
100.608813	CH ₂ CN	$5_{0,5}-4_{0,4}, J = 9/2-7/2,$ $F_1 = 11/2-9/2, F = 13/2-11/2$	10.1	−0.00(3)	0.045(2)	0.84(5)	0.036(12)	6.6

Table 2. (Continued)

Frequency (GHz)	Molecule	Transition	E_u (cm^{-1})	ΔV_{LSR}^* (km s^{-1})	T_{mb}^* (K)	Δv^* (km s^{-1})	$\int T_{\text{mb}} dv$ (K km s^{-1})	rms (mK)
100.609199	CH ₂ CN	$5_{0,5}-4_{0,4}, J = 9/2-7/2,$ $F_1 = 9/2-7/2, F = 11/2-$ $9/2$	10.1	-0.00(3)	0.0376(19)	0.84(5)	0.034(11)	6.6
100.609626	CH ₂ CN	$5_{0,5}-4_{0,4}, J = 9/2-7/2,$ $F_1 = 7/2-5/2, F = 9/2-$ $7/2$	10.1	-0.00(3)	0.0311(16)	0.84(5)	0.021(11)	6.6
100.609662	CH ₂ CN	$5_{0,5}-4_{0,4}, J = 9/2-7/2,$ $F_1 = 9/2-7/2, F = 7/2-$ $5/2$	10.1	-0.00(3)	0.0216(11) [‡]	0.84(5)	0.012(11)	6.6
100.610072	CH ₂ CN	$5_{0,5}-4_{0,4}, J = 9/2-7/2,$ $F_1 = 11/2-9/2, F = 9/2-$ $7/2$	10.1	-0.00(3)	0.0292(15)	0.84(5)	0.013(12)	6.6
100.683368	HCOOCH ₃	$9_{0,9}-8_{0,8}, A$	17.3	-	-	-	-	5.5
100.807872	c-C ₃ D	$2_{1,1}-1_{1,0}, J = 5/2-3/2$	3.7	...	0.052	8.6
101.036630	CH ₂ CO	$5_{0,5}-4_{0,4}$	10.1	...	0.065	9.4
101.174677	HC ₅ N	$38-37$	65.8	0.0(2)	0.029(10) [†]	1.4(6)	0.036(15)	10.2
101.314818	DC ₃ N	$12-11$	22.0	...	0.081	10.7
101.477810	H ₂ CS	$3_{1,3}-2_{1,2}$	15.9	0.03(7)	0.128(9)	0.82(9)	0.090(12)	8.9
101.981429	CH ₂ CO	$5_{1,4}-4_{1,3}$	19.3	0.18(5)	0.137(17)	1.16(19)	0.142(19)	11.8
102.298030	HCCCHO	$11_{0,11}-10_{0,10}$	20.5	...	0.025 [†]	12.4
102.423019	c-C ₃ HD	$4_{1,3}-4_{0,4}$	15.5	0.19(13)	0.051(9)	0.91(18)	0.030(11)	7.9
102.540145	CH ₃ CCH	$J_K = 6_2-5_2$	32.1	-0.00(5)	0.111(7)	0.92(7)	0.108(10)	7.2
102.546024	CH ₃ CCH	$J_K = 6_1-5_1$	17.0	0.012(16)	0.585(10)	0.77(2)	0.498(10)	7.6
102.547984	CH ₃ CCH	$J_K = 6_0-5_0$	12.0	0.048(14)	0.658(9)	0.789(16)	0.589(10)	7.7
102.636255	C ₅ H	$^2\Pi_{1/2}, J = 43/2-41/2, e$	38.5	-0.01(13)	0.041(7)	1.6(3)	0.063(11)	7.3
102.642695	C ₅ H	$^2\Pi_{1/2}, J = 43/2-41/2, f$	38.5	...	0.043	6.9
102.992379	l-C ₃ H ₂	$5_{1,5}-4_{1,4}$	19.6	0.03(6)	0.29(3)	0.75(10)	0.240(13)	10.4
103.040452	H ₂ CS	$3_{0,3}-2_{0,2}$	6.9	0.08(5)	0.153(9)	0.87(6)	0.162(9)	8.3
103.069925	c-H ₂ C ₃ O	$7_{1,6}-6_{1,5}$	14.7	0.10(15)	0.043(17)	0.9(4)	0.042(10)	7.1
103.319276	l-C ₃ H	$^2\Pi_{3/2}, J = 9/2-7/2,$ $F = 5-4, f$	22.9	0.3(5)	0.029(7) [‡]	4.2(11)	0.11(3)	8.4
103.319786	l-C ₃ H	$^2\Pi_{3/2}, J = 9/2-7/2,$ $F = 4-3, f$	22.9	1.7(5)	0.027(7) [†]	3.9(12)	0.08(3)	11.6
103.372483	l-C ₃ H	$^2\Pi_{3/2}, J = 9/2-7/2,$ $F = 5-4, e$	22.9	...	0.038	9.0
103.373094	l-C ₃ H	$^2\Pi_{3/2}, J = 9/2-7/2,$ $F = 4-3, e$	22.9	-0.20(14)	0.042(9)	1.2(3)	0.077(8)	6.4
103.575395	C ₂ H ₃ CN	$11_{0,11}-10_{0,10}$	20.8	0.4(4)	0.017(6) [†]	2.3(9)	0.048(17)	7.8

Table 2. (Continued)

Frequency (GHz)	Molecule	Transition	E_u (cm^{-1})	ΔV_{LSR}^* (km s^{-1})	T_{mb}^* (K)	Δv^* (km s^{-1})	$\int T_{\text{mb}} dv$ (K km s^{-1})	rms (mK)
103.640759	CCS	$N = 8-7, J = 8-7$	21.6	-0.08(14)	0.039(7)	0.86(20)	0.046(7)	6.2
103.836817	HC ₅ N	39-38	69.3	...	-1.765	7.3
103.952926	l-C ₃ H ₂	5 _{0,5} -4 _{0,4}	10.4	0.06(3)	0.179(14)	0.87(8)	0.169(9)	6.6
104.187126	c-C ₃ HD	3 _{0,3} -2 _{1,2}	7.5	0.092(14)	0.74(8)	0.79(8)	0.623(10)	8.1
104.297349	CC ¹³ CCH	$N = 11-10, J = 23/2-21/2$	20.9	...	0.019 [†]	10.6
104.302170	HCCCHO	11 _{1,10} -10 _{1,9}	23.0	-0.3(2)	0.023(11) [†]	1.3(5)	0.021(11)	8.3
104.335725	CC ¹³ CCH	$N = 11-10, J = 21/2-19/2$	20.9	...	0.025 [†]	11.3
104.617040	H ₂ CS	3 _{1,2} -2 _{1,1}	16.1	0.14(5)	0.113(9)	1.19(10)	0.154(14)	8.7
104.666568	C ₄ H	$N = 11-10, J = 23/2-21/2$	20.9	0.136(8)	0.717(8)	1.158(14)	0.902(14)	8.8
104.705108	C ₄ H	$N = 11-10, J = 21/2-19/2$	21.0	0.086(9)	0.655(9)	1.216(19)	0.863(15)	9.4
104.711404	¹³ C ¹⁸ O	1-0	3.5	0.33(8)	0.076(11)	1.1(2)	0.083(11)	9.0
104.799707	c-C ₃ HD	3 _{1,3} -2 _{1,2}	7.6	...	0.100	9.5
104.915583	l-C ₃ H ₂	5 _{1,4} -4 _{1,3}	19.8	0.14(4)	0.213(19)	0.93(10)	0.193(15)	10.5
105.476475	c-H ₂ C ₃ O	8 _{1,8} -7 _{1,7}	16.7	-0.07(14)	0.040(7)	1.5(3)	0.064(11)	7.7
105.799113	H ¹³ CCCN	12-11	22.9	...	0.041 [†]	15.0
105.835363	C ₃ O	11-10	21.2	0.15(10)	0.088(18)	1.0(2)	0.090(15)	13.0
106.007682	C ₄ D	$N = 12-11, J = 23/2-21/2$	23.0	...	0.030 [†]	11.4
106.256108	c-C ₃ HD	4 _{2,3} -4 _{1,4}	15.6	-0.06(7)	0.061(7)	1.10(13)	0.043(8)	6.5
106.347726	CCS	$N = 8-7, J = 9-8$	17.4	0.09(5)	0.098(6)	1.48(11)	0.166(10)	6.8
106.498910	HC ₅ N	40-39	72.8	0.00(18)	0.024(8) [‡]	1.2(5)	0.032(9)	7.1
106.726849	C ₄ H ₂	12 _{1,12} -11 _{1,11}	32.5	0.03(5)	0.112(9)	1.03(9)	0.116(13)	8.8
106.811090	c-C ₃ HD	3 _{0,3} -2 _{0,2}	7.5	0.07(4)	0.125(7)	0.98(6)	0.132(9)	6.4
106.913563	HCO ₂ ⁺	5 _{0,5} -4 _{0,4}	10.7	...	0.015 [†]	6.5
107.013803	CH ₃ OH	3 _{1,3} -4 _{0,4} , A^+	19.7	-0.00(13)	-0.030(7)	1.2(3)	-0.029(8)	6.1
107.175007	C ₄ H ₂	12 _{0,12} -11 _{0,11}	23.2	-0.14(5)	0.084(17)	0.85(19)	0.078(7)	5.4
107.409891	C ₅ H	$^2\Pi_{1/2}, J = 45/2-43/2, e$	42.0	...	0.018 [†]	8.3
107.416595	C ₅ H	$^2\Pi_{1/2}, J = 45/2-43/2, f$	42.0	0.28(17)	0.026(8) [‡]	1.2(5)	0.039(9)	7.1

Table 2. (Continued)

Frequency (GHz)	Molecule	Transition	E_u (cm^{-1})	ΔV_{LSR}^* (km s^{-1})	T_{mb}^* (K)	Δv^* (km s^{-1})	$\int T_{\text{mb}} dv$ (K km s^{-1})	rms (mK)
107.423671	c-C ₃ H ₂ D	3 _{1,3} -2 _{0,2}	7.6	0.030(9)	0.589(8)	0.966(14)	0.625(10)	6.8
107.622954	C ₄ H ₂	12 _{1,11} -11 _{1,10}	32.7	0.09(7)	0.097(10)	1.13(12)	0.124(15)	9.8
107.971554	l-C ₃ D	² Π _{1/2} , $J=11/2-9/2$, f	11.5	...	0.024 [†]	8.2
108.039986	l-C ₃ D	² Π _{1/2} , $J=11/2-9/2$, e	11.5	-0.28(20)	0.027(7) [‡]	1.6(5)	0.046(14)	7.5
108.426889	¹³ CN	$N=1-0$, $J=1/2-1/2$, $F_1=0-1$, $F=1-2$	3.6	-0.0(3)	0.025(9) [‡]	0.8(4)	0.006(6)	6.3
108.631121	¹³ CN	$N=1-0$, $J=1/2-1/2$, $F_1=1-0$, $F=0-1$	3.6	...	0.025 [†]	8.5
108.636923	¹³ CN	$N=1-0$, $J=1/2-1/2$, $F_1=1-0$, $F=1-1$	3.6	0.11(11)	0.052(9)	0.92(18)	0.054(9)	7.9
108.638212	¹³ CN	$N=1-0$, $J=3/2-1/2$, $F_1=1-1$, $F=1-0$	3.6	0.29(13)	0.037(8)	1.1(3)	0.050(9)	7.6
108.644346	¹³ CN	$N=1-0$, $J=3/2-1/2$, $F_1=1-1$, $F=0-1$	3.6	...	0.022 [†]	9.0
108.651297	¹³ CN	$N=1-0$, $J=1/2-1/2$, $F_1=1-0$, $F=2-1$	3.6	...	0.064	9.1
108.657646	¹³ CN	$N=1-0$, $J=3/2-1/2$, $F_1=1-1$, $F=2-2$	3.6	0.11(9)	0.071(12)	1.1(2)	0.091(16)	10.7
108.710532	HC ¹³ CCN	12-11	23.6	...	0.017 [†]	10.0
108.720999	HCC ¹³ CN	12-11	23.6	0.01(11)	0.060(15)	1.1(3)	0.057(14)	11.6
108.780201	¹³ CN	$N=1-0$, $J=3/2-1/2$, $F_1=2-1$, $F=3-2$	3.6	0.04(5)	0.127(12)	0.99(11)	0.146(11)	9.8
108.782374	¹³ CN	$N=1-0$, $J=3/2-1/2$, $F_1=2-1$, $F=2-1$	3.6	-0.05(14)	0.069(17)	0.9(3)	0.051(12)	11.6
108.786982	¹³ CN	$N=1-0$, $J=3/2-1/2$, $F_1=2-1$, $F=1-0$	3.6	...	0.034 [†]	14.8
108.793753	¹³ CN	$N=1-0$, $J=3/2-1/2$, $F_1=2-1$, $F=1-1$	3.6	...	0.021 [†]	7.2
108.796400	¹³ CN	$N=1-0$, $J=3/2-1/2$, $F_1=2-1$, $F=2-2$	3.6	...	0.025 [‡]	8.1
108.893963	CH ₃ OH	0 _{0,0} -1 _{-1,1} , E	9.1	0.07(5)	0.18(4)	0.77(17)	0.149(10)	8.0
109.029216	CH ₃ CCD	$J_K=7_1-6_1$	19.6	...	0.019 [†]	8.0
109.031214	CH ₃ CCD	$J_K=7_0-6_0$	14.5	...	0.027 [‡]	7.6
109.173634	HC ₃ N	12-11	23.7	-0.008(4)	2.310(15)	1.212(9)	2.967(11)	8.6
109.252220	SO	$N=3-2$, $J=2-1$	14.6	0.39(12)	0.057(7)	2.0(3)	0.111(14)	7.2
109.289095	HCCNC	11-10	21.9	-0.0(3)	0.022(8) [†]	1.5(6)	0.046(13)	9.0
109.757133	DC ₃ N	13-12	25.6	-0.14(8)	0.06(2)	0.9(4)	0.046(10)	8.7

Table 2. (Continued)

Frequency (GHz)	Molecule	Transition	E_u (cm^{-1})	ΔV_{LSR}^* (km s^{-1})	T_{mb}^* (K)	Δv^* (km s^{-1})	$\int T_{\text{mb}} dv$ (K km s^{-1})	rms (mK)
109.782173	C ¹⁸ O	1-0	3.7	-0.022(11)	4.41(9)	1.11(3)	5.582(12)	8.1
109.905749	HNCO	5 _{0,5} -4 _{0,4}	11.0	-0.05(2)	0.298(8)	0.81(3)	0.238(9)	7.4
110.024590	C ¹⁵ N	$N = 1-0, J = 3/2-1/2,$ $F = 2-1$	3.7	-0.23(14)	0.048(9)	1.5(3)	0.096(14)	10.0
110.153594	NH ₂ D	1 _{1,1} -1 _{0,1}	14.8	0.4(3)	0.027(8) [†]	1.7(6)	0.053(17)	9.3
110.201354	¹³ CO	1-0	3.7	0.240(12)	9.52(12)	1.96(3)	19.79(3)	14.5
110.381372	CH ₃ CN	$J_K = 6_1-5_1$	17.9	-0.10(16)	0.033(8)	1.4(4)	0.042(11)	8.0
110.383500	CH ₃ CN	$J_K = 6_0-5_0$	12.9	...	0.078	8.4
110.837830	D ₂ CO	2 _{1,2} -1 _{1,1}	9.3	0.15(4)	0.162(11)	1.04(8)	0.184(14)	10.0
112.254524	CH ₃ CHO	6 _{-1,6} -5 _{-1,5} , E	14.7	...	0.037 [‡]	12.2
112.358880	C ¹⁷ O	$J = 1-0, F = 3/2-5/2,$ $7/2-5/2$	3.7	-0.060(16)	0.99(2)	1.25(3)	1.39(2)	17.2
112.360007	C ¹⁷ O	$J = 1-0, F = 5/2-5/2$	3.7	0.04(4)	0.51(3)	1.21(9)	0.62(12)	94.4
112.520200	U	-	3.8	-0.33(8)	0.198(11)	3.09(19)	0.62(4)	19.7
112.805469	CH ₂ DCCH	7 _{1,7} -6 _{1,6}	18.8	...	0.038 [†]	15.2
113.123370	CN	$N = 1-0, J = 1/2-1/2,$ $F = 1/2-1/2$	3.8	-0.13(2)	0.517(17)	0.84(3)	0.472(19)	15.1
113.144157	CN	$N = 1-0, J = 1/2-1/2,$ $F = 1/2-3/2$	3.8	-0.200(11)	0.786(14)	1.31(3)	1.141(18)	11.4
113.170491	CN	$N = 1-0, J = 1/2-1/2,$ $F = 3/2-1/2$	3.8	-0.280(14)	0.811(17)	1.32(3)	1.241(19)	12.1
113.191279	CN	$N = 1-0, J = 1/2-1/2,$ $F = 3/2-3/2$	3.8	-0.290(15)	0.843(18)	1.48(4)	1.40(3)	15.4
113.258171	CH ₂ DCCH	7 _{0,7} -6 _{0,6}	15.1	...	0.059	13.4
113.313910	U	-	3.8	...	0.075	12.0
113.410186	CCS	$N = 9-8, J = 8-7$	23.3	-0.3(3)	0.037(13) [†]	0.9(7)	0.058(14)	13.0
113.488120	CN	$N = 1-0, J = 3/2-1/2,$ $F = 3/2-1/2$	3.8	-0.17(3)	1.09(6)	1.35(8)	1.759(20)	12.2
113.490970	CN	$N = 1-0, J = 3/2-1/2,$ $F = 5/2-3/2$	3.8	-0.11(2)	1.62(5)	1.68(6)	3.22(3)	15.9
113.499644	CN	$N = 1-0, J = 3/2-1/2,$ $F = 1/2-1/2$	3.8	-0.119(16)	0.97(3)	1.23(4)	1.424(19)	12.3
113.508907	CN	$N = 1-0, J = 3/2-1/2,$ $F = 3/2-3/2$	3.8	-0.081(11)	1.19(2)	1.20(3)	1.63(2)	14.3
113.520432	CN	$N = 1-0, J = 3/2-1/2,$ $F = 1/2-3/2$	3.8	0.059(10)	0.60(2)	0.95(4)	0.614(16)	12.1

Table 2. (Continued)

Frequency (GHz)	Molecule	Transition	E_u (cm^{-1})	ΔV_{LSR}^* (km s^{-1})	T_{mb}^* (K)	Δv^* (km s^{-1})	$\int T_{\text{mb}} dv$ (K km s^{-1})	rms (mK)
113.716762	CH ₂ DCCH	7 _{1,6} -6 _{1,5}	19.0	...	0.052	12.4
114.182515	C ₄ H	$N = 12-11, J = 25/2-23/2$	24.8	0.046(13)	0.770(18)	0.87(2)	0.783(18)	13.7
114.221041	C ₄ H	$N = 12-11, J = 23/2-21/2$	24.8	-0.013(14)	0.730(15)	0.856(20)	0.716(17)	13.4
114.381212	c- ¹³ CCCH ₂	3 _{0,3} -2 _{1,2}	8.2	-0.15(11)	0.079(15)	1.1(2)	0.076(17)	14.5
114.614995	H ¹³ CCCN	13-12	26.8	0.47(17)	0.054(14) [‡]	1.1(4)	0.06(2)	14.1
114.647951	c-C ₃ HD	3 _{1,2} -2 _{2,1}	9.8	0.21(7)	0.136(16)	1.25(16)	0.18(2)	14.7
114.897371	c-CC ¹³ CH ₂	3 _{0,3} -2 _{1,2}	8.2	0.00(4)	0.32(2)	0.90(6)	0.30(3)	19.6
114.940190	CH ₃ CHO	6 _{0,6} -5 _{0,5} , E	13.5	...	0.069	16.9
114.954995	c-CC ¹³ CH ₂	3 _{1,3} -2 _{1,2}	8.2	0.0(2)	0.11(3)	0.7(2)	0.10(3)	25.9
115.271202	CO	1-0	3.8	1.21(12)	8.8(7)	2.9(3)	32.28(13)	53.3
115.524356	c-CC ¹³ CH ₂	3 _{1,3} -2 _{0,2}	8.2	-0.00(6)	0.30(2)	0.78(7)	0.27(2)	22.0
115.619870	C ₄ H ₂	13 _{1,13} -12 _{1,12}	36.4	...	0.054 [‡]	17.5
116.118107	CH ₃ CHO	6 _{2,4} -5 _{2,3} , A^+	19.8	0.0(4)	0.11(10) [†]	0.9(9)	0.09(7)	69.6
116.594779	CCS	$N = 9-8, J = 9-8$	25.5	...	0.071 [†]	37.4
116.688420	D ₂ CO	2 _{0,2} -1 _{0,1}	5.8	-0.04(11)	0.23(4)	1.4(3)	0.24(5)	37.4

* Obtained from the Gaussian fit. ΔV_{LSR} represents the velocity shift from V_{LSR} of 5.85 km s^{-1} . Δv represents the FWHM line width. “...” shows that the fit is not successful due to the weak intensity or the insufficient resolution.

† Less than 3σ detection.

‡ Less than 4σ detection.

§ Blended.

|| The line is not detected. Three times the rms noise is used to derive the upper limit of the column density by assuming the line width of 1 km s^{-1} .

Table 3. Line parameters of the supplementary observation in the 4 mm band.

Frequency (GHz)	Molecule	Transition	E_u (cm^{-1})	ΔV_{LSR}^* (km s^{-1})	T_{mb}^* (K)	Δv^* (km s^{-1})	$\int T_{\text{mb}} dv$ (K km s^{-1})	rms (mK)
70.733206	D ¹³ CO+	1-0	2.4	0.12(3)	0.28(3)	0.53(7)	0.153(17)	32.4
71.024788	H ₂ ¹³ CO	1 _{0,1} -0 _{0,0}	2.4	0.13(5)	0.18(3)	0.63(11)	0.124(17)	30.2
72.039312	DCO ⁺	1-0	2.4	0.061(3)	3.31(3)	0.654(6)	2.308(17)	30.3
72.101715	CCD	$N = 1-0, J = 3/2-1/2,$ $F = 3/2-3/2$	2.4	-0.27(4)	0.20(3)	0.58(9)	0.147(16)	30.0
72.107700	CCD	$N = 1-0, J = 3/2-1/2,$ $F = 5/2-3/2$	2.4	-0.035(13)	0.61(3)	0.60(3)	0.395(16)	29.2
72.109114	CCD	$N = 1-0, J = 3/2-1/2,$ $F = 1/2-1/2$	2.4	0.40(3)	0.24(3)	0.43(6)	0.117(14)	29.8
72.112399	CCD	$N = 1-0, J = 3/2-1/2,$ $F = 3/2-1/2$	2.4	0.51(2)	0.33(3)	0.48(6)	0.144(15)	30.2
72.187704	CCD	$N = 1-0, J = 1/2-1/2,$ $F = 3/2-3/2$	2.4	-0.03(2)	0.36(3)	0.50(6)	0.165(20)	39.8
72.189505	CCD	$N = 1-0, J = 1/2-1/2,$ $F = 1/2-3/2$	2.4	-0.93(6)	0.19(3) [‡]	0.76(14)	0.12(3)	53.1
72.198388	CCD	$N = 1-0, J = 1/2-1/2,$ $F = 3/2-1/2$	2.4	0.81(5)	0.18(3)	0.43(8)	0.065(16)	33.3
72.413504	DCN	$J = 1-0, F = 1-1$	2.4	0.019(20)	0.50(3)	0.67(5)	0.325(19)	32.2
72.414933	DCN	$J = 1-0, F = 2-1$	2.4	0.013(18)	0.63(3)	0.74(4)	0.53(2)	33.5
72.417028	DCN	$J = 1-0, F = 0-1$	2.4	0.09(4)	0.26(4)	0.51(10)	0.126(18)	36.0
76.117439	C ₄ H	$N = 8-7, J = 17/2-15/2$	11.4	0.08(2)	2.01(16)	0.60(5)	1.26(9)	171.0
76.156028	C ₄ H	$N = 8-7, J = 15/2-13/2$	11.4	0.090(7)	1.91(5)	0.575(18)	1.19(3)	54.5
76.198726	l-C ₃ H	$^2\Pi_{3/2}, J = 7/2-5/2,$ $F = 4-3, e$	5.4	0.11(2)	0.56(4)	0.58(5)	0.36(2)	43.6
76.199928	l-C ₃ H	$^2\Pi_{3/2}, J = 7/2-5/2,$ $F = 3-2, e$	5.4	0.13(2)	0.51(5)	0.47(5)	0.24(2)	42.5
76.204182	l-C ₃ H	$^2\Pi_{3/2}, J = 7/2-5/2,$ $F = 4-3, f$	5.4	0.031(20)	0.59(4)	0.55(5)	0.31(2)	44.7
76.205103	l-C ₃ H	$^2\Pi_{3/2}, J = 7/2-5/2,$ $F = 3-2, f$	5.4	0.08(3)	0.42(4)	0.60(7)	0.29(2)	43.0
76.305700	DNC	1-0	2.5	0.014(13)	1.75(5)	0.96(3)	1.84(4)	55.6
77.100041	c-C ₃ H ₂	5 _{3,2} -5 _{2,3}	31.1	0.18(2)	0.202(11)	0.78(5)	0.168(8)	13.9
77.107760	N ₂ D ⁺	$N = 1-0, J = 1/2-1/2,$ $F = 2-2$	2.6	0.22(3)	0.038(4) [†]	0.58(7)	0.022(13)	13.1
77.109315	N ₂ D ⁺	$N = 1-0, J = 3/2-1/2,$ $F = 2-1$	2.6	0.22(3)	0.038(4) [†]	0.58(7)	0.046(13)	13.1

Table 3. (Continued)

Frequency (GHz)	Molecule	Transition	E_u (cm^{-1})	ΔV_{LSR}^* (km s^{-1})	T_{mb}^* (K)	Δv^* (km s^{-1})	$\int T_{\text{mb}} dv$ (K km s^{-1})	rms (mK)
77.109612	N_2D^+	$N = 1-0, J = 3/2-1/2,$ $F = 3-2$	2.6	0.22(3)	0.071(8)	0.58(7)	0.035(13)	13.1
77.109811	N_2D^+	$N = 1-0, J = 3/2-1/2,$ $F = 1-0$	2.6	0.22(3)	0.0170(18) [†]	0.58(7)	0.006(13)	13.1
77.112106	N_2D^+	$N = 1-0, J = 1/2-1/2,$ $F = 1-2$	2.6	0.22(3)	0.0170(18) [†]	0.58(7)	0.020(12)	13.1
77.880542	CH_3CCD	$J_K = 5_0-4_0$	7.8	0.05(9)	0.13(4) [†]	0.6(2)	0.13(2)	43.0
79.099313	CH_3CHO	$4_{1,3}-3_{1,2}, E$	8.2	-0.03(5)	0.079(15)	0.49(10)	0.014(7)	14.1
79.150166	CH_3CHO	$4_{1,3}-3_{1,2}, A^-$	8.2	0.13(7)	0.053(15) [‡]	0.52(17)	0.037(8)	15.7
79.150993	C_3N	$N = 8-7, J = 17/2-15/2$	11.9	0.10(4)	0.098(14)	0.55(9)	0.056(8)	15.5

* Obtained from the Gaussian fit. ΔV_{LSR} represents the velocity shift from V_{LSR} of 5.85 km s^{-1} . Δv represents the FWHM line width.

[†] Less than 3σ detection.

[‡] Less than 4σ detection.

Table 4. Derived column densities, rotation temperatures and optical depths of the lines used for the evaluation*

Molecule	N (cm^{-2})	T_{rot} (K)	τ range [†]	Molecule	N (cm^{-2})	T_{rot} (K)	τ range [†]
SO	$1.1(9) \times 10^{13}$	6(2)	< 0.21	C ₅ H	$5.3(11) \times 10^{11}$	33(26)	< 0.002
CCS	$6(2) \times 10^{12}$	6.1(8)	< 0.066	HC ₃ N	$1.22(6) \times 10^{13}$	25(4)	< 0.16
C ₃ O	$1.8(11) \times 10^{11}$	11(5)	< 0.034	H ¹³ CCCN	$1.4(4) \times 10^{11}$	25 (fix) [‡]	< 0.002
C ₃ N	$6(7) \times 10^{11}$	11(9)	< 0.009	HC ¹³ CCN	$2.4(3) \times 10^{11}$	25 (fix) [‡]	< 0.0028
l-C ₃ H	$3.5(2) \times 10^{12}$	11.5(12)	< 0.067	HCC ¹³ CN	$2.5(8) \times 10^{11}$	25 (fix) [‡]	< 0.003
c-C ₃ H	$1.4(5) \times 10^{13}$	15(6)	< 0.034	DC ₃ N	$4.7(12) \times 10^{11}$	25 (fix) [‡]	< 0.015
c-C ₃ H ₂	$4.4(5) \times 10^{13}$	8.9(6)	< 0.83	HC ₅ N	$2.4(18) \times 10^{12}$	22(7)	< 0.005
c- ¹³ CCCH ₂	$2.18(16) \times 10^{11}$	8.9 (fix) [‡]	< 0.013	CH ₃ CCH	$7.0(6) \times 10^{13}$	14.2(15)	< 0.070
c-CC ¹³ CH ₂	$1.07(16) \times 10^{12}$	8.9 (fix) [‡]	< 0.058	CH ₂ DCCH	$9.83(13) \times 10^{12}$	14.2 (fix) [‡]	< 0.008
c-C ₃ HD	$1.9(2) \times 10^{12}$	8.9 (fix) [‡]	< 0.11	CH ₃ OH	$2.3(10) \times 10^{13}$	13(8)	< 0.030
c-C ₃ D ₂	$2.2(8) \times 10^{11}$	8.9 (fix) [‡]	0.006	CH ₃ CN	$2.54(15) \times 10^{11}$	21(2)	< 0.005
l-C ₃ H ₂	$1.23(7) \times 10^{12}$	9.2(8)	< 0.049	CH ₂ CN	$2.2(4) \times 10^{12}$	8.6(19)	< 0.010
C ₄ H	$2.32(12) \times 10^{14}$	12.3(4)	< 0.26	CH ₂ CO	$7(3) \times 10^{12}$	27(23)	< 0.008
C ₄ H ₂	$1.9(2) \times 10^{12}$	12.7(11)	< 0.017	HCCCHO	$2.4(3) \times 10^{12}$	16(13)	< 0.004

* The numbers in parentheses represent the errors in units of last significant digits.

[†] The range of the optical depths of the lines used in the analysis.

[‡] The rotation temperature is assumed to be the same as that derived for the normal species.

Table 5. Derived column densities and optical depths of the lines used for the evaluation*

Molecule	$T_{\text{rot}} = 10 \text{ K}$		$T_{\text{rot}} = 15 \text{ K}$		Molecule	$T_{\text{rot}} = 10 \text{ K}$		$T_{\text{rot}} = 15 \text{ K}$	
	$N \text{ (cm}^{-2}\text{)}$	$\tau \text{ range}$	$N \text{ (cm}^{-2}\text{)}$	$\tau \text{ range}$		$N \text{ (cm}^{-2}\text{)}$	$\tau \text{ range}$	$N \text{ (cm}^{-2}\text{)}$	$\tau \text{ range}$
CO	$(4.4(16) \times 10^{18})^\dagger$	–	$(4.0(10) \times 10^{18})^\dagger$	–	DCN	$2.6(5) \times 10^{12}$	< 0.11	$3.1(6) \times 10^{12}$	< 0.061
^{13}CO	$(5.1(13) \times 10^{16})^\ddagger$	–	$(5.9(15) \times 10^{16})^\ddagger$	–	N_2H^+	$5.8(3) \times 10^{12}$	< 0.20	$6.6(13) \times 10^{12}$	< 0.11
C^{18}O	$8(3) \times 10^{15}$	1.07	$7.1(18) \times 10^{15}$	0.48	N_2D^+	$3.0(6) \times 10^{11}$	< 0.010	$3.6(7) \times 10^{11}$	< 0.006
C^{17}O	$1.90(4) \times 10^{15}$	< 0.16	$2.1(4) \times 10^{15}$	< 0.088	CCH	$1.4(3) \times 10^{15}$	< 0.25	$1.5(3) \times 10^{15}$	< 0.14
$^{13}\text{C}^{18}\text{O}$	$9(2) \times 10^{13}$	0.011	$1.1(3) \times 10^{14}$	0.007	^{13}CCH	$6.3(10) \times 10^{12}$	< 0.007	$7.5(15) \times 10^{12}$	< 0.004
CS	$(3.1(6) \times 10^{13})^\S$	–	$(3.4(7) \times 10^{13})^\S$	–	C^{13}CH	$9.4(19) \times 10^{12}$	< 0.009	$1.1(2) \times 10^{13}$	< 0.005
C^{34}S	$1.4(3) \times 10^{12}$	0.025	$1.6(3) \times 10^{12}$	0.014	CCD	$4.7(3) \times 10^{13}$	< 0.092	$5.6(11) \times 10^{13}$	< 0.053
C^{33}S	$2.1(6) \times 10^{11}$	0.007	$2.3(7) \times 10^{11}$	0.004	HCS ⁺	$3.8(8) \times 10^{11}$	0.008	$4.3(9) \times 10^{11}$	0.005
CN	$2.3(3) \times 10^{14}$	< 0.090	$2.6(5) \times 10^{14}$	< 0.051	HCO	$5.3(11) \times 10^{12}$	< 0.023	$7.2(14) \times 10^{12}$	< 0.013
^{13}CN	$3.7(7) \times 10^{12}$	< 0.018	$4.2(8) \times 10^{12}$	< 0.011	c- $\text{H}_2\text{C}_3\text{O}$	$5.4(16) \times 10^{11}$	< 0.009	$4.5(11) \times 10^{11}$	< 0.005
C^{15}N	$10(3) \times 10^{11}$	0.007	$1.1(2) \times 10^{12}$	0.004	H_2CO	$(1.2(3) \times 10^{14})^{\#,**}$	–	$(1.6(4) \times 10^{14})^{\#,**}$	–
HCO^+	$(2.9(7) \times 10^{14})^\#$	–	$(3.1(7) \times 10^{14})^\#$	–	H_2^{13}CO	$2.0(5) \times 10^{12}$	0.025	$2.6(7) \times 10^{12}$	0.015
H^{13}CO^+	$4.8(12) \times 10^{12}$	0.47	$5.2(12) \times 10^{12}$	0.25	D_2CO	$1.8(7) \times 10^{12}$	< 0.046	$2.2(8) \times 10^{12}$	< 0.026
HC^{18}O^+	$4.8(10) \times 10^{11}$	0.050	$5.7(11) \times 10^{11}$	0.029	CH_3CHO	$1.6(3) \times 10^{12}$	< 0.009	$1.6(4) \times 10^{12}$	< 0.005
DCO^+	$(1.5(3) \times 10^{13})^\#$	–	$(1.8(4) \times 10^{13})^\#$	–	H_2CS	$2.7(5) \times 10^{12}$	< 0.023	$2.8(5) \times 10^{12}$	< 0.013
D^{13}CO^+	$2.4(6) \times 10^{11}$	0.040	$3.0(7) \times 10^{11}$	0.023	HDCS	$6.3(18) \times 10^{11}$	0.008	$8(2) \times 10^{11}$	0.004
HNC	$(1.0(2) \times 10^{14})^\#$	–	$(1.2(3) \times 10^{14})^\#$	–	HCCNC	$5.2(16) \times 10^{11}$	0.005	$3.1(9) \times 10^{11}$	0.003
HN^{13}C	$1.6(4) \times 10^{12}$	0.092	$1.9(5) \times 10^{12}$	0.052	HNCO	$2.6(5) \times 10^{12}$	< 0.036	$2.6(3) \times 10^{12}$	< 0.023
H^{15}NC	$3.1(7) \times 10^{11}$	0.020	$3.7(8) \times 10^{11}$	0.012	NH_2D	$1.9(17) \times 10^{12}$	0.007	$1.5(14) \times 10^{12}$	0.004
DNC	$4.5(11) \times 10^{12}$	0.29	$5.2(11) \times 10^{12}$	0.16	OCS	< 2.3×10^{12}	–	< 1.9×10^{12}	–
HCN	$(5.5(11) \times 10^{13})^\#$	–	$(6.5(12) \times 10^{13})^\#$	–	HCOOCH_3	< 1.3×10^{13}	–	< 9.7×10^{12}	–
H^{13}CN	$9.1(18) \times 10^{11}$	< 0.028	$1.1(2) \times 10^{12}$	< 0.016	$(\text{CH}_3)_2\text{O}$	< 4.1×10^{12}	–	< 5.0×10^{12}	–
HC^{15}N	$2.2(5) \times 10^{11}$	0.015	$2.6(5) \times 10^{11}$	0.009					

* The numbers in parentheses represent the errors in units of last significant digits.

† The spectral line of C^{18}O is used for evaluation of the column density of CO, where the $^{16}\text{O}/^{18}\text{O}$ ratio is assumed to be 560 (Wilson & Rood 1994).

‡ The spectral line of $^{13}\text{C}^{18}\text{O}$ is used for evaluation of the column density of C^{18}O , where the $^{16}\text{O}/^{18}\text{O}$ ratio is assumed to be 560 (Wilson & Rood 1994).

§ The spectral lines of the ^{34}S species are used for evaluation of the column density, where the $^{32}\text{S}/^{34}\text{S}$ ratio is assumed to be 22 (Chin et al. 1996).

|| Two optically-thin hyperfine components are used for evaluation of the column density.

The spectral lines of the ^{13}C species are used for evaluation of the column density, where the $^{12}\text{C}/^{13}\text{C}$ ratio is assumed to be 60 (Lucas & Liszt 1998).

** No lines are observed in this survey.

Table 6. Comparison of column densities derived by the non-LTE and LTE analysis *

Molecule	N (cm^{-2})	
	Non-LTE [†]	LTE [‡]
C ¹⁸ O	$(0.7\text{--}1.0)\times 10^{16}$	$7.1(18)\times 10^{15}$
CS	$(1.4\text{--}2.0)\times 10^{13}$	$3.4(7)\times 10^{13}$
SO	$(4.0\text{--}6.5)\times 10^{12}$	$1.1(9)\times 10^{13}$
HC ¹⁸ O ⁺	$(3.5\text{--}7.5)\times 10^{11}$	$5.7(11)\times 10^{11}$
HC ¹⁵ N	$(1.5\text{--}2.6)\times 10^{11}$	$2.6(5)\times 10^{11}$
H ¹³ CN	$(0.7\text{--}1.4)\times 10^{11}$	$1.1(2)\times 10^{11}$
CCH	$(1.2\text{--}2.2)\times 10^{15}$	$1.5(3)\times 10^{15}$
CH ₃ OH [#]	$(2.3\text{--}3.4)\times 10^{13}$	$2.3(10)\times 10^{13}$

* The H₂ density and the kinetic temperature are set to be $3\times 10^5\text{--}3\times 10^6\text{ cm}^{-3}$ and 10–30 K, respectively.

[†] Calculated with RADEX (van der Tak et al. 2007). The collisional rate coefficients are taken from Yang et al. (2010) for C¹⁸O, Lique, Spielfiedel, & Cernicharo (2006) for CS and SO, Flower (1999) for HC¹⁸O⁺, Green & Thaddeus (1974) for HC¹⁵N and H¹³CN, Spielfiedel et al. (2012) for CCH, and Rabli & Flower (2010) for CH₃OH.

[‡] The numbers in parentheses represent the errors in units of last significant digits. For molecules listed in Table 5, the column density derived with $T_{\text{rot}} = 15$ K is shown.

^{||} Two optically-thin hyperfine components are used.

[#] The H₂ density is restricted to $3\times 10^5\text{--}1\times 10^6\text{ cm}^{-3}$ to reproduce the absorption feature of $3_{1,3}\text{--}4_{1,4}, A^+$ line.

Table 7. Fractal abundance relative to H₂, calculated from Tables 4 and 5.*

Molecule	X	Molecule	X	Molecule	X
CO	$(4.8(16) \times 10^{-5})^\dagger$	N ₂ H ⁺	$8(2) \times 10^{-11}$	HCC ¹³ CN	$3.0(11) \times 10^{-12}$
¹³ CO	$(7(2) \times 10^{-7})^\ddagger$	N ₂ D ⁺	$4.4(12) \times 10^{-12}$	DC ₃ N	$5.7(18) \times 10^{-12}$
C ¹⁸ O	$9(3) \times 10^{-8}$	CCH	$1.9(5) \times 10^{-8}$	HC ₅ N	$3(2) \times 10^{-11}$
¹³ C ¹⁸ O	$1.3(4) \times 10^{-9}$	¹³ CCH	$9(3) \times 10^{-11}$	c-H ₂ C ₃ O	$5.5(17) \times 10^{-12}$
CS	$(4.2(12) \times 10^{-10})^\#$	C ¹³ CH	$1.4(4) \times 10^{-10}$	H ₂ CO	$(1.9(6) \times 10^{-9})^\#,**$
C ³⁴ S	$1.9(5) \times 10^{-11}$	CCD	$6.9(19) \times 10^{-10}$	H ₂ ¹³ CO	$3.1(10) \times 10^{-11}$
C ³³ S	$2.8(10) \times 10^{-12}$	HCS ⁺	$5.2(15) \times 10^{-12}$	D ₂ CO	$2.7(11) \times 10^{-11}$
CN	$3.2(9) \times 10^{-9}$	HCO	$9(2) \times 10^{-11}$	H ₂ CS	$3.5(9) \times 10^{-11}$
¹³ CN	$5.2(14) \times 10^{-11}$	CCS	$7(3) \times 10^{-11}$	HDCS	$10(3) \times 10^{-12}$
C ¹⁵ N	$1.4(4) \times 10^{-11}$	C ₃ O	$2.2(14) \times 10^{-12}$	NH ₂ D	$1.8(17) \times 10^{-11}$
SO	$1.3(11) \times 10^{-10}$	l-C ₃ H	$4.3(9) \times 10^{-11}$	HCCNC	$3.8(14) \times 10^{-12}$
HCO ⁺	$(3.8(11) \times 10^{-9})^\#$	c-C ₃ H	$1.7(7) \times 10^{-10}$	HNCO	$3.2(7) \times 10^{-11}$
H ¹³ CO ⁺	$6.3(19) \times 10^{-11}$	c-C ₃ H ₂	$5.3(12) \times 10^{-10}$	CH ₃ CHO	$2.0(7) \times 10^{-11}$
HC ¹⁸ O ⁺	$6.9(19) \times 10^{-12}$	c- ¹³ CCCH ₂	$2.6(6) \times 10^{-12}$	CH ₃ CCH	$8.5(18) \times 10^{-10}$
DCO ⁺	$(2.2(7) \times 10^{-10})^\#$	c-CC ¹³ CH ₂	$1.3(3) \times 10^{-11}$	CH ₂ DCCH	$1.2(2) \times 10^{-10}$
D ¹³ CO ⁺	$3.6(11) \times 10^{-12}$	c-C ₃ HD	$2.4(5) \times 10^{-11}$	CH ₃ OH	$2.8(13) \times 10^{-10}$
HNC	$(1.4(4) \times 10^{-9})^\#$	c-C ₃ D ₂	$2.7(11) \times 10^{-12}$	CH ₃ CN	$3.1(6) \times 10^{-12}$
HN ¹³ C	$2.3(7) \times 10^{-11}$	l-C ₃ H ₂	$1.5(3) \times 10^{-11}$	CH ₂ CN	$2.6(7) \times 10^{-11}$
H ¹⁵ NC	$4.5(13) \times 10^{-12}$	C ₄ H	$2.8(6) \times 10^{-9}$	CH ₂ CO	$9(4) \times 10^{-11}$
DNC	$6.3(19) \times 10^{-11}$	C ₄ H ₂	$2.4(5) \times 10^{-11}$	HCCCHO	$3.0(7) \times 10^{-11}$
HCN	$(8(2) \times 10^{-10})^\#$	C ₅ H	$6.4(18) \times 10^{-12}$	OCS	$< 2.3 \times 10^{-11}$
H ¹³ CN	$1.3(4) \times 10^{-11}$	HC ₃ N	$1.5(3) \times 10^{-10}$	HCOOCH ₃	$< 1.2 \times 10^{-10}$
HC ¹⁵ N	$3.1(9) \times 10^{-12}$	H ¹³ CCCN	$1.8(6) \times 10^{-12}$	(CH ₃) ₂ O	$< 6.1 \times 10^{-11}$
DCN	$3.8(11) \times 10^{-11}$	HC ¹³ CCN	$2.9(7) \times 10^{-12}$		

* The numbers in parentheses represent the errors in units of last significant digits. The column density of H₂ is evaluated from that of C¹⁷O to be $(8.2 \pm 1.6) \times 10^{22}$ cm⁻². For molecules listed in Table 5, the column density derived with $T_{\text{rot}} = 15$ K is assumed.

†,‡,||, #, ** See the footnotes in Table 5.

Table 8. D/H ratios*

Ratios	This work		Previous works
	Abundance ratio	D/H ratio [†]	Abundance ratio
D ¹³ CO ⁺ /H ¹³ CO ⁺	0.057(19)		0.048 [‡]
N ₂ D ⁺ /N ₂ H ⁺	0.054(15)		0.06(1) [§]
DCN/HCN	0.048(13)		0.037(8) ^{, #}
DNC/HNC	0.045(14)		0.046(4) ^{, **}
CCD/CCH	0.037(10)		–
DC ₃ N/HC ₃ N	0.039(10)		0.0370(7) ^{††}
c-C ₃ HD/c-C ₃ H ₂	0.044(7)	0.022(4)	0.071(23) ^{††}
c-C ₃ D ₂ /c-C ₃ H ₂	0.0050(18)	0.071(13)	–
c-C ₃ D ₂ /c-C ₃ HD	0.11(4)	0.23(8)	–
CH ₂ DCCH/CH ₃ CCH	0.141(12)	0.047(4)	–
HDCS/H ₂ CS	0.29(10)	0.14(5)	–
D ₂ CO/H ₂ CO	0.014(6)	0.12(3)	0.016(5) ^{§,} , 0.44 ^{+0.60} _{-0.29} ^{§§}

* The numbers in parentheses represent the errors in units of the last significant digits.

[†] The D/H ratio means the abundance ratio for the single deuteration, which is corrected for the statistical weight caused by molecular symmetry (Persson et al. 2018).

[‡] The [DCO⁺]/[HCO⁺] ratio reported by Jørgensen, Schöier & van Dishoeck (2004), where the column density of HCO⁺ is derived from the H¹³CO⁺ lines by assuming the ¹²C/¹³C ratio of 60.

[§] Roberts & Millar (2007)

^{||} The column density of the normal species is derived from the ¹³C species, where the ¹²C/¹³C ratio is assumed to be 60.

[#] Roberts et al. (2002)

^{**} Hirota, Ikeda & Yamamoto (2001)

^{††} Araki et al. (2016)

^{††} Sakai et al. (2009b)

^{§§} Parise et al. (2006)

Table 9. $^{12}\text{C}/^{13}\text{C}$ ratios*

Ratios	This work	Previous works
$[\text{C}^{18}\text{O}]/[^{13}\text{C}^{18}\text{O}]$	70(20)	–
$[\text{CN}]/[^{13}\text{CN}]$	61(17)	–
$[\text{CCH}]/[^{13}\text{CCH}]$	210(60)	$> 135^\dagger$
$[\text{CCH}]/[\text{C}^{13}\text{CH}]$	140(40)	$> 80^\dagger$
$[\text{HC}_3\text{N}]/[\text{H}^{13}\text{CCCN}]$	85(22)	$86.4(16)^\ddagger$
$[\text{HC}_3\text{N}]/[\text{HC}^{13}\text{CCN}]$	51(7)	$85.4(17)^\ddagger$
$[\text{HC}_3\text{N}]/[\text{HCC}^{13}\text{CN}]$	49(15)	$64.2(11)^\ddagger$
$[\text{c-C}_3\text{H}_2]/[\text{c-}^{13}\text{CCCH}_2]$	200(30)	$310(80)^\S$
$[\text{c-C}_3\text{H}_2]/[\text{c-CC}^{13}\text{CH}_2]$	41(8)	$61(11)^\S$

* The numbers in parentheses represent the errors in units of the last significant digits.

† Sakai et al. (2010b)

‡ Araki et al. (2016)

§ Yoshida et al. (2015)

Table 10. $^{14}\text{N}/^{15}\text{N}$ ratios*

Ratios	L1527 [†]	B1 [‡]	OMC-2 FIR4 [§]
$[\text{CN}]/[\text{C}^{15}\text{N}]$	230(80)	290_{-80}^{+160}	270(60)
$[\text{HCN}]/[\text{HC}^{15}\text{N}]$	250(80)	330_{-50}^{+60}	270(50)
$[\text{HNC}]/[\text{H}^{15}\text{NC}]$	300(100)	225_{-45}^{+75}	290(50)

* The numbers in parentheses represent the errors in units of the last significant digits.

[†] This work

[‡] Daniel et al. (2013)

[§] Kahane et al. (2018)

^{||} The column density of the normal species are derived from the ^{13}C species, where the $^{12}\text{C}/^{13}\text{C}$ ratio is assumed to be 60.

Table 11. Column density ratios of organic species relative to CH₃OH*

Species	L1527	TMC-1 (CP [†])	TMC-1 (MP [‡])	IRAS16293-2422
H ₂ CO	7(3)	–	–	1.1(8)
CH ₃ CHO	0.08(5)	0.046(16) [§]	0.09(4) [§]	0.06(3)
CH ₂ CO	0.31(19)	0.20(7)	0.09(4)	–
c-H ₂ C ₃ O	0.020(10)	0.011(2)	–	–
HCOOCH ₃	< 0.42 (3 σ)	–	0.026(11) [§]	1.2(4)
(CH ₃) ₂ O	< 0.22 (3 σ)	< 0.13 [§]	0.031(17) [§]	11(6)

* The numbers in parentheses represent the errors in units of the last significant digits.

The column densities are taken from Soma et al. (2018) for TMC-1. The beam-averaged column densities of CH₃OH and other COMs (CH₃CHO, HCOOCH₃, and (CH₃)₂O) in IRAS16293-2422 are evaluated by the least-squares fit of the observation data reported by Caux et al. (2011) and Cazaux et al. (2003), respectively, under the assumption of the LTE condition.

[†] Cyanopolyne Peak

[‡] Methanol Peak

[§] The column density is the sum of two velocity components.

Table 12. Comparison of rest frequencies of the CCD $N = 1-0$ transition between our observation and calculation*

Transition	Rest frequency (GHz)	
	Observation [†]	Calculation [‡]
$N = 1-0, J = 3/2-1/2, F = 3/2-3/2$	72.101780(10)	72.1017155
$N = 1-0, J = 3/2-1/2, F = 5/2-3/2$	72.1077085(3)	72.1077000
$N = 1-0, J = 3/2-1/2, F = 1/2-1/2$	72.1090173(7)	72.1091138
$N = 1-0, J = 3/2-1/2, F = 3/2-1/2$	72.112277(5)	72.1123994
$N = 1-0, J = 1/2-1/2, F = 3/2-3/2$	72.187710(6)	72.1877041
$N = 1-0, J = 1/2-1/2, F = 1/2-3/2$	72.189729(15)	72.1895050
$N = 1-0, J = 1/2-1/2, F = 3/2-1/2$	72.198193(12)	72.1983880

* The numbers in parentheses represent the errors in units of last significant digits.

[†] V_{LSR} of 5.85 km s^{-1} is assumed.

[‡] Taken from CDMS.

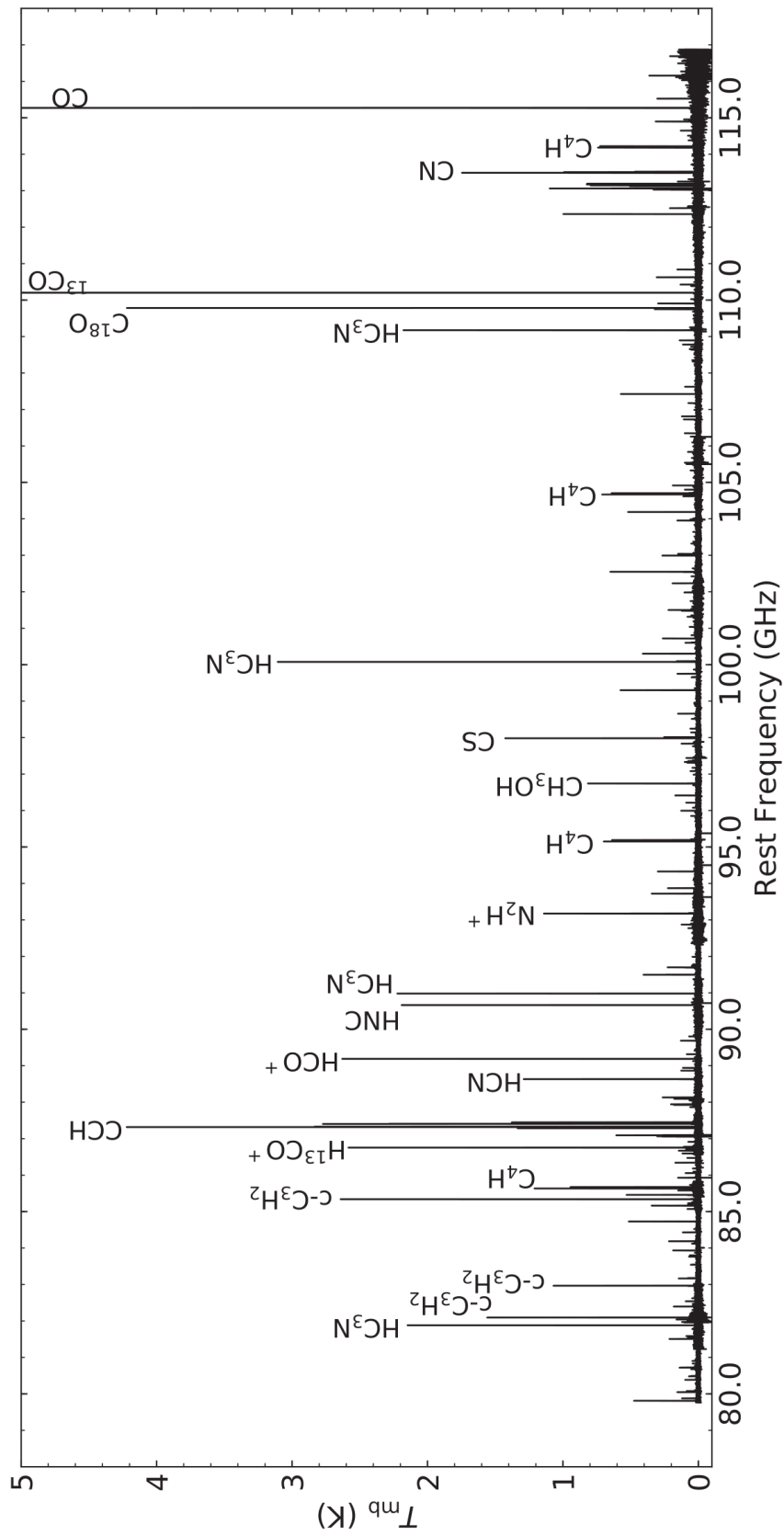


Fig. 1. The overall spectrum of L1527 in the 3 mm band. Lines of some representative molecular species are indicated.

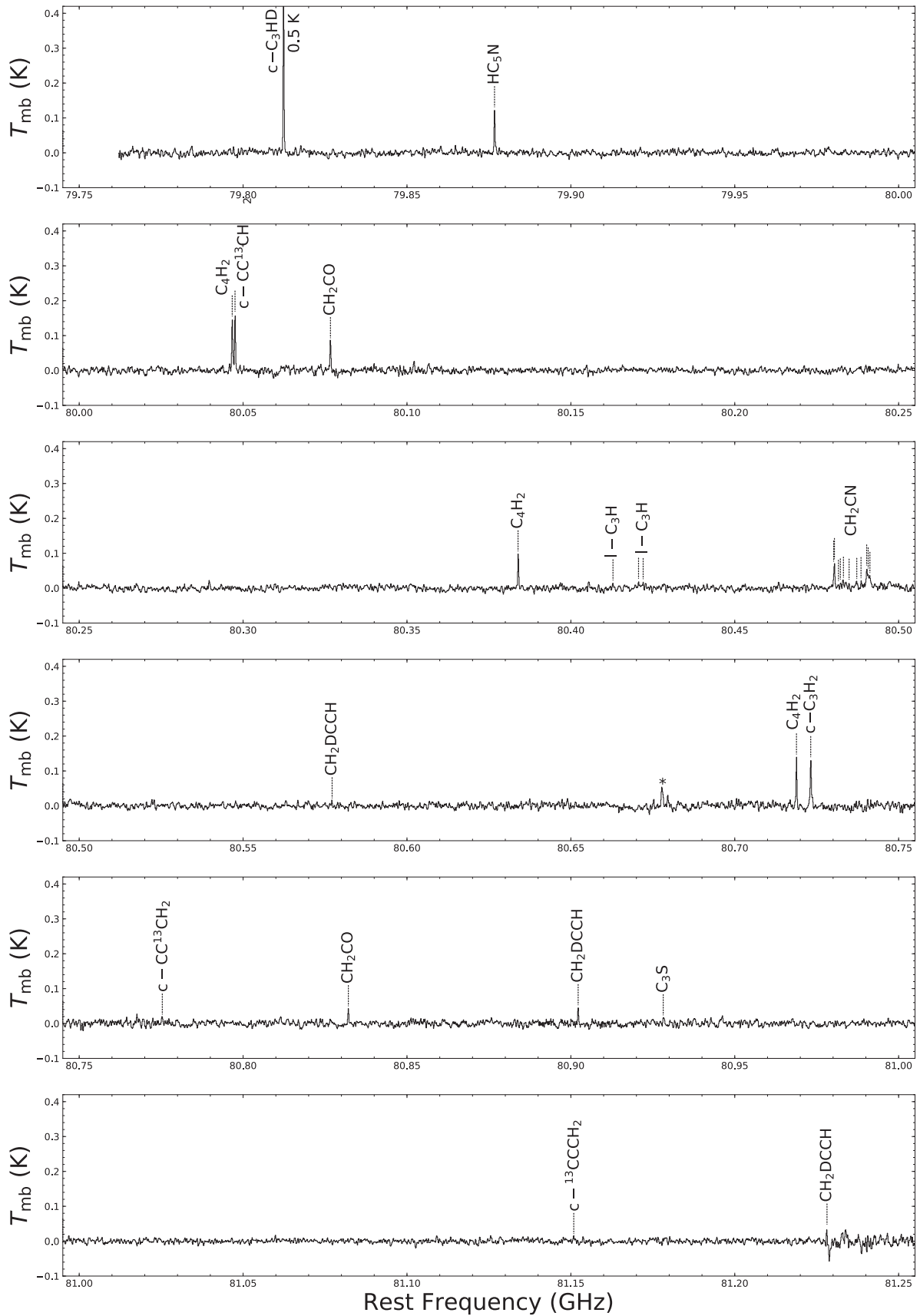


Fig. 2. Spectrum of L1527 in the 3 mm band. Spurious lines are indicated with asterisks.

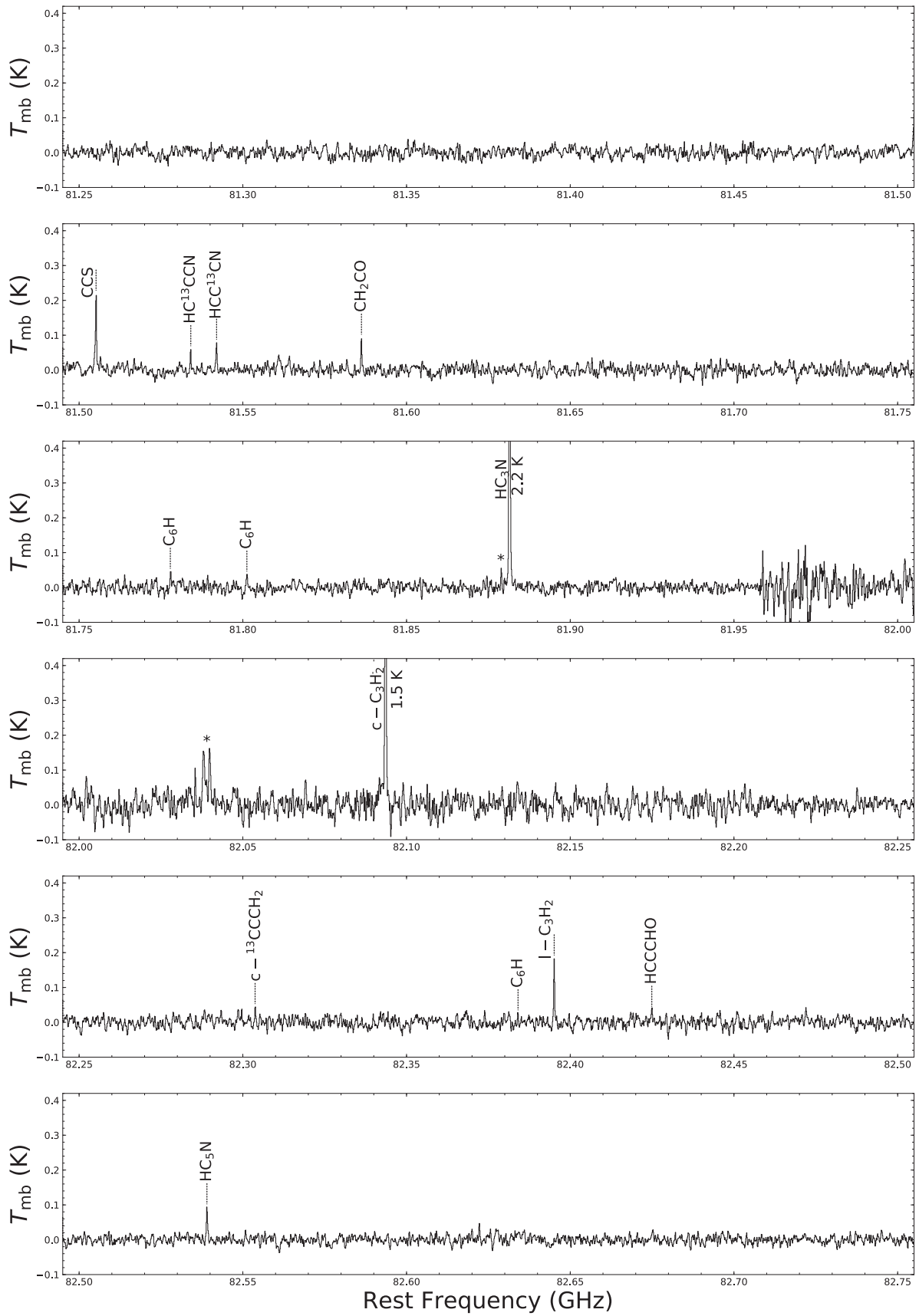


Fig. 2. (Continued.)
49

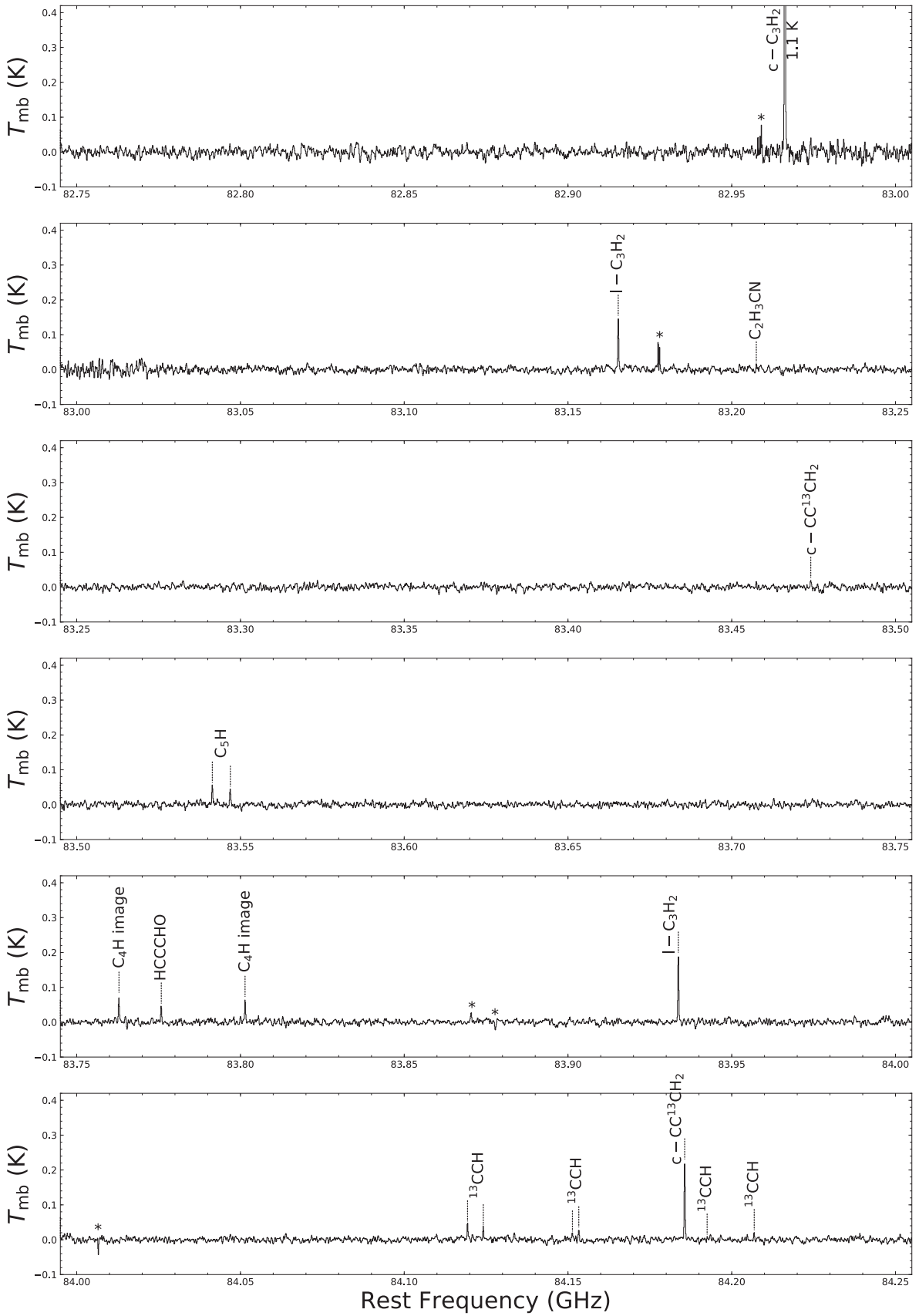


Fig. 2. (Continued.)
50

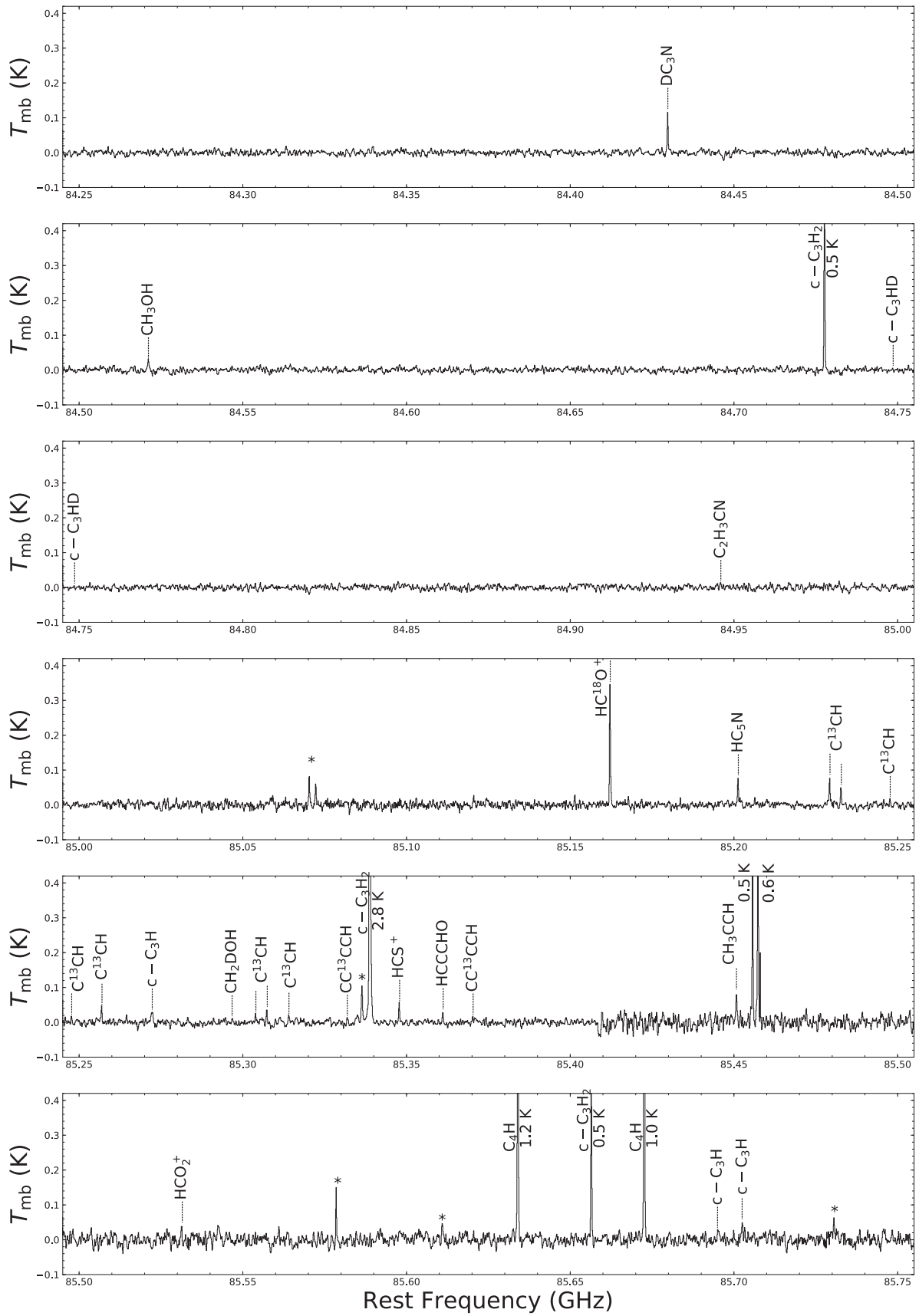


Fig. 2. (Continued.)
51

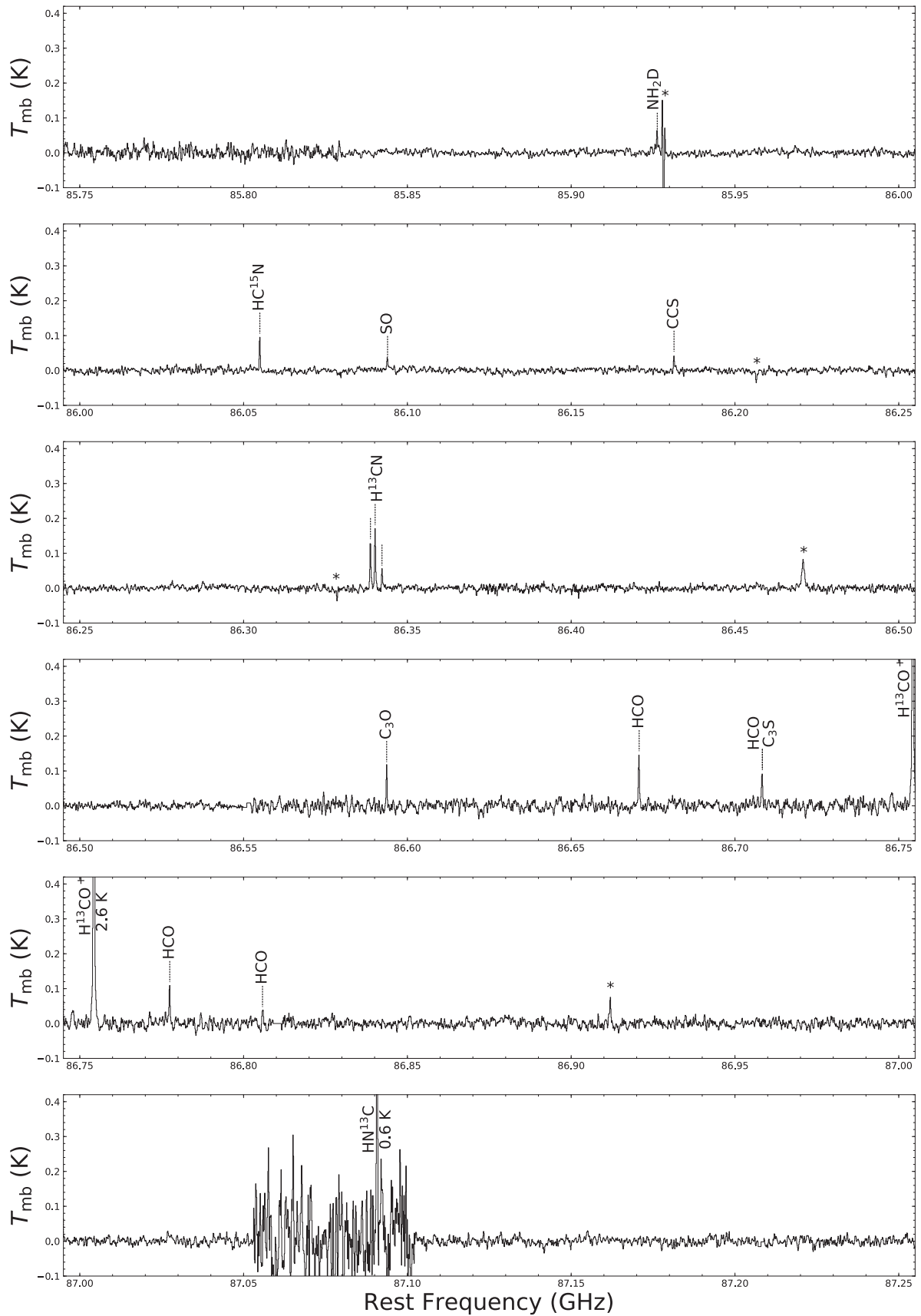


Fig. 2. (Continued.)
52

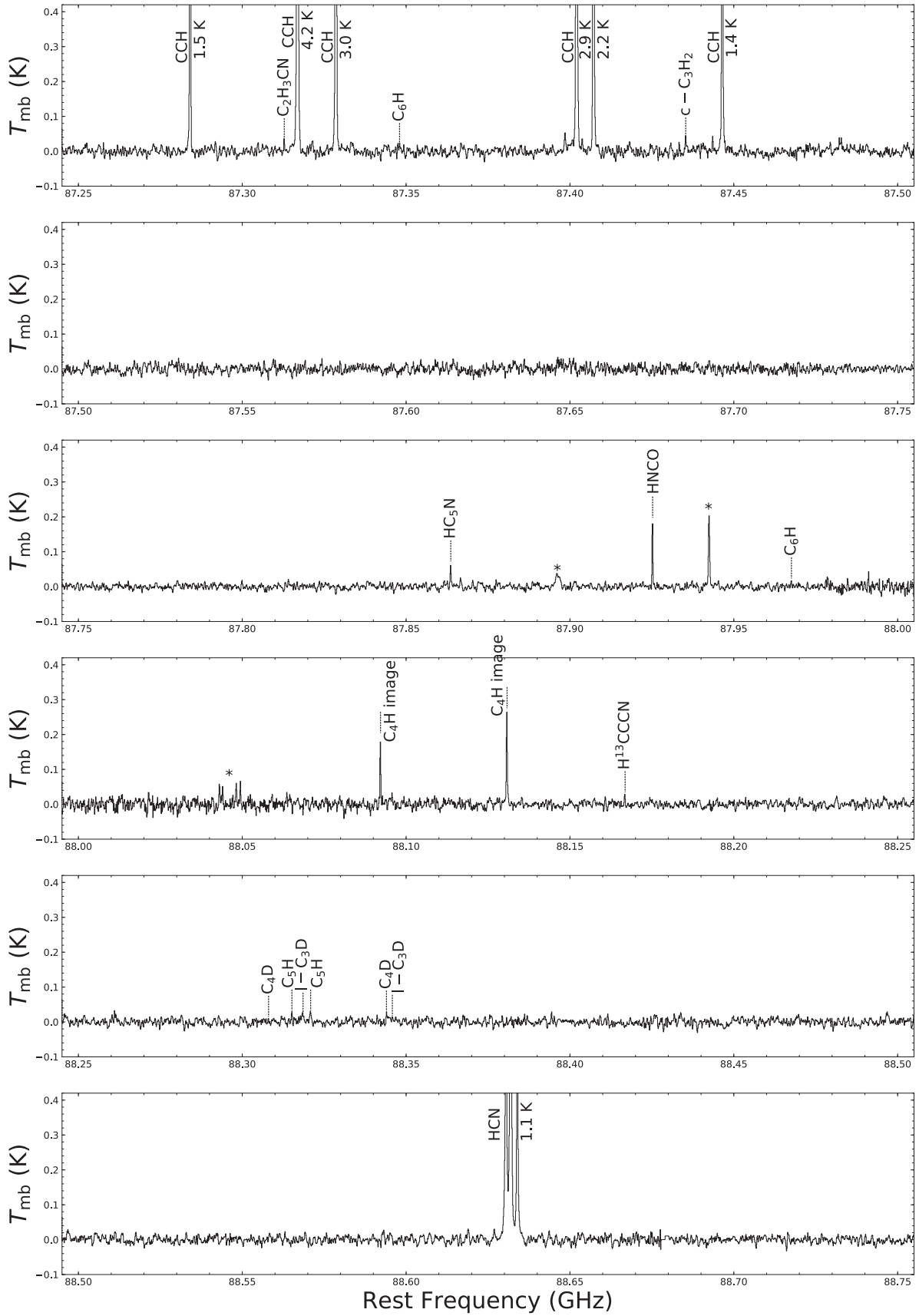


Fig. 2. (Continued.)

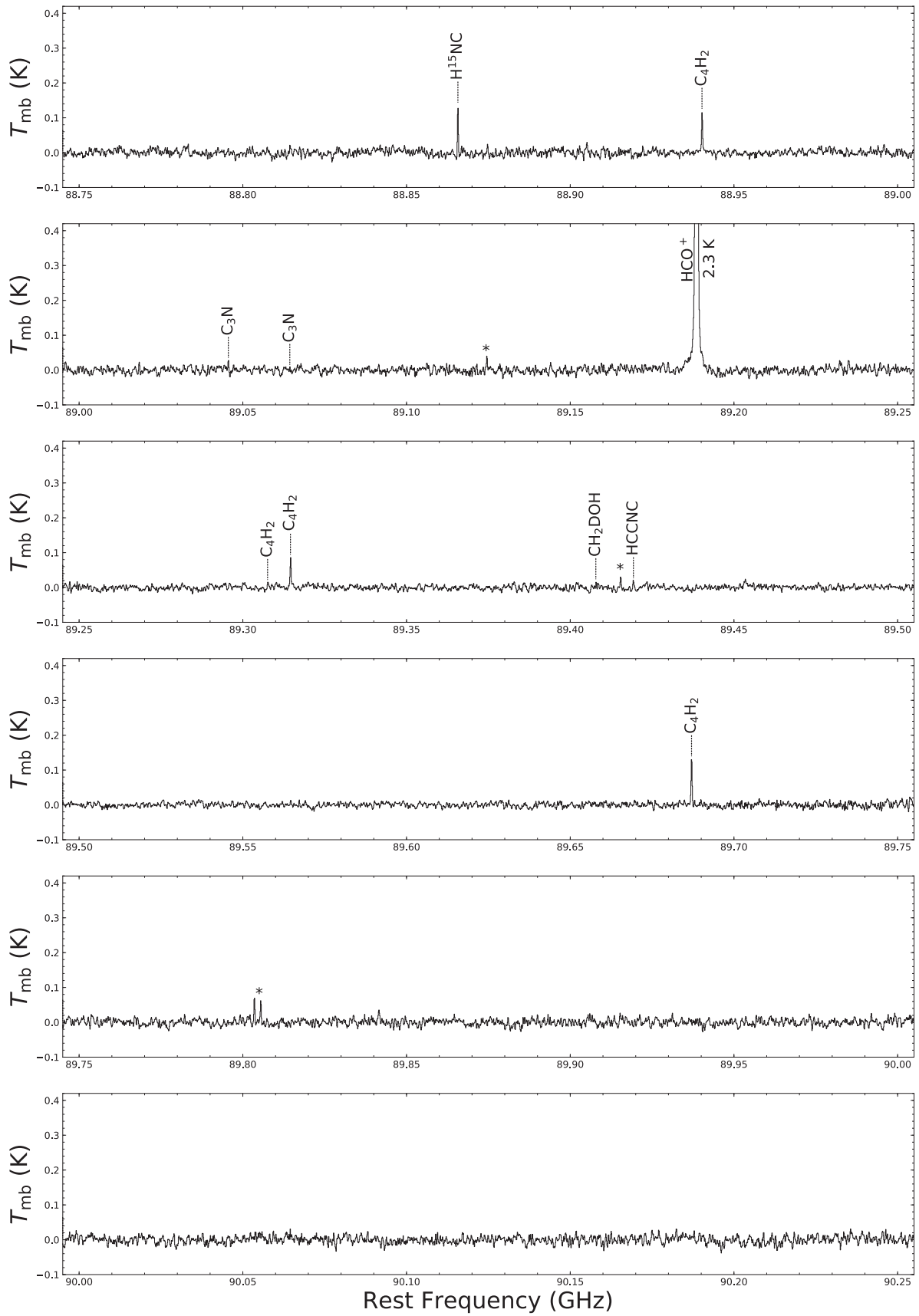


Fig. 2. (Continued.)

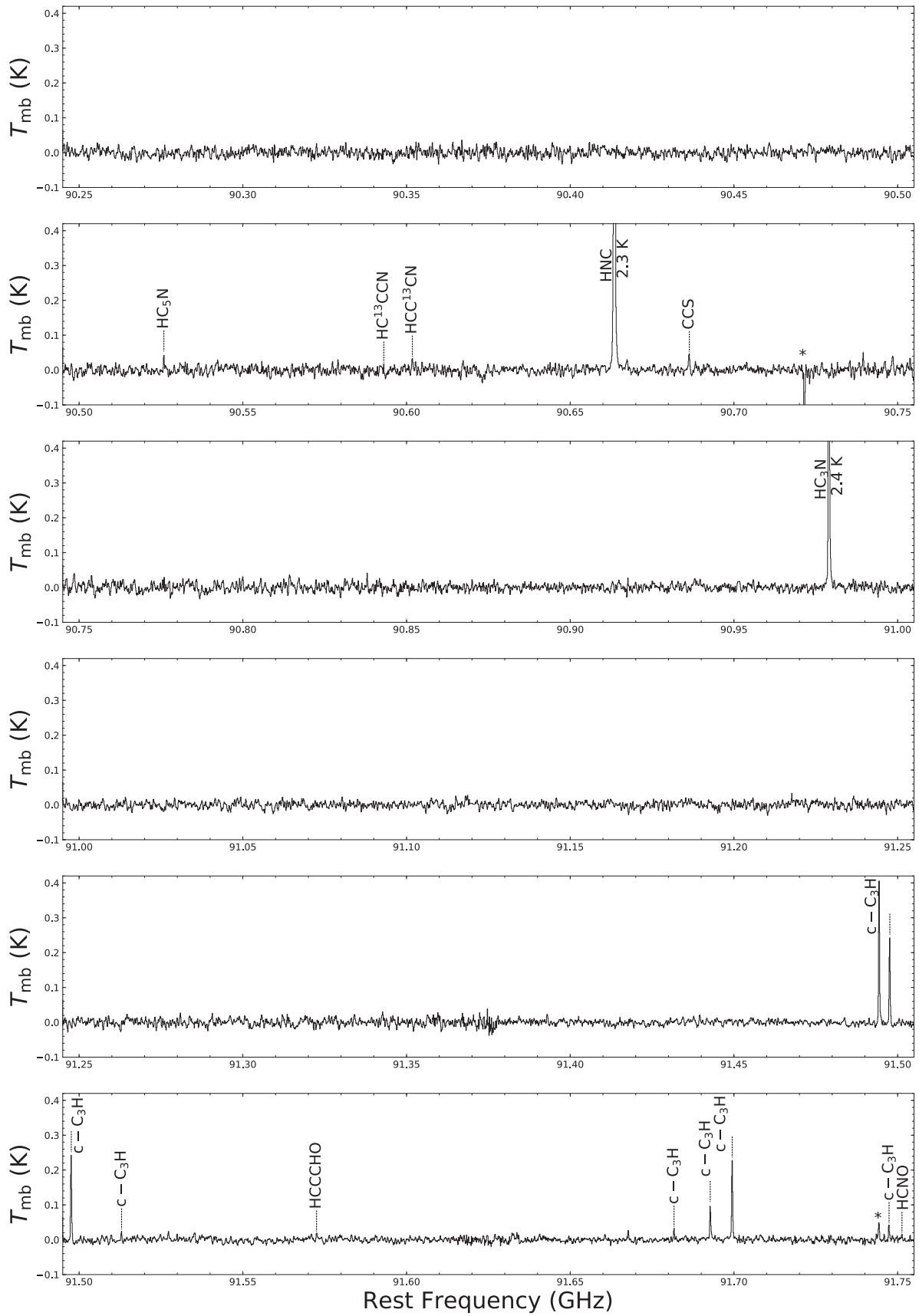


Fig. 2. (Continued.)
55

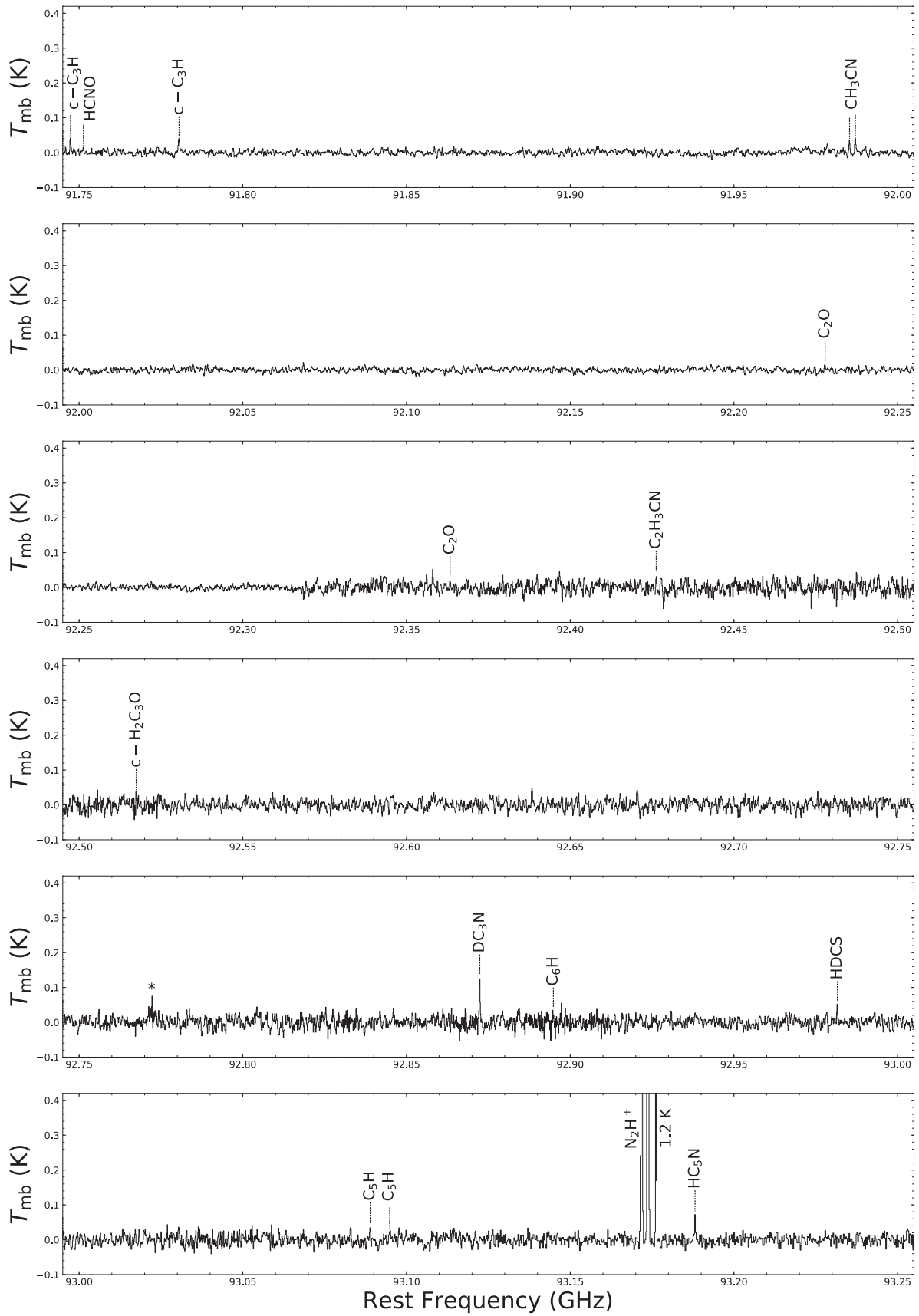


Fig. 2. (Continued.)
56

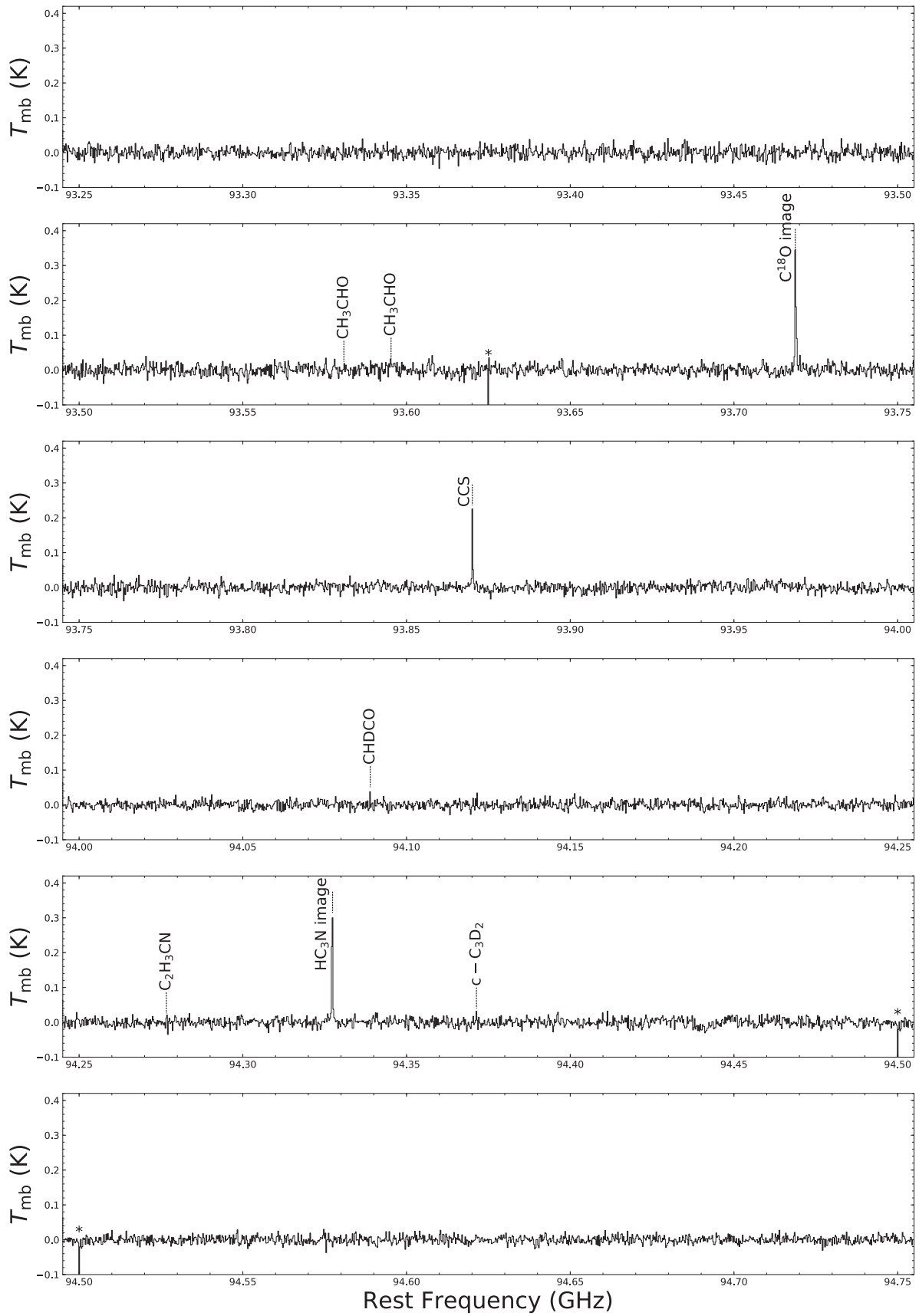


Fig. 2. (Continued.)
57

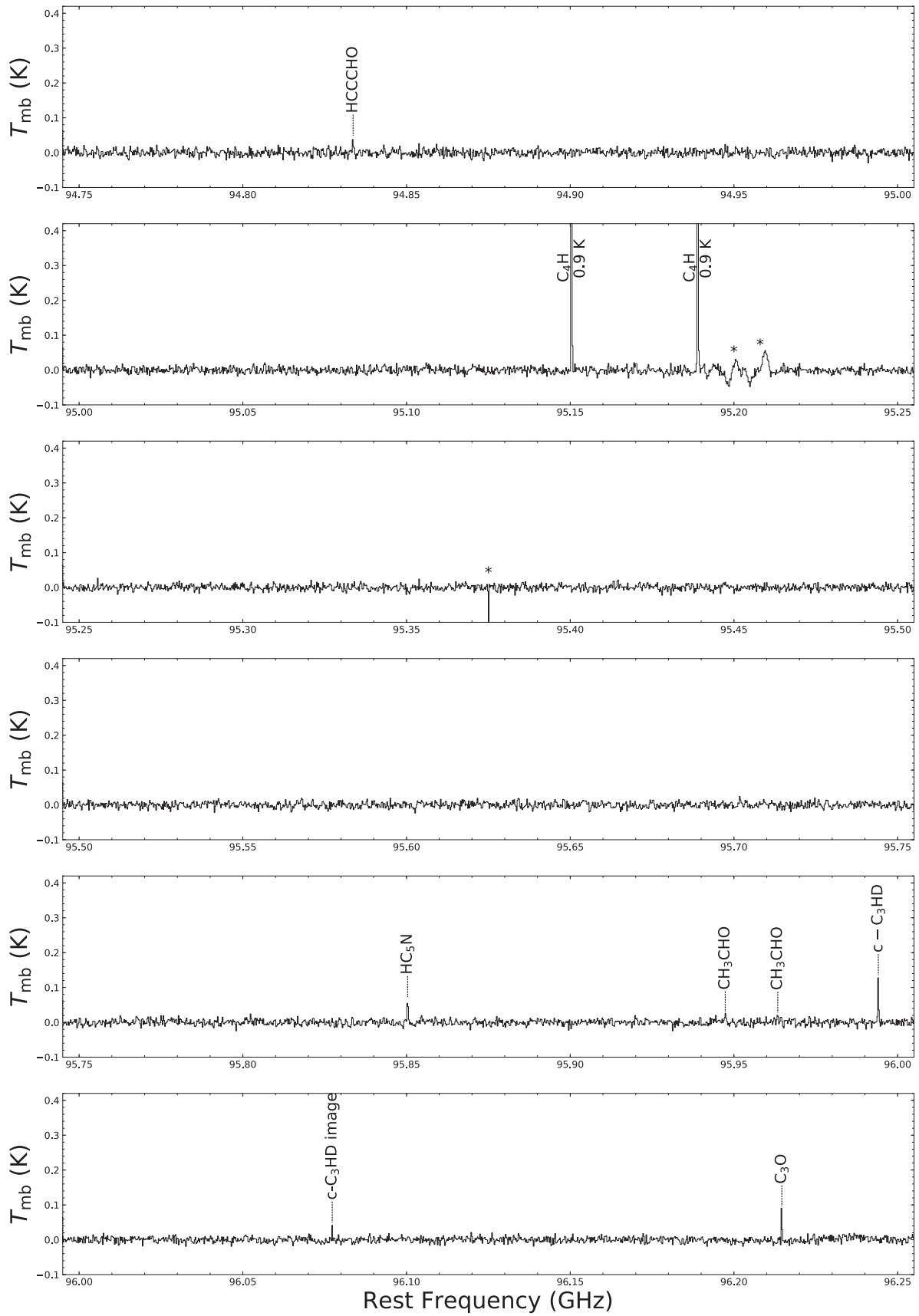


Fig. 2. (Continued.)
58

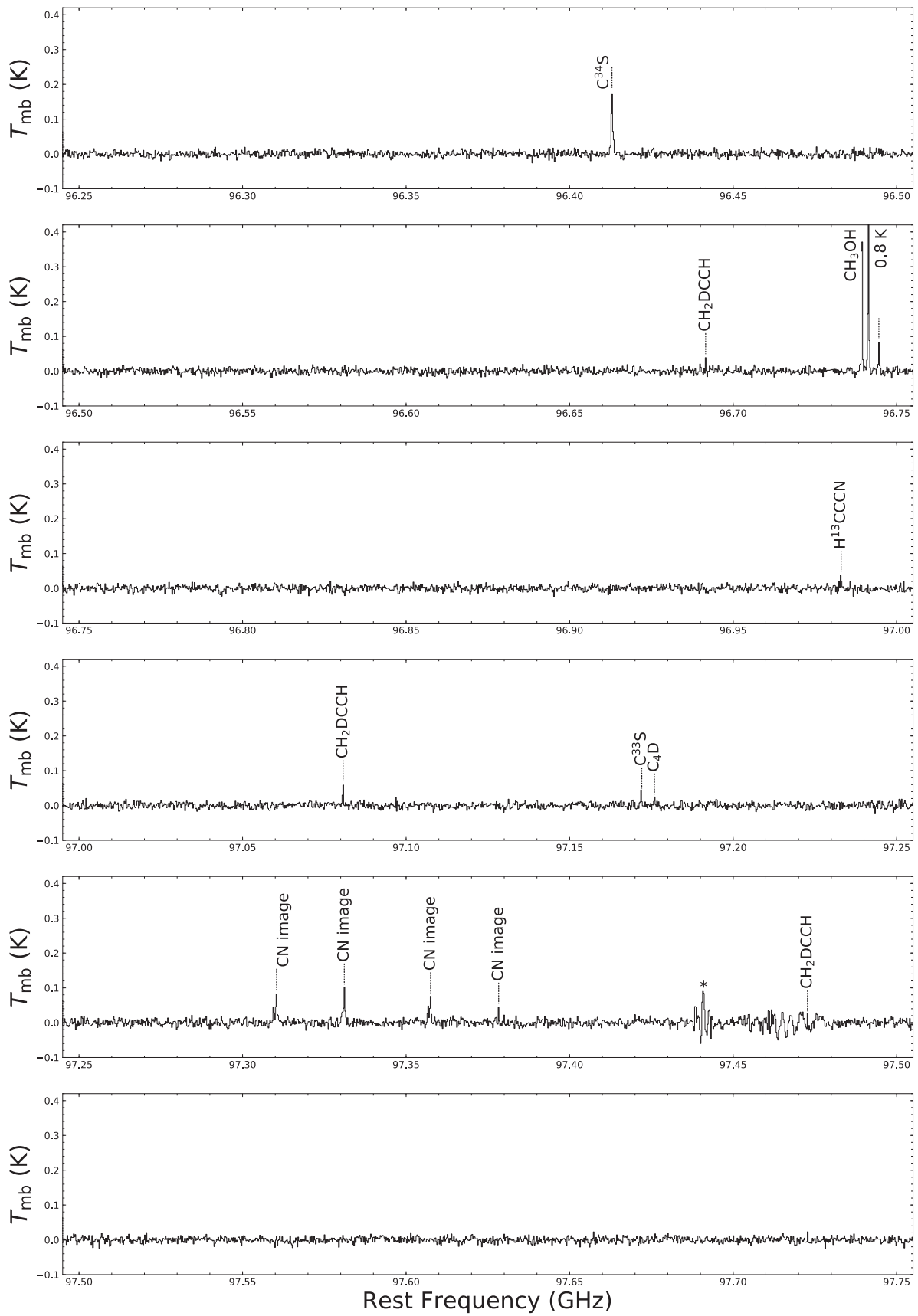


Fig. 2. (Continued.)
59

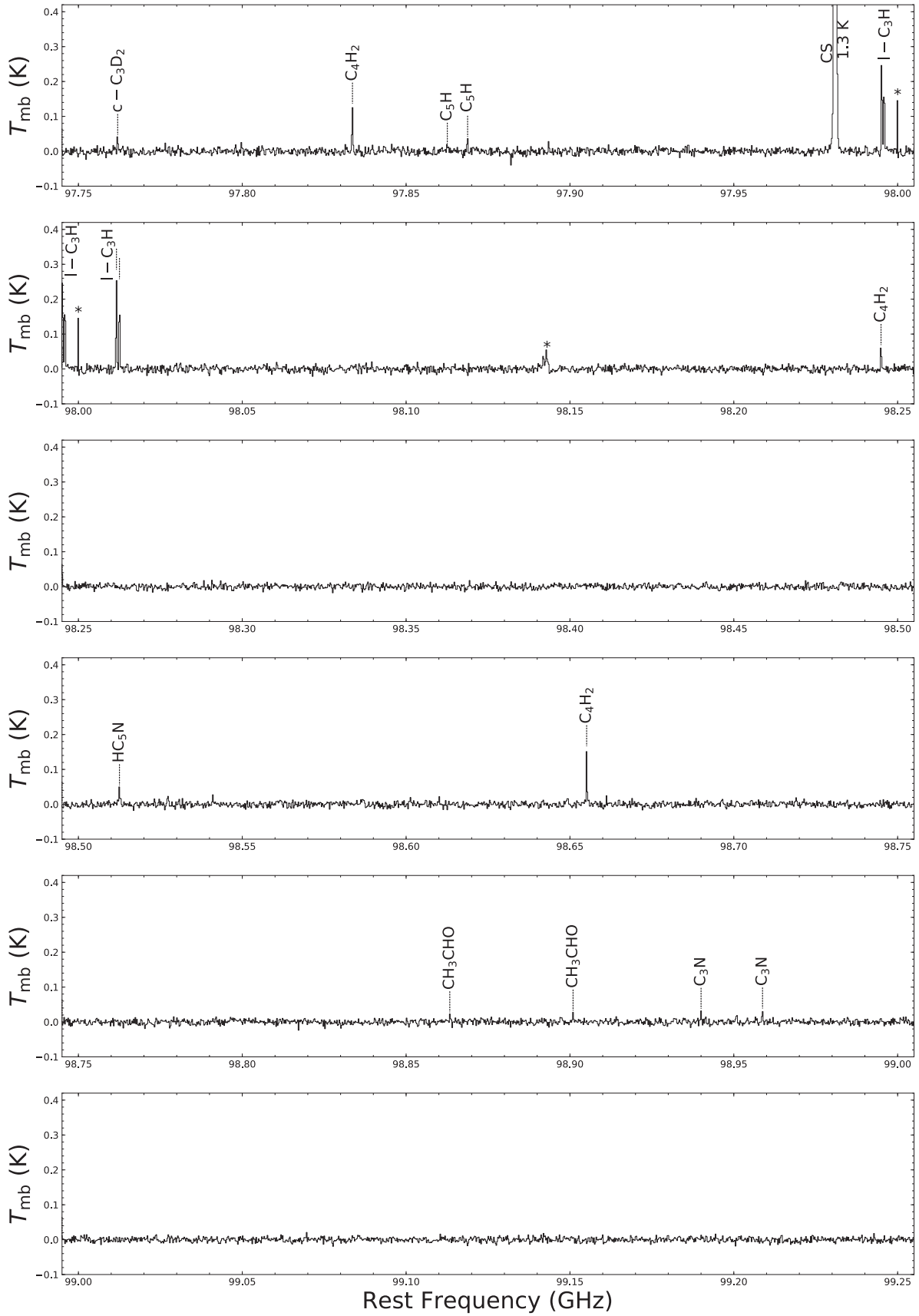


Fig. 2. (Continued.)
60

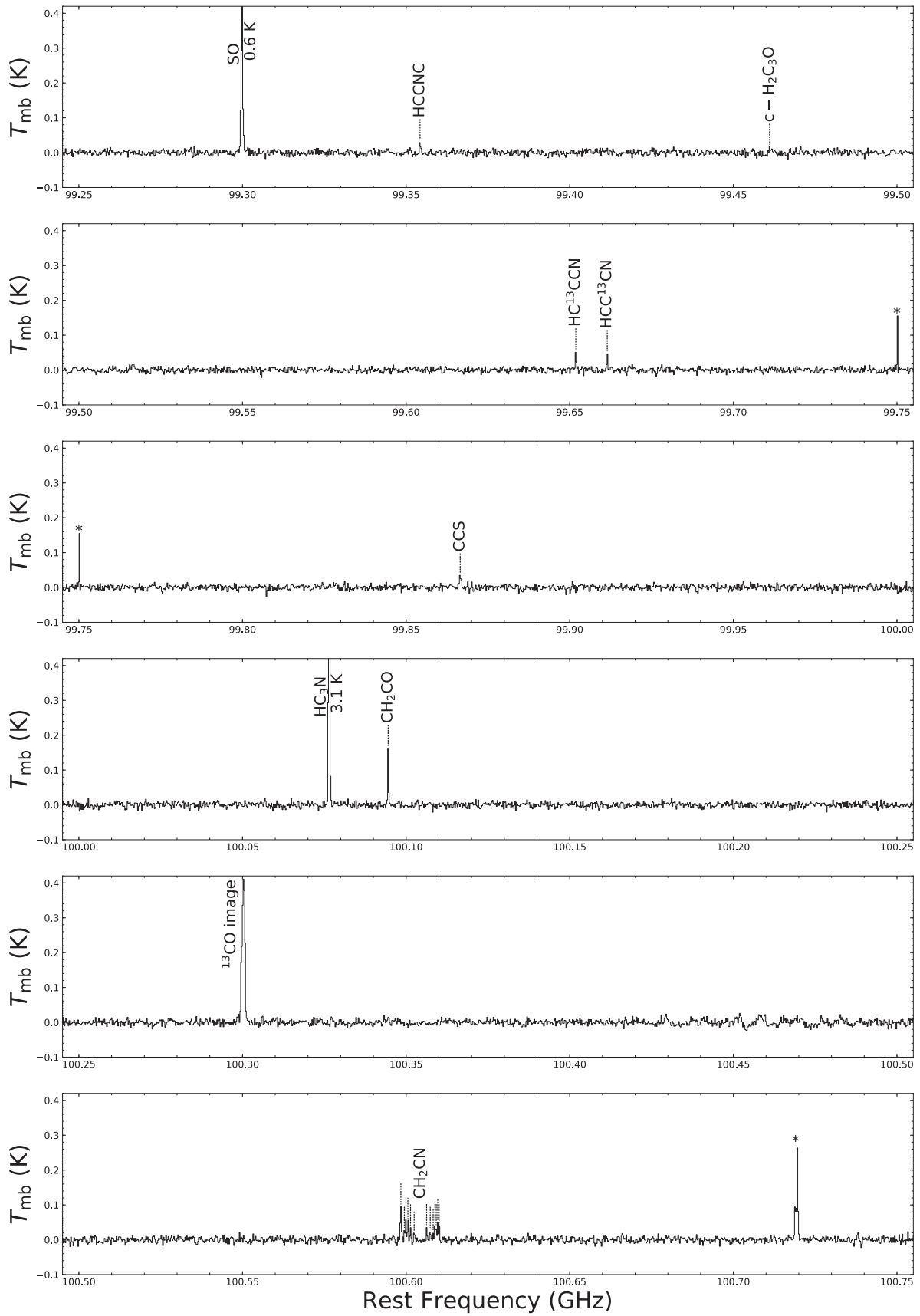


Fig. 2. (Continued.)
61

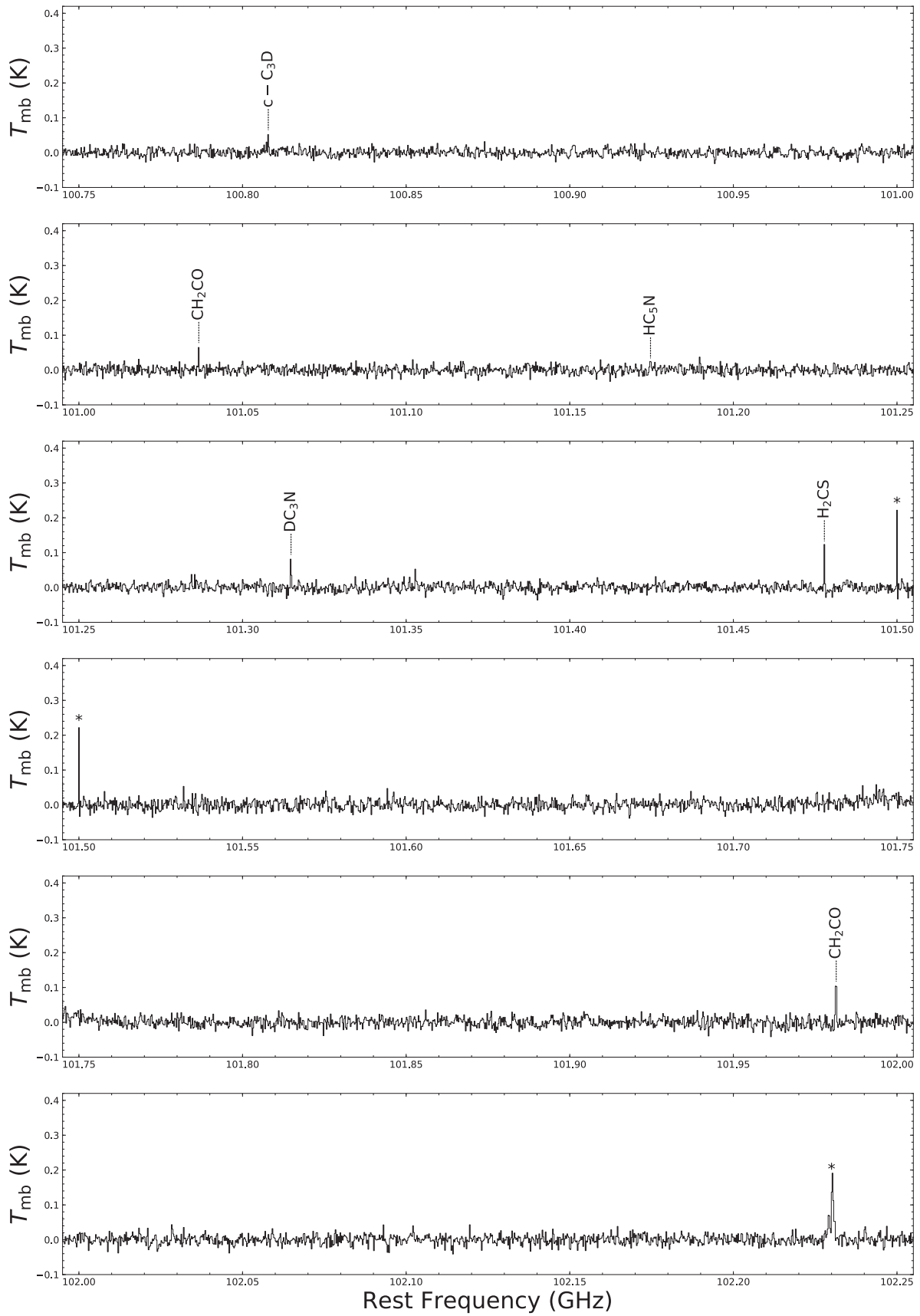


Fig. 2. (Continued.)
62

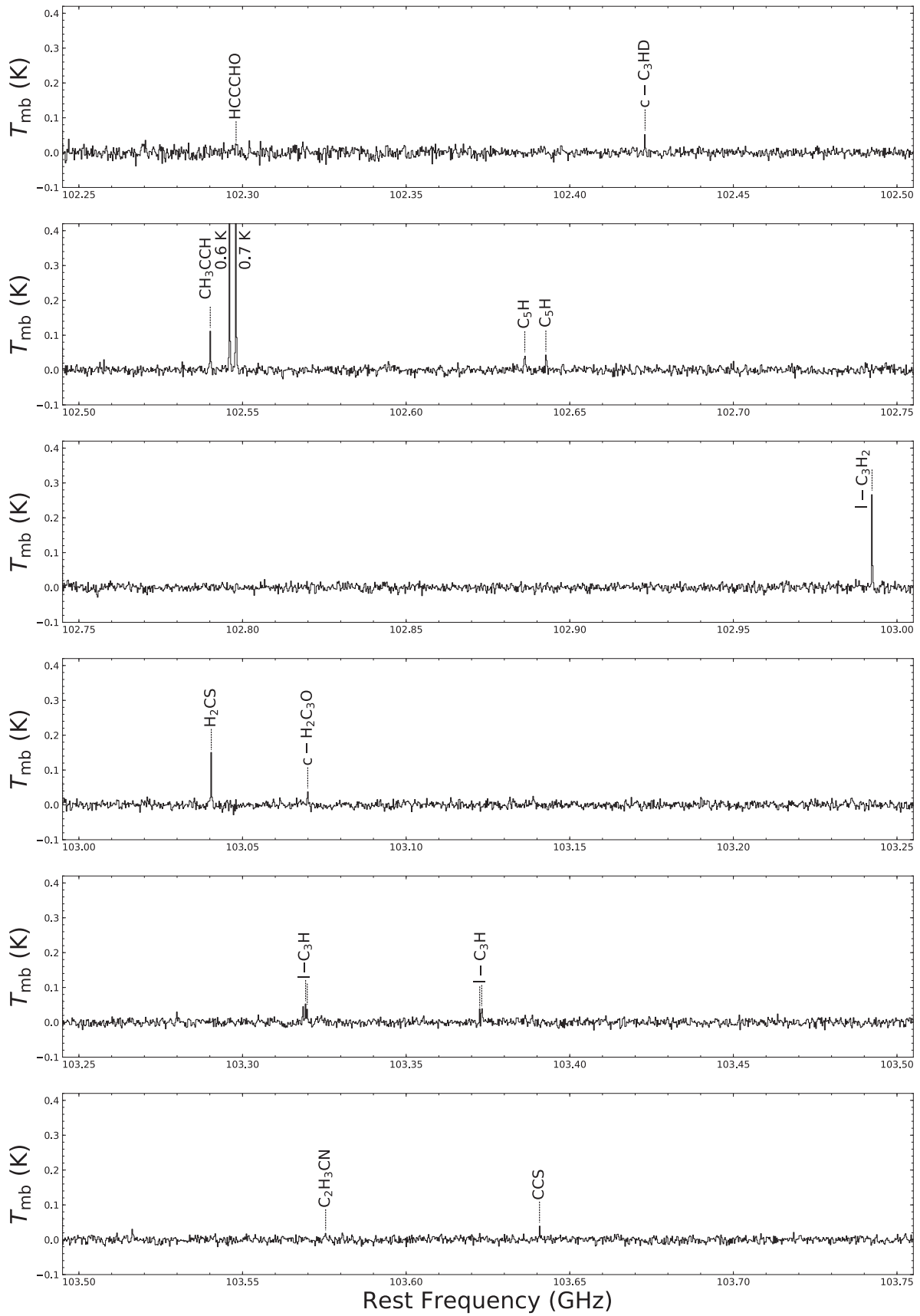


Fig. 2. (Continued.)
63

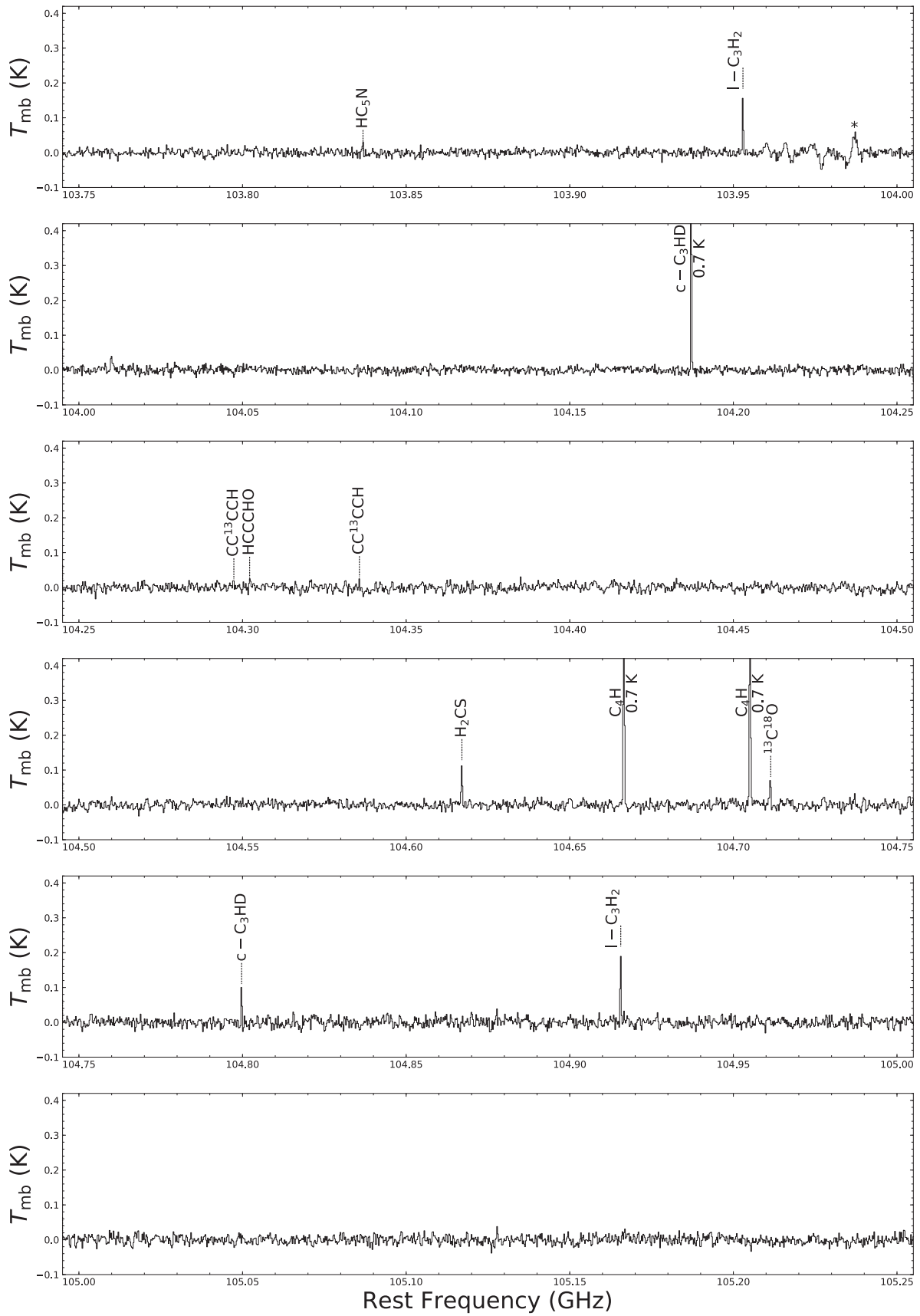


Fig. 2. (Continued.)

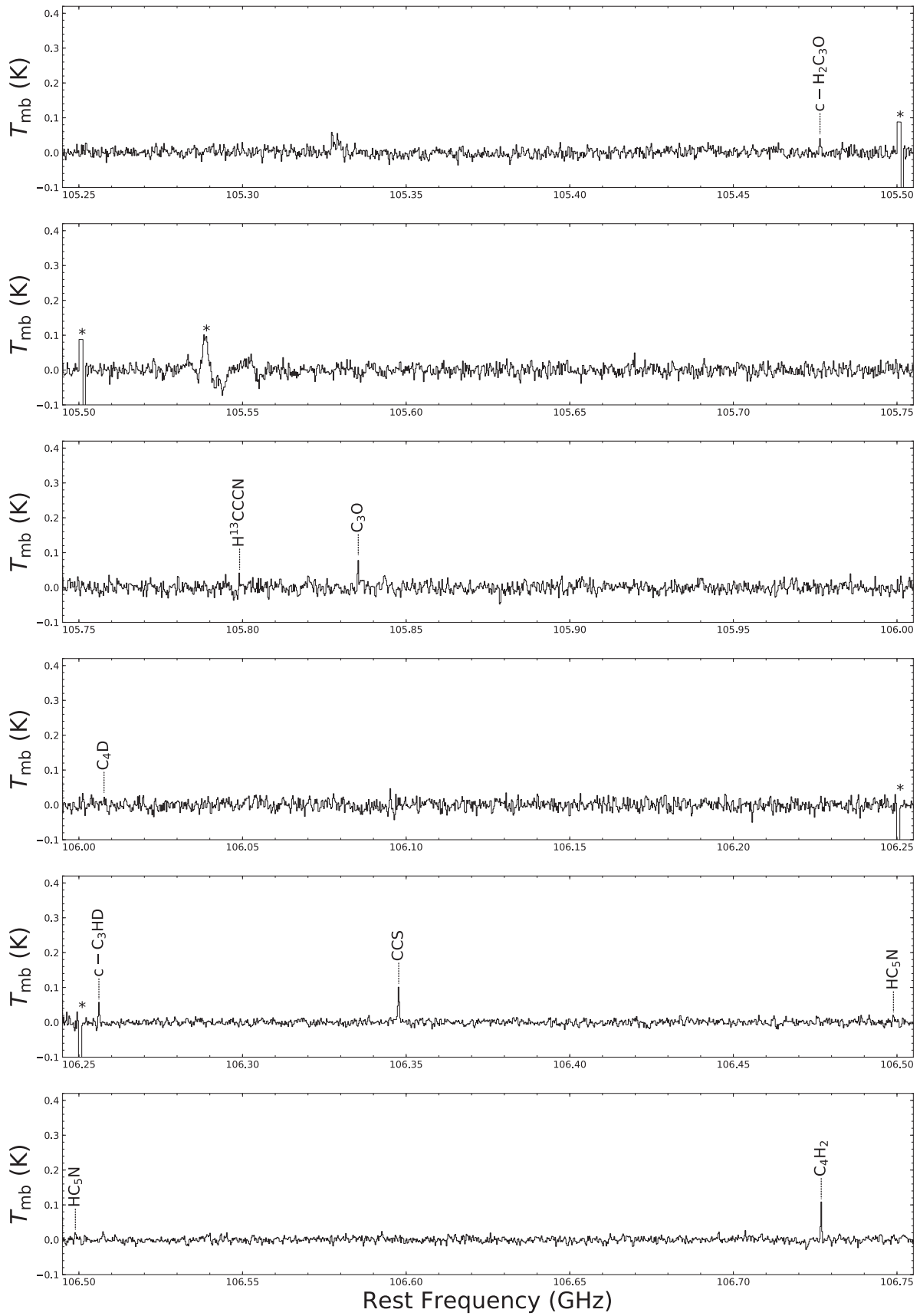


Fig. 2. (Continued.)
65

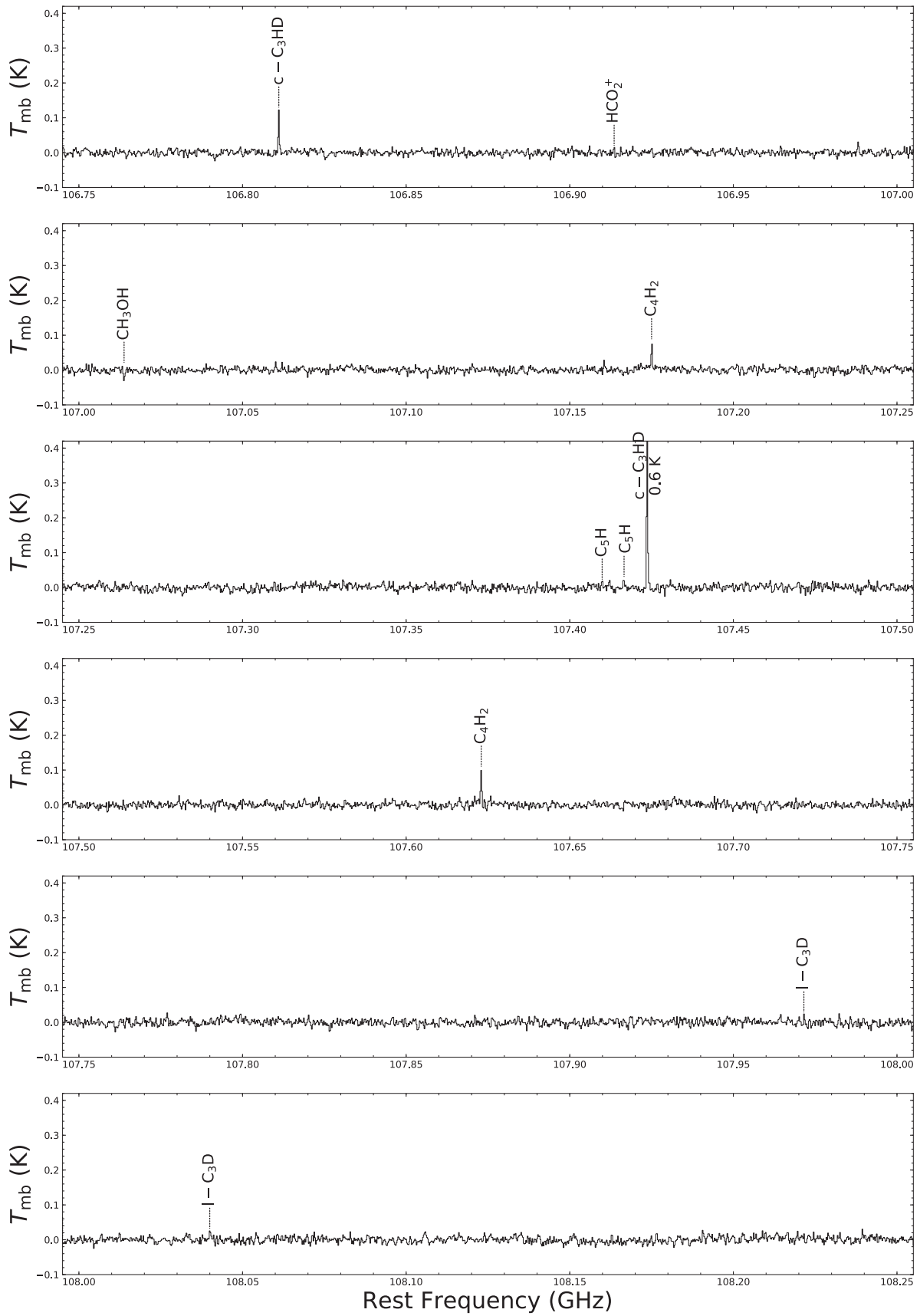


Fig. 2. (Continued.)
66

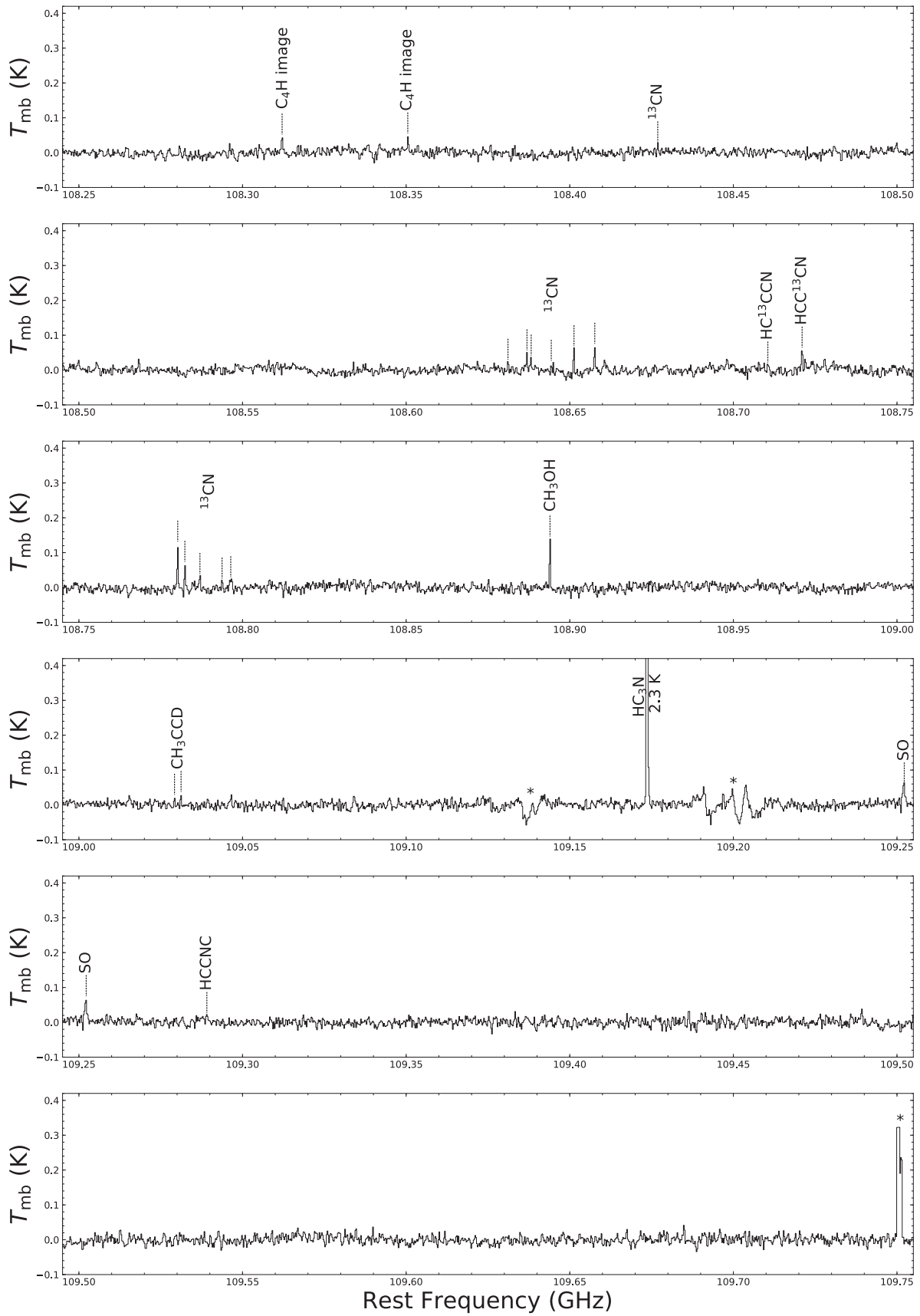


Fig. 2. (Continued.)
67

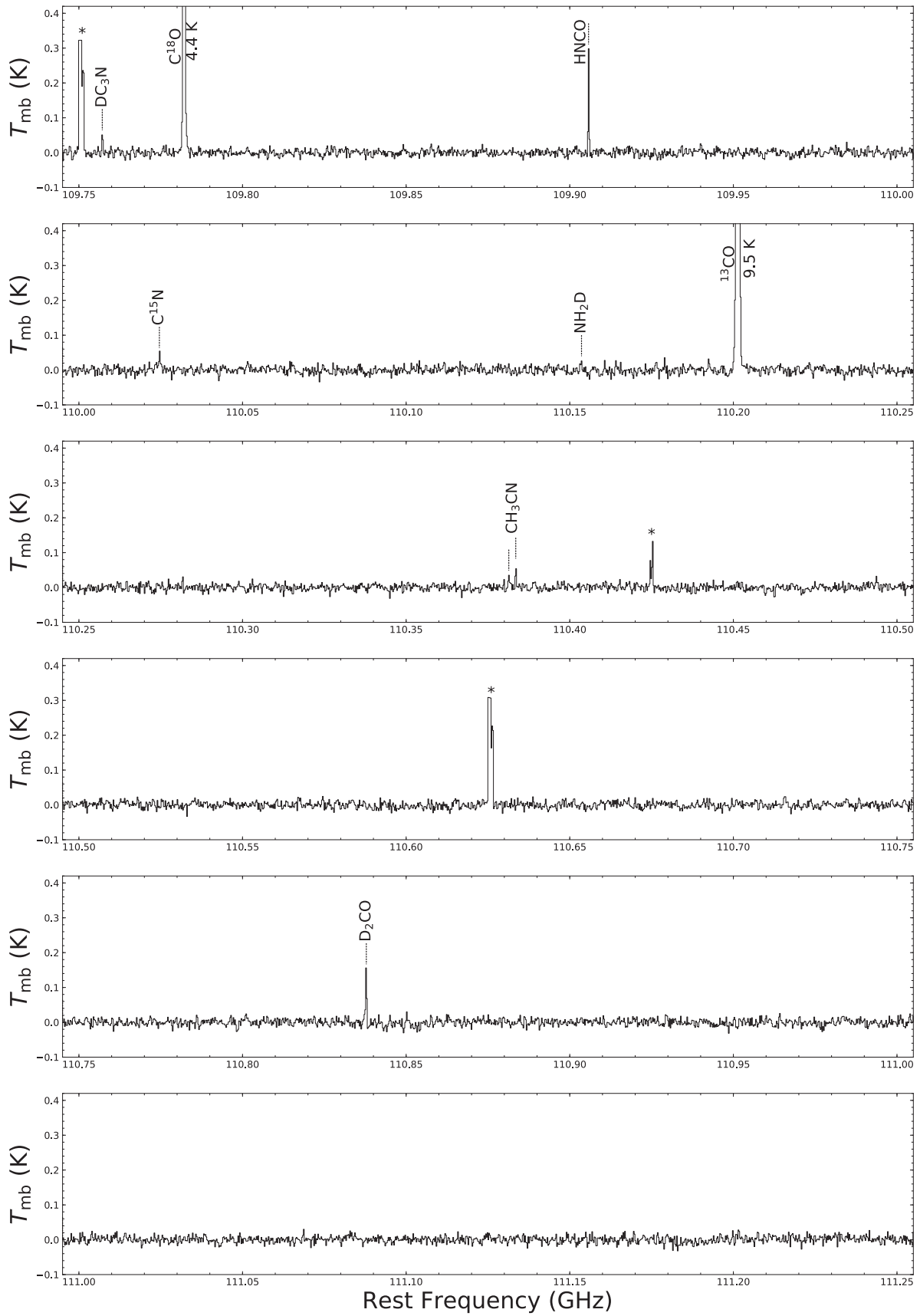


Fig. 2. (Continued.)
68

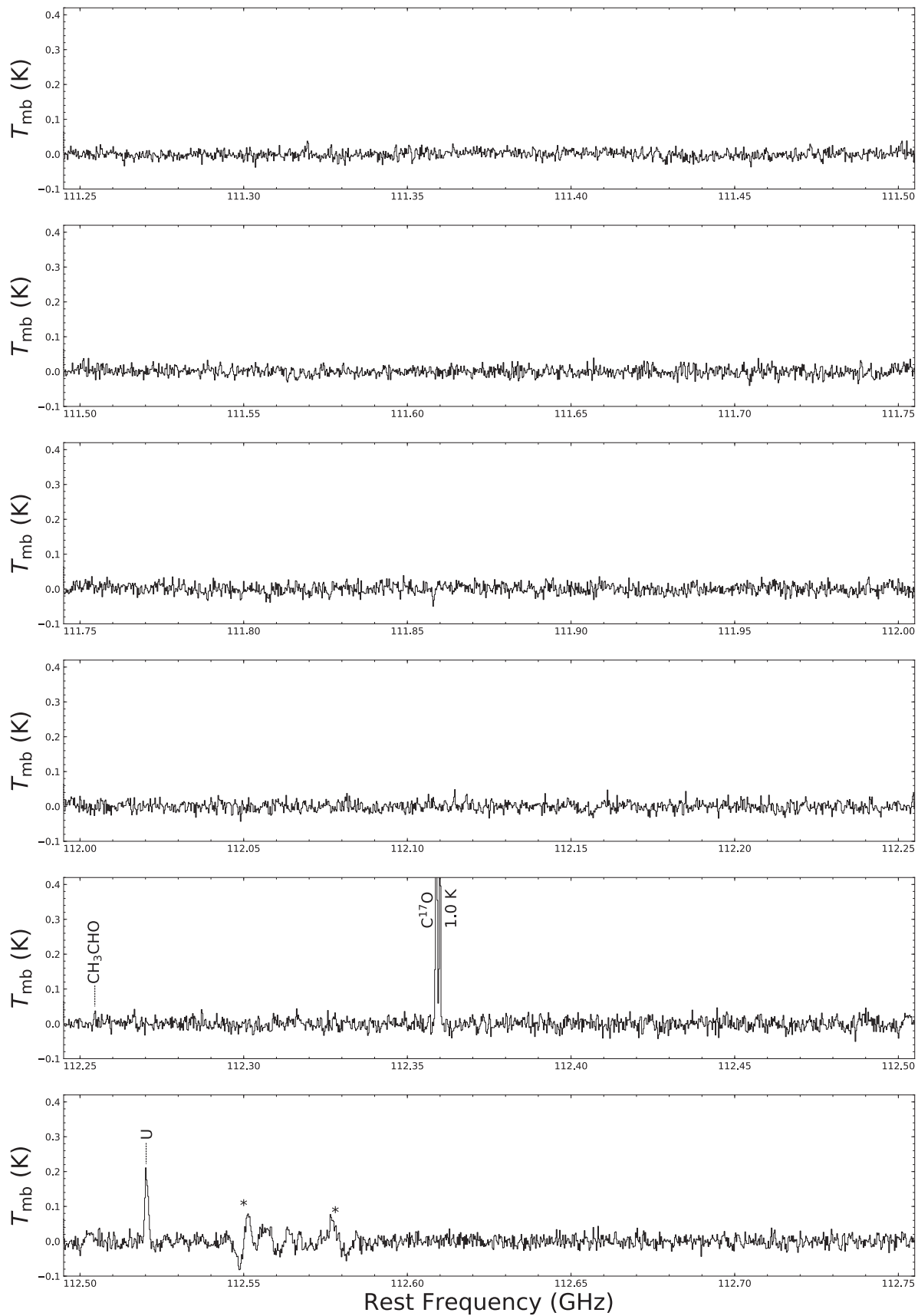


Fig. 2. (Continued.)
69

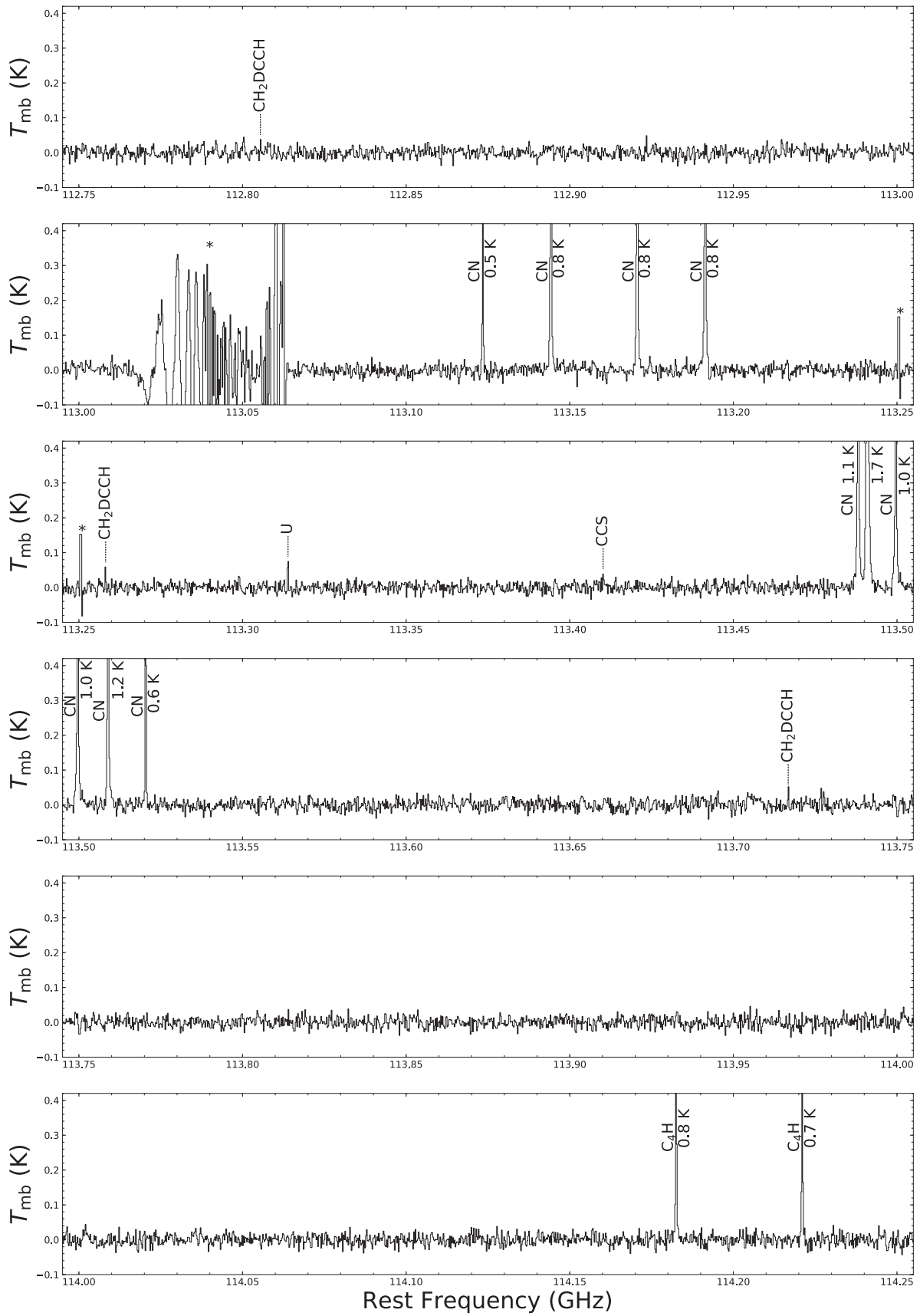


Fig. 2. (Continued.)
70

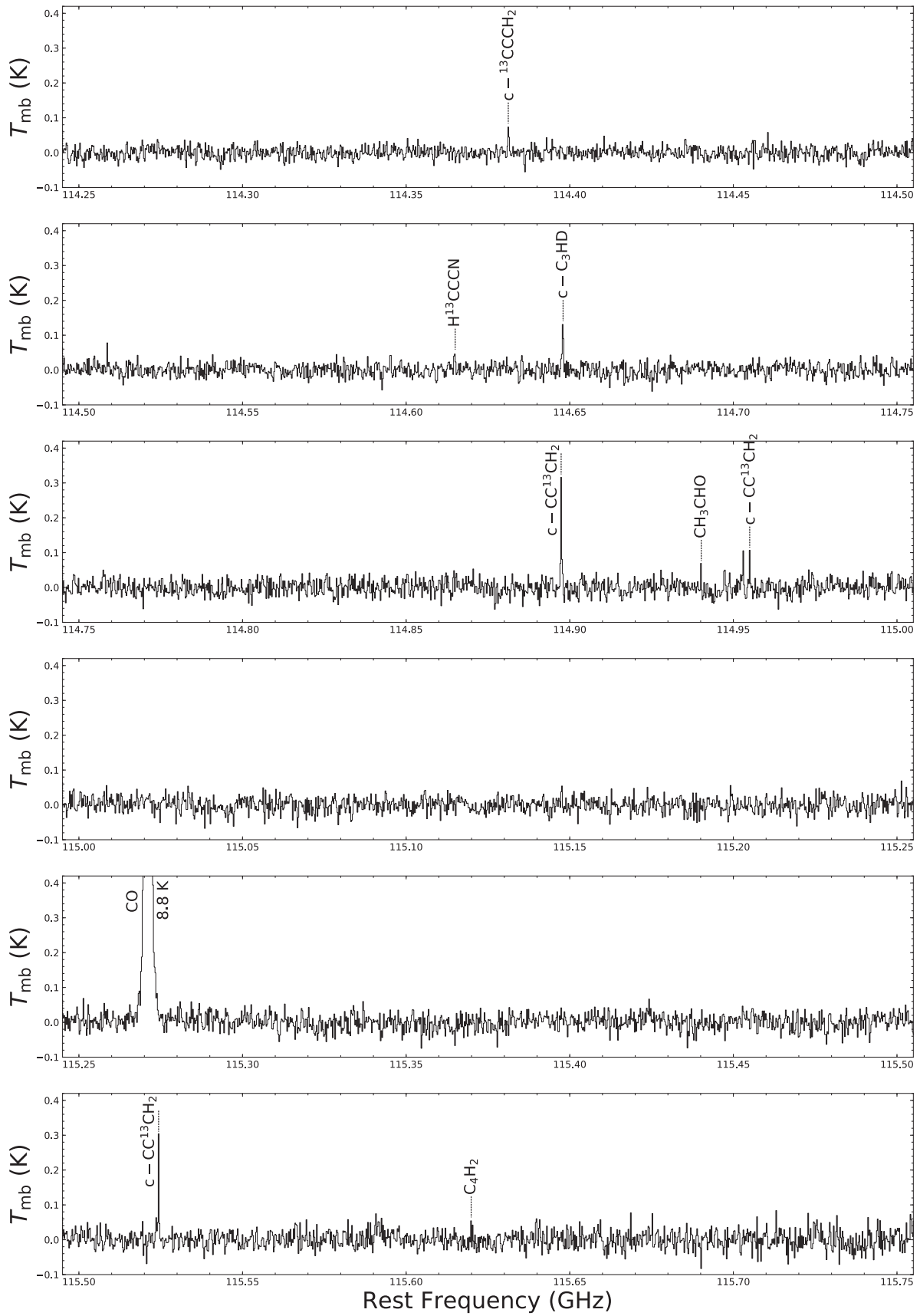
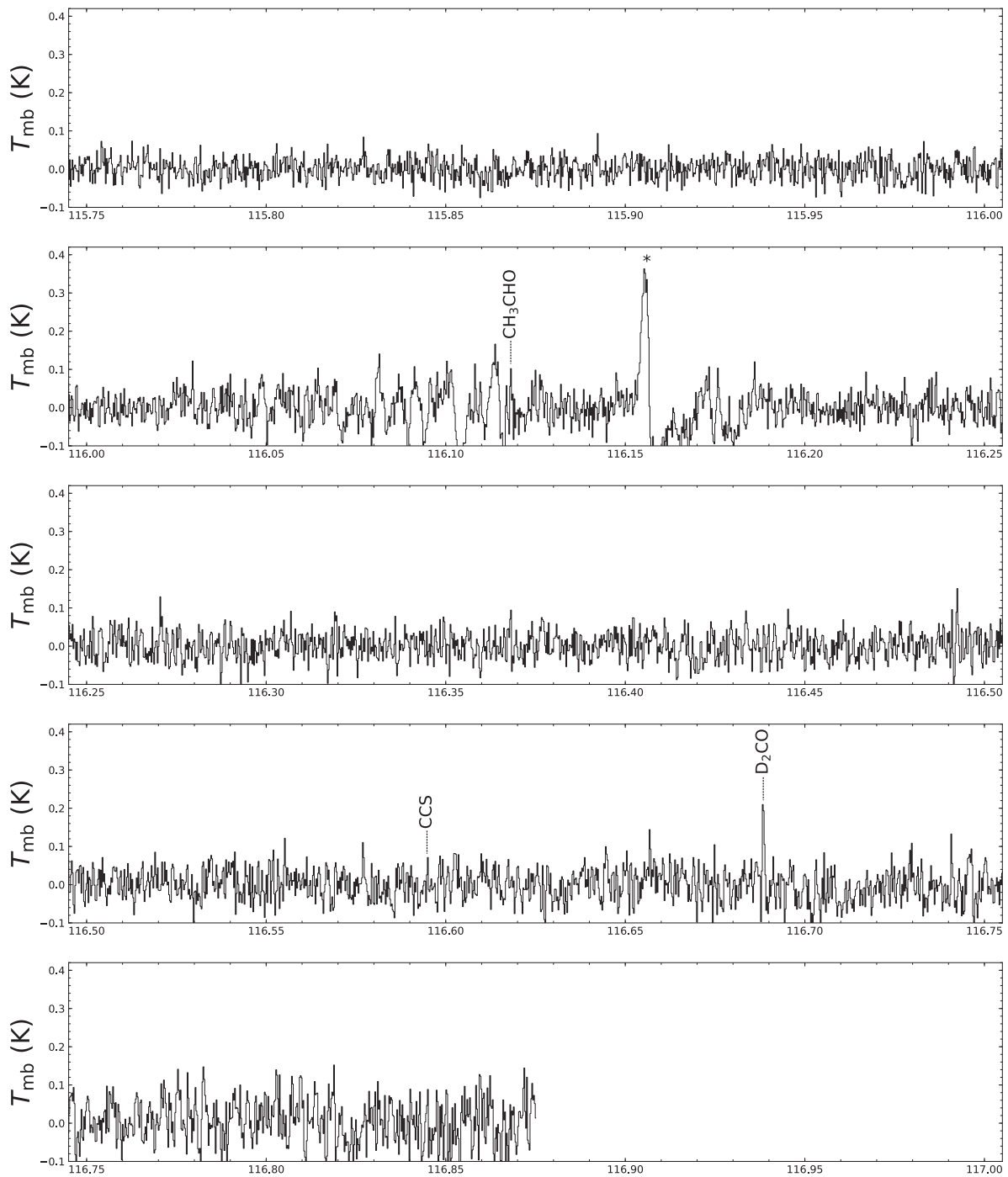


Fig. 2. (Continued.)



Rest Frequency (GHz)

Fig. 2. (Continued.)
72

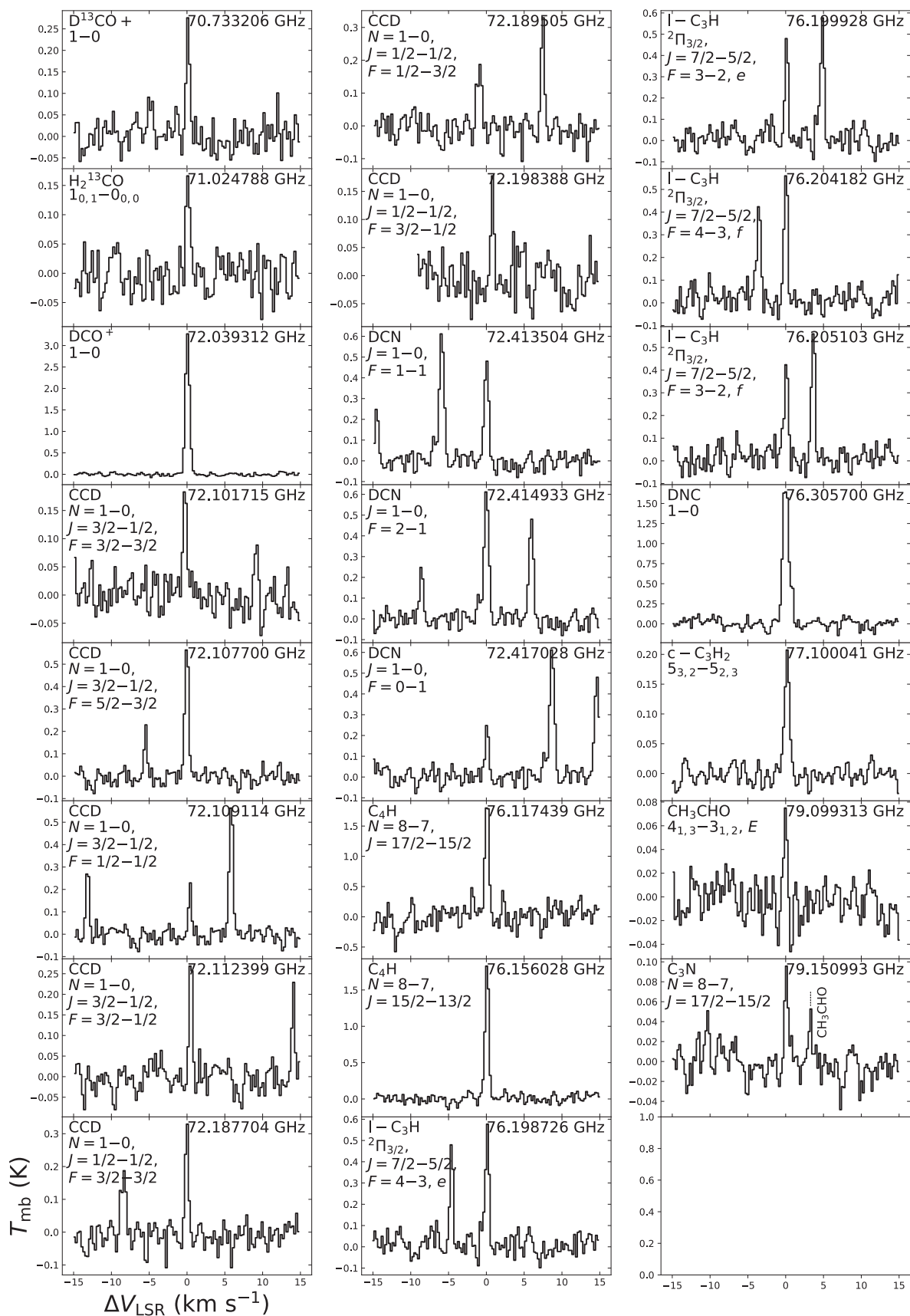


Fig. 3. Individual spectral line profiles of molecules detected in the 70 GHz band. The $N = 1-0$ lines of N_2D^+ are shown in Figure 4.

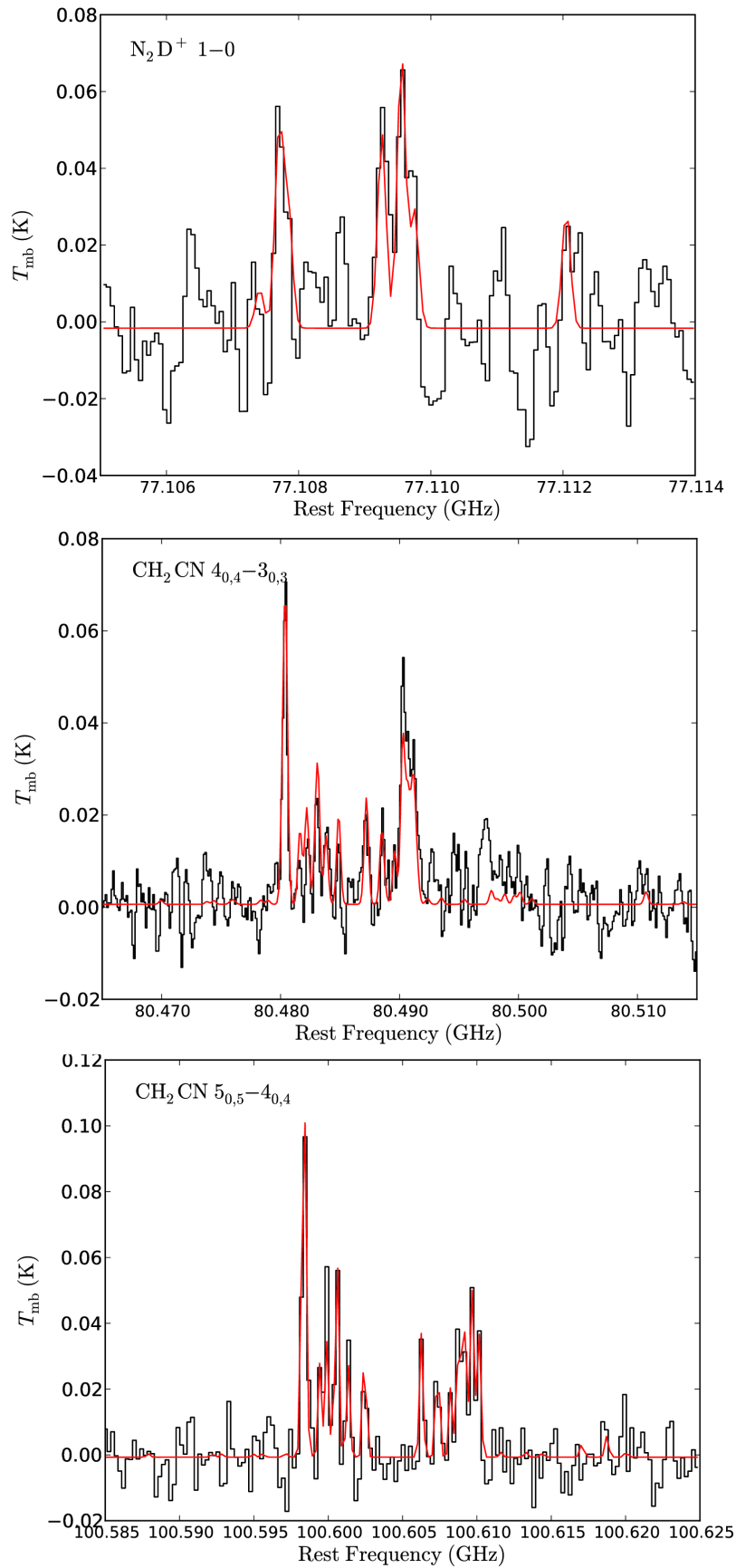


Fig. 4. The hyperfine components of N_2D^+ and CH_2CN . The results of the multiple Gaussian fitting are also shown in red.

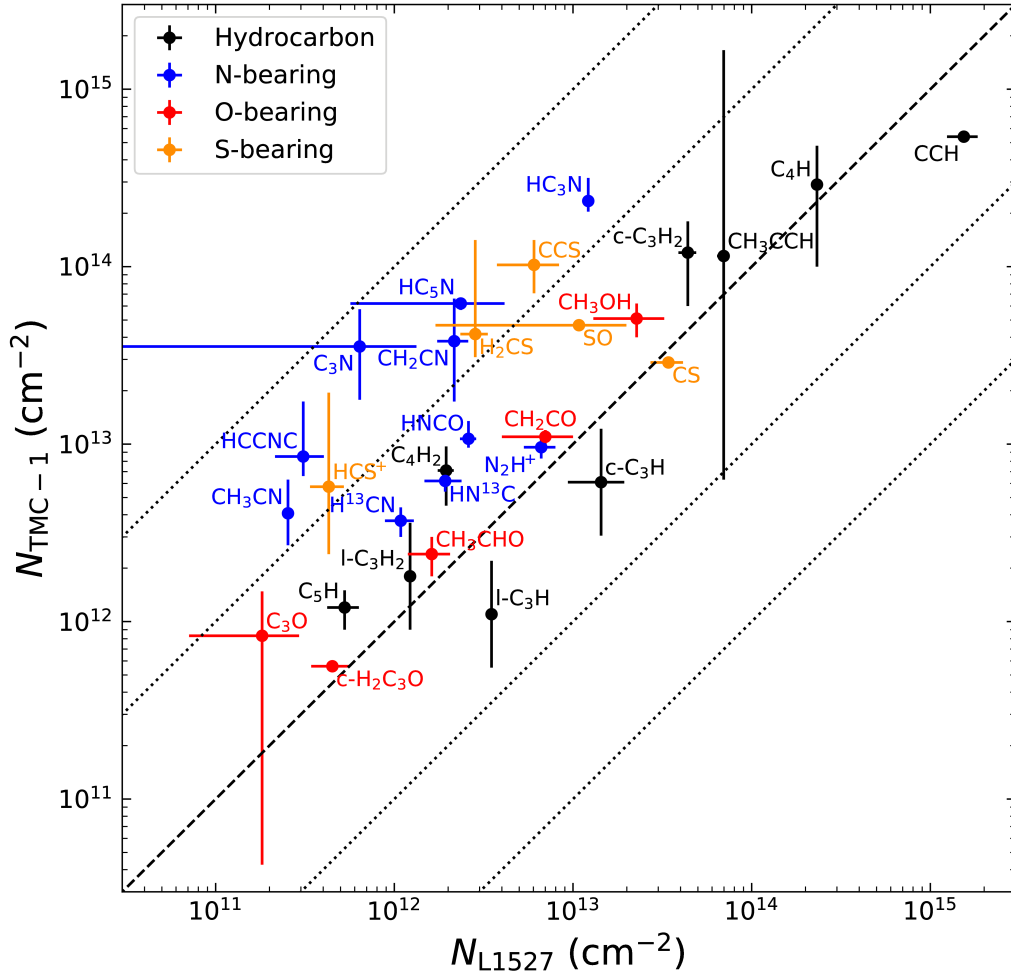


Fig. 5. The correlation plot of the column densities in L1527 (N_{L1527}) and in TMC-1 (N_{TMC-1}). The dashed line represents $N_{L1527} = N_{TMC-1}$. The four dotted lines show the column density ratio of 100, 10, 0.1, and 0.01. Column densities in TMC-1 are taken from: Loison et al. (2017; $c\text{-C}_3\text{H}$, $I\text{-C}_3\text{H}$, $c\text{-C}_3\text{H}_2$, and $I\text{-C}_3\text{H}_2$), Sakai (2008; C_4H , C_4H_2 , and C_5H), Sakai et al. (2008b; C_4H , C_4H_2 , and C_5H , 2010b; CCH), Gratier et al. (2016; CH_3CCH , HC_5N , HCCNC , CH_2CN , CH_3CN , HNCO , C_3N , CH_2CN , C_3O , SO , CS , CCS , H_2CS , and HCS^+), Taniguchi et al. (2016; HC_5N), Soma et al. (2015; CH_3OH , 2018; CH_2CO and $c\text{-H}_2\text{C}_3\text{O}$), Crapsi et al. (2005; N_2H^+), and Hirota et al. (1998; HN^{13}C and H^{13}CN)

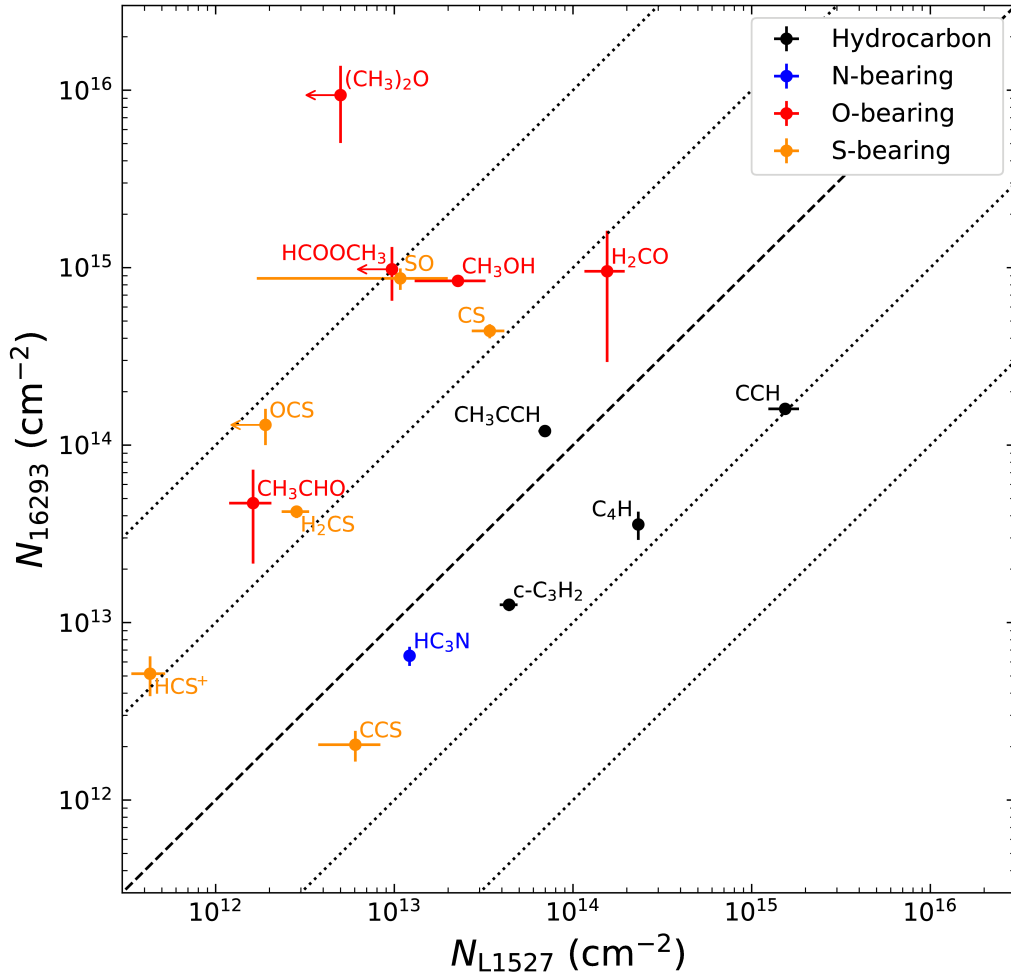


Fig. 6. The correlation plot of the column densities of carbon-chain molecules, COMs, and S-bearing molecules in L1527 (N_{L1527}) and in IRAS 16293-2422 (N_{L16293}). The dashed line represents $N_{L1527} = N_{L16293}$. The four dotted lines show the column density ratio of 100, 10, 0.1, and 0.01. The beam-averaged column densities in IRAS 16293-2422 are derived from Cazaux et al. (2003) for CH_3CHO , HCOOCH_3 , and $(\text{CH}_3)_2\text{O}$. The column densities of other species are derived from Caux et al. (2011).